TÉCNICO LISBOA

Quantum Solitonic Turbulence in Low-Dimensional Bose-Einstein Condensates

Maria Clara Robalo Pereira

Thesis to obtain the Master of Science Degree in

Engineering Physics

Supervisor(s): Prof. Hugo Fernando Santos Terças

Examination Committee

Chairperson:	Prof. Horácio João Matos Fernandes
Supervisor:	Prof. Hugo Fernando Santos Terças
Members of the Committee:	Prof. João Pedro Saraiva Bizarro
	Prof. Marija Vranic

January 2021

Dedicated to my parents, for all the love distilled into patience.

Acknowledgments

I would like to thank first my supervisor Prof. Hugo Terças, for all the patience, guidance, and in general for being a source of infectious passion for physics and its beautiful quirks. I am very grateful to have been introduced to this subject matter and for the opportunity to develop this work.

I must thank as well the quantum plasmas research group inside IPFN at IST, for the warm welcome and for all the enlightening physics' discussions and the weekly meetings which i do sincerely miss.

Finally, It would be beyond remiss not to mention those that, although not directly involved in the development of this work, have supported me, loved me and held me. And in doing so were the reason it was able to come to fruition.

So to my brother, for being my first and closest ally, and in general for always being in my corner.

To Carolina Amoedo, for being there in all and every moment during this degree. You were my companion for the years.

To Alice, for all the love, support and understanding.

To my one little cousin Adriana and my aunt Teresa and uncle Aníbal, for fostering me and for all the love, kindness and warmth.

To my unexpected sister Carolina, for liking me albeit begrudgingly.

To Suze Dercksen, my one Erasmus buddy and constant friend.

To my parents, for the endless stream of support. And to my uncle Carlos, for the good friendship and affection.

And not in the least, to all the kind people from QueerIST, especially the little physics family who started it all. Violeta, Mariana, Diana, Diogo, Rafael, Rita, and many others, I am beyond humbled.

Resumo

Turbulência forte em fluidos quânticos a baixas dimensões implica o surgimento e interacção dinâmica de solitões escuros. Estas estruturas surgem naturalmente em fluidos quânticos sujeitos a perturbações e, especificamente, em condensados de Bose-Einstein. Por sua vez, a evolução deste fluido é descrita pela equação de Gross-Pitaevskii (GP), da qual os solitões constituem soluções estacionárias. Ora, se os solitões constituem uma manifestação de turbulência, então a descrição de um ensemble destas excitações a interagir dinamicamente conduzir-nos-á no sentido da produção de uma descrição de turbulência quântica.

Com isto em mente, propõe-se uma descrição cinética de um gás de solitões derivada a partir da equação de Vlasov com o objectivo de captar as componentes estatística e dinâmica do gás de solitões. Para além disto, é desenvolvido também um código que resolve numericamente a equação GP para estabelecer uma base de comparação e interpretação dos nossos resultados.

As simulações numéricas produzem um espectro de excitações que apresenta dois modos: um modo acústico mais energético e identificado com excitações do condensado, e um modo menos energético que, esse sim, é o correspondente ao modelo cinético desenvolvido e a um modo solitónico. Estes resultados estabelecem a possibilidade do desenvolvimento de uma descrição cinética e analítica de regimes turbulentos em fluidos quânticos a baixas dimensões.

Palavras-chave: Condensação de Bose-Einstein, Solitões, Fluidos Quânticos, Teoria Cinética, Turbulência Quântica

Abstract

Strong turbulence in one-dimensional quantum fluids entails the emergence and dynamical interaction of dark solitons. These structures arise naturally in quantum fluids subject to perturbation and, specifically, in Bose-Einstein condensates (BEC). In turn, the evolution of this quantum fluid is described by the Gross-Pitaevskii(GP) equation, of which solitons are stationary solutions. If solitons constitute a manifestation of turbulence, then a description of an ensemble of these excitations dynamically interacting would lead one in the direction of producing a description of quantum turbulence.

With this in mind, we propose a kinetic description of dark-soliton gases which we derive from the Vlasov equation to capture the statistical and dynamical features of the soliton gas. Beside this, we also develop a code which numerically solves the GP equation to provide a basis to compare and interpret our results to. The numerical simulations yield a spectrum of excitations which show two modes: a more energetic acoustic mode identified with BEC excitations, and a less energetic mode which is the one linked to our kinetic model and to a solitonic mode. These findings establish the possibility for a kinetic analytical description of turbulent regimes in low-dimensional superfluids.

Keywords: Bose-Einstein Condensation, Solitons, Quantum Fluids, Kinetic Theory, Quantum Turbulence

Contents

List of Tables

List of Figures

Nomenclature

Greek symbols

∇	Gradient
$\boldsymbol{\nabla}\times$	Curl
$\boldsymbol{\nabla}\cdot$	Divergence
Δ	Laplacian operator
$\hat{\Psi}$	Creation field operator
$\hat{\Psi}^\dagger$	Annihilation field operator
λ	Simulation parameter
ω	Frequency
ω_x	Trapping frequency
∂	Partial derivative
φ	Wavefunction
ξ	Healing length
ζ	Riemann Zeta Function

Roman symbols

ϵ	Excitation energy
ϵ_s	Single soliton energy
γ	Interaction parameter
$\hat{H}$	Hamiltonian operator
$\hbar$	Reduced Planck's constant
μ	chemical potential
a	s-wave scattering length

c	Sound velocity
d	Interparticle distance
E	Energy
E'	Grand canonical energy
E_d	Deformation energy
E_s	Soliton energy
E_{ph}	Phonon energy
$f(E)$	Energy distribution function
$f(r_i, p_i; t)$	Probability distribution
f_0	Soliton velocity distribution function
$f_1(r, p; t)$	One-particle distribution function
g	Interaction parameter
$g(E)$	Density of states
g_{1D}	Two-body Lieb-Liniger interaction strength
j	Current density
k	Wavevector
k_c^{LL}	Lieb-liniger critical wavevector
K_B	Boltzmann constant
L	Box length
m	Mass
m^*	Effective soliton mass
N	Number of particles
n	Density
N_0	Soliton density
n_0	Equilibrium density
n_c	Critical density
n_f	COndensate Fraction
n_i	Occupation number

p	Momentum
r	Cartesian coordinate
S	Condensate phase
T	Temperature
t	Time
T_C	Critical transition temperature
V	Volume
v	Velocity
$V(q-q')$	Interaction potential
v_F	Fermi velocity
v_s	Soliton velocity
V_{ext}	External potential
x	Position
$\hat{a}_i^\dagger$	Creation operator
$\hat{a}_i$	Annihilation operator
E_g	Ground-state BEC energy

Subscripts

i, j, k	Indexes
n	number index
x, y, z	Cartesian components
ref	Reference condition

Superscripts

*	Adjoint.
†	Conjugate Transpose
T	Transpose.

Chapter 1

Introduction

1.1 Quantum Turbulence in 1D

Turbulence has been described by Feynman [1] as the most important unsolved problem of classical physics. And once one starts delving into it, it is not too difficult to understand his reasoning; actually, the more one looks, the more one comes face to face with the undeniable and constant presence of turbulent effects in nature and all around us. Be it in the transport of salinity in the oceans, in the motion of molten iron in the Earth's core, in the behaviour of clouds in our atmosphere [2] or even in the rough surface of our seas; this problem of difficult definition is ever-present, and represents the most general, and most complex, dynamical motion of fluids.

Turbulence has been on the minds of scientists ever since Da Vinci, approx. 500 years ago, first recognised it as a distinct phenomenon. Despite this, it was only in the 1950s that Feynman introduced the notion of quantum turbulence (QT), which looks to understand the phenomenon of turbulence occurring in quantum fluids. Feynman theoretically suggested that turbulence in this regime would exhibit a rather distinct set of effects from its classical counterpart. Since then, QT has been garnering attention from scientists from all fields, specially in the last decade, having become one of the most lively topics of research in low temperature physics.

The growing interest in this topic cannot be solely attributed to its academic interest. It is also due, among other things, to its relevance for the development of a new generation of quantum technologies. In this sense, a better understanding of turbulent behaviour in quantum regimes will allow for a better description of quantum many-body systems, whether it be on ultracold gases or in Bose-Einstein condensates (BECs), something that is of fundamental importance towards the realisation of quantum technologies and may represent a basis of important developments on quantum information and quantum technologies [3, 4].

In addition to this, there is also hope that knowledge on QT may shed some light on the phenomenon of (classical) turbulence in general. Recently, weakly interacting dilute atomic BECs have emerged as a promising prototype system to explore the quantum mechanical form of turbulence [4], having proven to be an attractive context for the study of nonlinear dynamics and quantum effects at the macroscopic

scale [5].

1.1.1 A better understanding of the problem

Even though both classical and quantum turbulence are characterised by chaotic, aperiodic spatial and temporal dynamical motion, the latter is quite distinct in a few key aspects namely superfluidity, i.e., the fluid ability to flow freely without the dissipative effects of viscosity (so characteristic of classical fluidics) [5]; and quantised vorticity, the phenomenon whereby the quantisation of angular momentum in quantum fluids, like BECs, restricts the vorticity (circulating flow is constrained to discrete vortex lines around topological defects). This quantised quality of vortices is strongly contrasting with the eddies of classical fluids, which are continuous and of arbitrary size and shape.

In low-dimensional systems, the additional dimensional constraints give rise to new non-negligible effects. In the first place, the development of quantum fluctuations around a background density (also shifting the ground-state energy of a Bose gas) and secondly the emergence of quantum topological effects — local density minima in the fluid with a sharp phase gradient of the wavefunction — the so-called *dark solitons*.

Gathering up these concepts, one can surmise the 1D quantum fluid (such as BEC) subject to turbulence to be a sufficiently coherent large-scale structure of dark solitons (with fermionic statistics, as we should see later on) immersed in a turbulent, incoherent "sea" of small-scale fluctuations with which they interact — phonons (with bosonic statistics). The phonons, the aforemenioned quantum fluctuations, are low-energy excitations of the medium which arise as a consequence of the $\mathrm{U}(1)$ symmetry breaking in BECs — the Goldstone mode.

This thesis concerns weakly-interacting, dilute atomic BECs. These quantum fluids have been used to investigate quantum turbulence both experimentally and theoretically, which has been largely stimulated by the high degree of control available in the experiments with these quantum gases [6–8]. Their definition, characteristics and behaviour will be explored in detail in further sections.

1.2 Quantum Turbulence Overview

It was only in 1995 that Bose-Einstein condensation was experimentally observed [9]. And even though Feynman proposed quantum fluids as good candidates for a prototypical approach to classical turbulence as far back as in 1955 [10], the first theoretical proposals in this direction came about only in the mid 2000's [11–13]. However, the advent and rapid development of quantum optic techniques, which allow the control and manipulation of the fluid, has supported the emergence of Bose-Einstein condensates as a promising model system to understand quantum turbulence in the past decade [4, 14–16]. This is, in sum, our framework: Modelling quantum turbulence through the study of its manifestations in BECs. In turn, knowledge on QT may be key to understanding common features with its classical counterpart [17–19].

Having now an understanding of our goals, it is necessary to establish the necessary formalism to

tackle them. With this in mind, and because this thesis will focus on turbulence in one-dimensional BECs, we firstly summarise the phenomenon of Bose-Einstein condensation from the statistical physics and quantum field theoretical perspectives, culminating with a brief description of the mean-field theory which will be relevant in the development of our model. This model is materialised in the Gross-Pitaevskii equation, followed by the description of dark-solitons, which are shown to constitute particular solutions of this equation. The study of a collection of dark solitons naturally prompts kinetic theory as the tool to study such a many-body system.

1.3 Objectives

The main goal of this thesis is to establish a theoretical framework for turbulence in low-dimensional BECs, which are the most suitable platforms to understand the features of quantum turbulence occurring at ultracold temperatures.

The description of strong turbulence in one-dimensional BECs must account for the excitation of topological defects, the so-called dark-solitons (DS), and their interaction with the other arising structures, phonons. While so far a full treatment of strong turbulence in this context can only be achieved through complex numerical simulation, a route to a comprehensive treatment involving the statistical mechanics of dark solitons is desirable and, most importantly, treatable.

In this sense, the search for a theoretical model of turbulence in BECs will consist on the devising of a minimal kinetic model for a statistical distribution of dark-solitons in this fluid. By doing this, we also aim to understand to which extent strong quantum turbulence in 1D BECs can be described in terms of the already established tools for effective weak-turbulence theory of soliton gases.

Parallel to this, the work will also entail a computer simulation wherein the system in study will be modelled by solving the Gross-Pitaevskii equation. The purpose of this simulation is to provide a comparison with the theory, and understanding of the physics involved, and allow for a verification of the results.

1.4 Thesis Outline

This thesis is divided into 5 chapters. In chapter 1 the contents present in the work are introduced, and a brief motivation is given as to the relevance of the work hereby developed. The work is also contextualised in its field and the goals of the thesis are outlined. Secondly, in chapter 2, a more detailed overview of the physics involved is explored, and the formalism and knowledge needed to develop the proposed model (1D gas of interacting solitons) is thoroughly detailed. This chapter includes as well a small foray into Lieb-Liniger theory, presented as a theory with a few similar aspects whose comparison to ours is interesting to explore. Chapter 3 describes the developed theory — a kinetic model which seeks to describe the behaviour of a gas of dark-solitons in a one-dimensional BEC. Next, an account of the developed code is presented in chapter 4, full with the discretisation of the Gross-Pitaevskii equation and a description of the adopted computational methods. This chapter includes an important section

where the code is employed to a few physical representative cases in order to test and validate its working condition, and ultimately make sure that the physics obtained are correct and meaningful.

In chapter 5, A comparison between the analytical predictions of the developed model and the simulations is provided. Finally, in chapter 6, final remarks on the achievements of the work developed as well as future prospects on possible further work are stated.

Chapter 2

Background

2.1 Theoretical Overview

2.2 Bose-Einstein Condensation

The phenomenon of Bose-Einstein condensation, initially predicted by Bose and Einstein in 1924, consists in a state of matter of a gas of bosons cooled to temperatures very close to absolute zero [20]. Under such conditions a large fraction of bosons occupy the lowest quantum state, at which point microscopic quantum mechanics become apparent on a macroscopic scale — the condensate exhibits collective behaviour. In particular, when a gas of bosonic particles is cooled below a critical transition temperature T_c, the particles merge into this state, in which a macroscopic number of particles share the same quantum state [21].

2.2.1 Statistical Physics

To better understand this phenomenon let us consider Bose-Einstein condensation in the context of statistical physics [22]. Ultimately, because we expect a macroscopic ocupation of the lowest energy state, we aim to find an expression for the population of states at very low temperatures. To process this statistically, we will need to use the usual trick of replacing sums over discrete momenta by an integral over the energies, while taking into account the correction due to the density of states, $g(E)$, which counts the available states in a system in a certain energy interval E to $E + dE$,

$$\sum_n \approx \int d^3n = \frac{V}{(2\pi)^3}\int d\boldsymbol{k} = \frac{4\pi V}{(2\pi)^3}\int_0^\infty dk k^2 \equiv \int dE\, g(E), \tag{2.1}$$

where $(2\pi\hbar)^3$ is the volume of each phase space cell, V is the volume of each cell in momentum space and $k = |\boldsymbol{k}|$ is the modulus of the wavevector. In order to compute the density of states, we first write an expression for the number of states with momenta within a sphere of radius p for which we have used the relation $E = p^2/2m$,

$$G(E) = \frac{V}{(2\pi\hbar)^3}\frac{4}{3}\pi p^3 = \frac{V}{3\pi^2}\left(\frac{8m}{\hbar^2}\right)^{\frac{3}{2}} E^{\frac{3}{2}}. \tag{2.2}$$

Using Eq. (2.2), we can finally determine the density of states:

$$g(E) = \frac{dG(E)}{dE} = \frac{V}{4\pi^2}\left(\frac{2m}{\hbar^2}\right)^{\frac{3}{2}} E^{\frac{1}{2}}. \tag{2.3}$$

Because we wish to inspect how the population of states behaves at very low temperatures, we search for an expression for the density parameter, $n = \frac{N}{V}$. Starting with the numerator, the total number of particles, N, will depend not only on $g(E)$ but also on the system distribution function $f(E)$ (probability to populate a certain state with energy E), which is given by the Bose-distribution,

$$f(E) = \frac{1}{e^{\frac{E-\mu}{k_B T}} - 1} = \frac{1}{z^{-1}e^{\beta E} - 1}\ , \qquad \text{with} \quad \beta = \frac{1}{K_b T} \ \text{ and } \ z = e^{\beta\mu}. \tag{2.4}$$

Together with the Eqs. (2.4) and (2.3), we can compute N,

$$N = \int_0^\infty dE\ f(E)g(E) = \frac{V}{4\pi^2}\left(\frac{2m}{\hbar^2}\right)^{\frac{3}{2}} \int_0^\infty dE\ \frac{E^{\frac{1}{2}}}{z^{-1}e^{\beta E} - 1}. \tag{2.5}$$

From this, we can obtain the system density,

$$n = \frac{N}{V} = \frac{1}{4\pi^2}\left(\frac{2m}{\hbar^2}\right)^{\frac{3}{2}} \int_0^\infty dE \frac{E^{\frac{1}{2}}}{z^{-1}e^{\beta E} - 1}. \tag{2.6}$$

Analysing Eq. (2.6) we notice that, because the chemical potential is always negative*, the minimum of the denominator is found when $\mu = 0$, or equivalently $z = 1$. When this happens, the integral can be evaluated by using the identity: $\int_0^\infty dx \frac{x^{\alpha-1}}{e^x - 1} = \Gamma(\alpha)\zeta(\alpha)$, yielding an exact finite bound for the density of the system, n_c. However, something seems to be amiss here, given that theoretically one could keep adding particles to the system even after the density bound had been reached. What would happen to these particles then? The answer lies in the fact that the approximation made in Eq. (2.1) is not entirely correct — we inadvertently lost the contribution of the ground state $E = 0$ to the integral. As such, by using the Bose-Einstein distribution in Eq. (2.4), we determine this contribution and add it manually to our density,

$$n = n_0 + n_{\text{exc}} = \frac{1}{V}\frac{1}{z^{-1} - 1} + \frac{1}{4\pi^2}\left(\frac{2m}{\hbar^2}\right)^{\frac{3}{2}} \int_0^\infty dE \frac{E^{1/2}}{z^{-1}e^{\beta E} - 1}. \tag{2.7}$$

We now realise that while the n_{exc} term is still bound by the critical density n_c, the n_0 term is unbound, representing a macroscopic occupation of the level $n_0 \to \infty$ as $\mu \to 0$ or $z \to 1$. This means that as we keep adding particles to the system after n_c is reached, all these particles are accommodated in the ground state of the system. David Tong describes this phenomenon as "a macroscopic number of atoms discarding their individual identities and merging into a communist collective, a single quantum state so large that it can be seen with the naked eye" [22].

*The number of particles summed over all states $N = \sum_i n_i$ must be positive. In accordance, in Bosonic statistics $e^{\beta(E_i - \mu)} > 1$, see Eq. (2.5), which implies $\mu < E_i$. Because this must be true for all states and in the ground state we have $E_0 = 0$ then we must have $\mu < 0$.

Making use of the found expression for the critical density n_c it is now straightforward to define critical temperature,

$$T_c = \left(\frac{2\pi\hbar^2}{k_B m}\right)\left(\frac{1}{\zeta(3/2)}n\right)^{2/3}. \tag{2.8}$$

Through this quantity, one can also define the condensate fraction,

$$n_f = \frac{N_0}{N} = 1 - \left(\frac{T}{T_c}\right)^{3/2}. \tag{2.9}$$

Finally, we conclude that Bose-Einstein condensation can be seen as a consequence of purely statistical effects. Even though BEC was theoretically predicted by Satyendra Nath Bose and Albert Einstein in 1924-25, it was only in 1938 that more attention was payed to the phenomenon as Fritz London argued that BEC could be at the basis of the superfluid properties observed in liquid $^4_2$He below 17K [23]. The experimental observation of BECs was achieved only in 1995 when Eric Cornell and Carl Wieman were able to produce BEC in dilute (rubidium) gases confined in magnetic traps and cooled down to temperatures of the order of a few nK. The experimental observation of BEC yielded Cornell, Wieman and Ketterle the 2001 Nobel Prize in Physics.

2.2.2 Quantum Field Theory

Although quantum statistics are quite useful at demonstrating the phenomenon of Bose-Einstein condensation, the study of such many-body systems is performed within the Quantum Field Theoretical (QFT) framework. The fundamental idea behind QFT is that particles and quasiparticles are field quanta, i.e. they manifest the quantisation of matter fields, whose degrees of freedom are described by an operator defined in space and time [24]; the interactions between particles are mediated via the corresponding field interactions.

Our goal is to study the dynamics of Bose-Einstein condensation. The formalism we will be using falls into the so-called 'mean-field' regime [20]. In this chapter, starting from simple base concepts in QFT, such as the field operators, $\hat{\Psi}$, and the creation and annihilation operators, $\hat{a}_i^\dagger$ and $\hat{a}_i$, we will introduce the one-body density matrix and build our way up to single-particle states, particularly the macroscopically occupied ground-state, Ψ_0, whose wave function provides a natural starting point for the introduction of the Bogoliubov approximation and consequent establishment of the mean-field picture.

The basis for the development of QFT are therefore the field operators $\hat{\Psi}^\dagger(\boldsymbol{r})$ and $\hat{\Psi}(\boldsymbol{r})$ which annihilate and create particles at position $\boldsymbol{r}$, respectively. Let us consider a system of N identical bosons (such that $\hat{\Psi}^\dagger(\boldsymbol{r})$ and $\hat{\Psi}(\boldsymbol{r})$ obey bosonic commutation relations,

$$[\hat{\Psi}(\boldsymbol{r}), \hat{\Psi}^\dagger(\boldsymbol{r}')] = \delta(\boldsymbol{r} - \boldsymbol{r}')\ ; \quad [\hat{\Psi}(\boldsymbol{r}), \hat{\Psi}(\boldsymbol{r}')] = 0. \tag{2.10}$$

The field operators allow us to define the one-body density matrix,

$$n^{(1)}(\boldsymbol{r},\boldsymbol{r}') = \langle\hat{\Psi}^\dagger(\boldsymbol{r})\hat{\Psi}(\boldsymbol{r}')\rangle. \tag{2.11}$$

From the diagonal terms ($\boldsymbol{r}=\boldsymbol{r}'$), we may obtain the diagonal density of the system which is then used to define the total number of particles $N = \int n(\boldsymbol{r})d\boldsymbol{r} = \int n^{(1)}(\boldsymbol{r},\boldsymbol{r})d\boldsymbol{r}$. In the momentum representation, it reads

$$n(\boldsymbol{r}) = n^{(1)}(\boldsymbol{r},\boldsymbol{r}) = \langle\hat{\Psi}^\dagger(\boldsymbol{r})\hat{\Psi}(\boldsymbol{r})\rangle, \tag{2.12}$$

$$n(\boldsymbol{p}) = \langle\hat{\Psi}^\dagger(\boldsymbol{p})\hat{\Psi}(\boldsymbol{p})\rangle. \tag{2.13}$$

Because $n^{(1)}(\boldsymbol{r},\boldsymbol{r}')$ is Hermitian, we can rewrite the one-body density matrix in terms of its eigenvalues, n_i, and an orthonormal set of single-particle wave functions, φ_i,

$$n^{(1)}(\boldsymbol{r},\boldsymbol{r}') = \sum_i n_i\varphi_i^*(\boldsymbol{r})\varphi_i(\boldsymbol{r}'). \tag{2.14}$$

Eq. (2.14) identifies n_i as the single-particle occupation numbers corresponding to each of the respective single-particle wave functions, φ_i. The introduction and identification of the latter is not only quite useful, but also of key importance in the understanding and development of the theory. These functions verify the completeness condition, $\sum_i \varphi_i^*(\boldsymbol{r})\varphi_i^*(\boldsymbol{r}') = \delta(\boldsymbol{r}-\boldsymbol{r}')$, and normalisation $N = \sum_i n_i$; together with the creation and annihilation operators of second quantisation, they can be used to construct the field operators:

$$\hat{\Psi}(\boldsymbol{r}) = \sum_i \varphi_i(\boldsymbol{r})\hat{a}_i, \tag{2.15}$$

$$\hat{\Psi}^\dagger(\boldsymbol{r}) = \sum_i \varphi_i^*(\boldsymbol{r})\hat{a}_i^*, \tag{2.16}$$

with $\hat{a}_i$ ($\hat{a}_i^*$) the annihilation (creation) operators of a single particle in the state φ_i, verifying the bosonic commutation relations $[a_i, a_j^\dagger] = \delta_{ij}$. Taking into account these considerations, it becomes straightforward to redetermine the one-body density matrix

$$n^{(1)}(\boldsymbol{r},\boldsymbol{r}') = \langle\hat{\Psi}^\dagger(\boldsymbol{r})\hat{\Psi}(\boldsymbol{r}')\rangle \tag{2.17}$$

$$= \sum_i \hat{a}_i^*\hat{a}_i\varphi_i(\boldsymbol{r})\varphi_i(\boldsymbol{r}'), \tag{2.18}$$

and thus $n_i = \langle\hat{n}_i\rangle = \langle a_i^\dagger a_i\rangle$.

If condensation takes place in our system, one of the single-particle states — the condensate (lowest energy) state, $i=0$ — is macroscopically occupied. As such, it becomes useful to separate the contributions from the ground-state and all the other remaining states, and write

$$n^{(1)}(\boldsymbol{r},\boldsymbol{r}') = N_0\varphi_0^*(\boldsymbol{r})\varphi_0(\boldsymbol{r}') + \sum_{i\neq 0} n_i\varphi_i^*(\boldsymbol{r})\varphi_i^*(\boldsymbol{r}') \tag{2.19}$$

and

$$\hat{\Psi}(\boldsymbol{r}) = \varphi_0(\boldsymbol{r})\hat{a}_0 + \sum_{i\neq 0} \varphi_i(\boldsymbol{r})\hat{a}_i, \tag{2.20}$$

where the state represented by φ_0 is the Bose-Einstein condensate, whose corresponding occupation number is $n_0 \equiv N_0$.

Bogoliubov Approximation

In a BEC we have $N_0 \gg 1$, as opposed to the microscopic occupation of all other states, $n_{i\neq 0} \sim 1 \ll N_0$. As such, the Bogoliubov approximation is

$$\begin{aligned} \hat{a}_0^\dagger &\simeq \sqrt{N_0}, \\ \hat{a}_0 &\simeq \sqrt{N_0}. \end{aligned} \tag{2.21}$$

In order to motivate this substitution we start by looking at the effect of the aforementioned operators over the eigenstates of the system. These operators, by construction, respectively *add* or *subtract* a particle onto a given eigenstate - e.g. $\hat{a}_i^*$ adds a particle to the p_i momentum eigenstate,

$$\hat{a}_i^\dagger |n_1 n_2 ... n_i ...\rangle = \sqrt{n_i + 1}\, |n_i n_2 ... (n_i + 1) ...\rangle, \tag{2.22}$$

$$\hat{a}_i |n_1 n_2 ... n_i ...\rangle = \sqrt{n_i}\, |n_i n_2 ... (n_i - 1) ...\rangle. \tag{2.23}$$

Now, we may notice that because there is a macroscopic occupation of the condensate state, $n_0 \gg 1$, adding or subtracting a single particle is negligible, as $n_0 \pm 1 \simeq n_0$. As a consequence, we may re-write Eqs. (2.22) and (2.23) as

$$\hat{a}_0^\dagger |n_0 n_1 ... n_i ...\rangle = \sqrt{n_0 + 1} |(n_0 + 1) n_2 ... n_1 ...\rangle \simeq \sqrt{n_0} |n_0 ...\rangle, \tag{2.24}$$

$$\hat{a}_0 |n_0 n_1 ... n_i ...\rangle = \sqrt{n_0} |(n_0 - 1) n_2 ... n_1 ...\rangle \simeq \sqrt{n_0} |n_0 ...\rangle. \tag{2.25}$$

As such we may obtain a new expression for the field operator (2.20), which becomes

$$\hat{\Psi}(\boldsymbol{r}) \simeq \sqrt{N_0}\, \varphi_0(\boldsymbol{r}) + \delta\hat{\Psi}(\boldsymbol{r}, t), \tag{2.26}$$

where we have performed the substitution $\sum_{i\neq 0} \varphi_i(\boldsymbol{r})\hat{a}_i \equiv \delta\hat{\Psi}(\boldsymbol{r}, t)$. We make a further step by treating the macroscopic component of the field operator as a classical field, $\Psi_0 = \sqrt{N_0}\, \varphi_0$, and thus write

$$\hat{\Psi}(\boldsymbol{r}) = \Psi_0(\boldsymbol{r}) + \delta\hat{\Psi}(\boldsymbol{r}). \tag{2.27}$$

This "classical" field $\Psi_0(\boldsymbol{r})$ is called the wave function of the condensate and plays the role of an order parameter [20]. As we will see later, Eq. (2.27) is actually the basis for the development of the mean-field theory used to describe BEC physics. This subject will be further discussed in section 2.3.1.

Even though we only briefly mentioned the momentum space representation (2.13), the latter is

actually adequate, given that condensation occurs in momentum space, with the meaning that the condensed phase consists of particles in the momentum ground state (minimum energy), $n(p = 0)$. As such, we write

$$n(\boldsymbol{p}) = N_0\delta(\boldsymbol{p}) + \sum_{\boldsymbol{p}_i \neq 0} n_{\boldsymbol{p}_i}\delta(\boldsymbol{p} - \boldsymbol{p}_i). \tag{2.28}$$

Analogously to Eq. (2.7), the first term represents the macroscopic occupation of the single-particle state with momentum $\boldsymbol{p} = 0$, and the second term is the momentum distribution for the excited/non-condensed particle states, $\tilde{n}(\boldsymbol{p}) = \sum_{\boldsymbol{p}' \neq 0} n_{\boldsymbol{p}'}\delta(\boldsymbol{p} - \boldsymbol{p}')$. Through the relation (2.28), we may define the quantity N_0/N representing the condensate fraction, with $N = \int d\boldsymbol{p}\, n(\boldsymbol{p}) = \int d\boldsymbol{r}\, n(\boldsymbol{r})$. At $T = 0$, $N_0 \to N$ and above the critical temperature T_c the condensate fraction tends to zero $N_0 \to 0$.

It is interesting to notice that by defining the eigenfunctions $\varphi_{\boldsymbol{p}_i}$ as plane-waves with energy and momentum defined as usual, and using statistical mechanics to determine the value of the mean occupation numbers,

$$\bar{n_i} = \frac{1}{z^{-1}e^{\beta E} - 1}, \tag{2.29}$$

we are able to re-obtain the expressions for the critical temperature, Eq. (2.8), and the condensate fraction, Eq. (2.9).

2.3 The Gross-Pitaevskii Equation

For a wide range of experimentally relevant conditions and diverse physical phenomena, the dynamics of a BEC can be aptly described by means of a classical nonlinear differential equation, the so-called Gross-Pitaevskii (GP) equation. In fact, this equation is a variant of the most common nonlinear Schrödinger (NLS) equation — a universal model describing the evolution of complex field envelopes in nonlinear dispersive media — and constitutes the main theoretical tool for investigating nonuniform dilute Bose gases at low temperature, including most of its important features [20].

In the case of BECs, the macroscopic features will be shown to be adequately accounted for in an effective mean-field regime, which ultimately consists on the treatment of the field operators of the microscopic many-body problem as a single, macroscopic, classical object. This approach is valid for dilute Bose gases at very low temperature ($T \ll T_c$), where thermal and quantum depletion are small and the total number of atoms is approximately the number of atoms in the BEC state ($N_0 \approx N$).

In this section, we will see how this framework significantly simplifies the problem and eliminates the necessity of treating the full many-body Schrödinger equation. We will arrive at the Gross-Pitaevskii equation starting from the non-uniform dilute gas Hamiltonian, motivate the mean-field approximation and detail the corresponding validity requirements.

2.3.1 The Mean-Field Description of BECs

Before progressing with a review of Gross-Pitaevskii theory, it is paramount we state a few crucial factors of this theory. First of all, in the dilute, weakly-interacting gas, and at temperatures lying well below the critical value, there is an interaction parameter which is key in characterising all interaction effects on the physical properties of the gas, the s-wave scattering length of the atoms, a[†] [20]. This gas parameter is used to define the diluteness condition, which determines the range of validity of the mean-field description, and states that the range of inter-atomic forces must be much smaller than the average distance between particles d,

$$|a| \ll d = n^{-\frac{1}{3}}. \tag{2.30}$$

In the context of quantum scattering theory, all information about scattering is encoded in the phase shifts between the ingoing and outgoing waves. Particularly, low energy scattering is always dominated by the s-wave ($l = 0$) whose phase shift scales as $\delta_0 \sim -ka + O(k^3)$, where k is the wavenumber of the interacting waves. As such, a comes about in the diluteness condition as an expression of the order of magnitude of inter-atomic interaction. Secondly, provided that the diluteness condition is satisfied, it is only relevant to consider binary interactions between the particles [25–28], ergo, the interaction in this formalism is fully accounted for by a two-body interaction potential, $V(\mathbf{r}' - \mathbf{r})$. Hence, one is able to produce a Hamiltonian which fully describes a dilute gas of N interacting bosons of mass m [28]:

$$\hat{H} = \int \left(\frac{\hbar^2}{2m} \boldsymbol{\nabla}\hat{\Psi}^\dagger \boldsymbol{\nabla}\hat{\Psi} + V_{ext}\hat{\Psi} \right) d\boldsymbol{r} + \frac{1}{2} \int \int \hat{\Psi}^\dagger \hat{\Psi}^{\dagger\prime} V(\boldsymbol{r}' - \boldsymbol{r}) \hat{\Psi}\hat{\Psi}' d\boldsymbol{r}' d\boldsymbol{r}, \tag{2.31}$$

where $V_{ext}(\boldsymbol{r})$ accounts for the presence of an external potential, $V(\boldsymbol{r} - \boldsymbol{r}')$ is the two-body interaction potential and the $\hat{\Psi} \equiv \hat{\Psi}(\boldsymbol{r}, t)$, $\hat{\Psi}^\dagger \equiv \hat{\Psi}^\dagger(\boldsymbol{r}, t)$ are the boson annihilation and creation field operators which satisfy the commutation relations in (2.10). We are thus able to obtain an equation describing the behaviour of the BEC wave function at the mean-field level in two steps:

1. Apply the Heisenberg equation $i\hbar\frac{\partial\hat{\Psi}}{\partial t} = [\hat{\Psi}, \hat{H}]$ to the Hamiltonian (2.31). Following the procedure sketched in app. A.1, we get:

$$i\hbar \frac{\partial \hat{\Psi}(\boldsymbol{r}, t)}{\partial t} = \left[\frac{-\hbar^2}{2m} \nabla^2 + V_{ext}(\boldsymbol{r}) + \int d\mathbf{r}' \hat{\Psi}^\dagger(\mathbf{r}', t) \mathsf{V}(\mathbf{r}' - \boldsymbol{r}) \hat{\Psi}(\mathbf{r}', t) \right] \hat{\Psi}(\boldsymbol{r}, t). \tag{2.32}$$

2. Simplify the inter-atomic interaction potential $V(\boldsymbol{r}' - \boldsymbol{r})$. For a dilute ultracold gas with binary collisions, the interacting potential can be approximated by an effective interaction point-like pseudopotential [28, 29],

$$V(\boldsymbol{r}' - \boldsymbol{r}) = g\delta(\boldsymbol{r}' - \boldsymbol{r}), \tag{2.33}$$

[†]Common values: for a gas of Rubidium ^{87}Rb atoms, $a = 2.4116 \times 10^6 m$; for a gas of Sodium ^{23}Na atoms, $= 4.6896 \times 10^{-6} m$.

where $g = 4\pi\hbar^2 a/m$ is the coupling constant [29]. A positive value of the scattering length $a > 0$ reflects a repulsive interaction, whereas a negative value, $a < 0$, reflects an attractive interaction [27, 28]. Replacing this effective interaction potential, Eq. (2.32) becomes:

$$i\hbar\frac{\partial\hat{\Psi}(\boldsymbol{r},t)}{\partial t} = \left[-\frac{\hbar^2}{2m}\boldsymbol{\nabla}^2 + V_{ext}(\boldsymbol{r},t) + g\hat{\Psi}^\dagger(\boldsymbol{r},t)\hat{\Psi}(\boldsymbol{r},t)\right]\hat{\Psi}(\boldsymbol{r},t) \tag{2.34}$$

The previously established mean-field approximation in (2.27) becomes once again useful by allowing the decomposition of the field operator into a sum of two terms (2.35) — a classical field, $\Psi_0(\boldsymbol{r},t) \equiv \langle\hat{\Psi}(\boldsymbol{r},t)\rangle$, which assumes the value of the expectation value of the field operator and is commonly known as the macroscopic wave function of the condensate — and the quantum fluctuation field, $\hat{\Psi}'(\boldsymbol{r},t)$, which verifies $\langle\hat{\Psi}'(\boldsymbol{r},t)\rangle = 0$. Here, $\hat{\Psi}'$ describes condensate depletion,

$$\hat{\Psi}(\boldsymbol{r},t) = \Psi_0(\boldsymbol{r},t) + \hat{\Psi}'(\boldsymbol{r},t), \quad \text{with } |\hat{\Psi}'(r,t)| \ll |\Psi_0|. \tag{2.35}$$

In an ideal, non-interacting Bose gas, all particles occupy the ground state at $T = 0$ and the classical field $\Psi_0(\boldsymbol{r},t)$ correctly describes the properties of all N particles in the system; However, for an interacting gas, even at zero temperature some particles lie outside the lowest energy state; this phenomenon is called *quantum depletion*. What this means is that besides considering very small temperatures $T \ll T_c \approx 0K$ one must also consider a weakly interacting dilute gas wherein the non-condensate fraction is very small and can consequently be neglected. This of course allows one to neglect the atoms out of the condensate [30]. Thus the mean field theory can be applied by taking $\hat{\Psi}(\boldsymbol{r},t) \approx \Psi_0(\boldsymbol{r},t)$. We have thus arrived at the Gross-Pitaevskii (GP) equation,

$$i\hbar\frac{\partial\Psi_0(\boldsymbol{r},t)}{\partial t} = \left[-\frac{\hbar^2}{2m}\boldsymbol{\nabla}^2 + V_{ext}(\boldsymbol{r},t) + g|\Psi_0(\boldsymbol{r},t)|^2\right]\Psi_0(\boldsymbol{r},t), \tag{2.36}$$

where one can identify the condensate density with $n(\boldsymbol{r},t) \equiv |\Psi(\boldsymbol{r},t)|^2$. The GP equation was first introduced in 1961 and it is the main theoretical tool for investigating dilute Bose gases at low temperatures [20, 23]. We assume the following normalisation:

$$N = \int |\Psi(\boldsymbol{r},t)|^2 d\boldsymbol{r}. \tag{2.37}$$

The GPE (2.36) appears to be very similar to the Schrödinger equation for a single particle. The difference lies in the presence of the self-interacting potential $g|\Psi|^2$, generated by the mean-field of the condensate. It should be remarked that Eq. (2.36) is valid only on length scales which are much larger than the scattering length, $L \gg a$. The assumption leading to this equation, especially replacing $V(\boldsymbol{r}'-\boldsymbol{r})$ with a point-like potential, are no longer justified on a microscopic scale, $L \lesssim a$ [29].

2.3.2 Conservation Laws

Some relevant conservation laws are associated with the GPE, such as the conservation of energy, $dE/dt = 0$ [20] [29]. This quantity, the energy functional of the system (2.38), is obtained directly from

the Hamiltonian (2.31). Its derivation can be found in the appendix (A.2).

$$E = \int \left(\frac{\hbar^2}{2m} |\boldsymbol{\nabla}\Psi|^2 + V_{ext}(\boldsymbol{r}, t)|\Psi|^2 + \frac{g}{2}|\Psi|^4 \right) d\boldsymbol{r} \tag{2.38}$$

Secondly, Eq. (2.36) also conserves the number of particles in the system,

$$\frac{dN}{dt} = 0. \tag{2.39}$$

The latter conservation law follows from the continuity equation (2.41), obtained from the GP equation (2.36) by applying the Madelung ansatz [31]:

$$\Psi(\boldsymbol{r}, t) = \sqrt{n(\boldsymbol{r}, t)}\, e^{iS(\boldsymbol{r},t)}, \tag{2.40}$$

where $S(\boldsymbol{r}, t)$ is the condensate phase. By multiplying Eq. (2.36) by Ψ and subtracting its complex conjugate, one is able to obtain the continuity equation

$$\frac{\partial n}{\partial t} + \boldsymbol{\nabla} \cdot \boldsymbol{j} = 0, \tag{2.41}$$

where $\boldsymbol{j}$ represents the current density,

$$\boldsymbol{j}(\boldsymbol{r}, t) = -i\frac{\hbar}{2m}(\Psi^\dagger \boldsymbol{\nabla}\Psi - \Psi \boldsymbol{\nabla}\Psi^\dagger) = \tag{2.42a}$$

$$= n(\boldsymbol{r}, t)\frac{\hbar}{m}\boldsymbol{\nabla} S(\boldsymbol{r}, t) \tag{2.42b}$$

The conservation of the number of particles then follows by integrating the continuity equation; the derivation can be found explicitly (see appendix A.3). The fact that the GPE satisfies the continuity equation, along with the introduction of the current density, reveals that the GPE is an equation which describes the motion of a fluid (the condensate) with density n and current density $\boldsymbol{j} = n\boldsymbol{v}$, whose velocity field is given by

$$\mathbf{v}(\boldsymbol{r}, t) = \frac{\hbar}{m}\boldsymbol{\nabla} S(\boldsymbol{r}, t). \tag{2.43}$$

2.3.3 Stationary Solutions

The GP equation (2.36) admits stationary solutions, i.e., states whose probability density is independent of time (2.44). Proceeding analogously to the Schrödinger equation case, for which stationary solutions are $\Psi(\boldsymbol{r}, t) = \Psi(\boldsymbol{r})e^{-iEt/h}$, with $\Psi(\boldsymbol{r}) \equiv \Psi(\boldsymbol{r}, t = 0)$ an eigenstate with eigenvalue E — the following stationary solution ansatz may be put forward,

$$\Psi_0(\boldsymbol{r}, t) = \Psi_0(\boldsymbol{r})e^{-i\frac{\mu t}{\hbar}}. \tag{2.44}$$

The fact that Ψ_0 is actually an average value over stationary states, in a system with N particles, leads to the conclusion that the eigenvalues of $\Psi_0(\boldsymbol{r})$ are approximately $\mu = E(N) - E(N-1) \approx \partial E/\partial N$,

which is identified as the chemical potential of the system [20].

Replacing equation (2.44) in the GPE (2.36) yields the time-independent equation for $\Psi_0(\boldsymbol{r})$:

$$\left(-\frac{\hbar^2}{2m}\nabla^2 + V_{ext}(\boldsymbol{r}) - \mu + g|\Psi_0(\boldsymbol{r})|^2\right)\Psi_0(\boldsymbol{r}) = 0. \tag{2.45}$$

Equation (2.45) describes stationary solutions of a dilute Bose gas interacting via repulsive forces [20] and as such may be used to gather profound insight into its characteristics. By rearranging the terms in Eq.(2.45), it is possible to obtain an equation for the chemical potential,

$$\mu\Psi_0(\boldsymbol{r}) = \left(-\frac{\hbar}{2m}\boldsymbol{\nabla}^2 + V_{ext}(\boldsymbol{r}) + g|\Psi_0(\boldsymbol{r})|^2\right)\Psi_0(\boldsymbol{r}), \tag{2.46}$$

which may be solved to yield,

$$\mu = E + \int \frac{1}{2}|\Psi_0|^4 d\boldsymbol{r}. \tag{2.47}$$

Now, returning to equation (2.45), we may note that the solutions to this equation actually constitute stationary points for the grand canonical energy functional,

$$E' = E - \mu\int |\Psi_0(\boldsymbol{r})|^2 d\boldsymbol{r} = E - \mu N. \tag{2.48}$$

This fact not only allows us to regain insight on the statistical nature of BECs, but also reiterates the physical purpose of this equation — Eq. (2.48) locates stationary points of the system energy under the constraint that the number of particles is fixed to some $N = \int |\Psi_0(\boldsymbol{r})|^2 d\boldsymbol{r}$, which is the normalization condition (2.37), with the chemical potential μ acting as a Lagrange multiplier.

Thomas-Fermi Approximation

For sufficiently large systems $N \gg 1$, an accurate expression for the ground-state energy may be obtained by neglecting the kinetic energy term in the Gross-Pitaevskii equation [20, 32]; in such a case the spatial variations of density are slow and small in the bulk of the BEC, and the action of the kinetic term is negligible in comparison with the interaction and potential terms. This approximation is thus valid as long as the typical distances characterising density variations are much larger than the healing length, $L \gg \xi$, which implies not only the absence of a confining external potential but also the inexistence of local excitations — the system must be in the ground state. Neglecting the dispersive term in (2.46) yields:

$$\left(V_{ext}(\boldsymbol{r}) + |\Psi_0(\boldsymbol{r})|^2\right)\Psi_0(\boldsymbol{r}) = \mu\Psi_0(\boldsymbol{r}), \tag{2.49}$$

which has the solution:

$$n_{TF}(\boldsymbol{r}) \equiv n(\boldsymbol{r}) = \begin{cases} \frac{\mu - V_{ext}(\boldsymbol{r})}{g} & ;\ \mu > V_{ext}(\boldsymbol{r}) \\ 0 & ;\ \text{otherwise.} \end{cases} \tag{2.50}$$

Equation (2.50) defines a region with a boundary at $V_{ext}(\boldsymbol{r}) = \mu$ and is a very good approximation to the ground state of the condensate wave function, provided the previously mentioned conditions are verified.

In a uniform Bose gas, the external potential is absent, and thus the Thomas-Fermi approximation reduces to

$$\mu = gn_0, \tag{2.51}$$

where n_0 is the equilibrium uniform density of the gas. In the presence of an external potential, V_{ext}, a value for the chemical potential within this approximation may be found by setting the adequate boundary conditions. Assuming for instance harmonic trapping in one-dimension, $V_{ext} = m\omega^2 x^2/2$, we set $n(x) = 0$ at the border — $\Psi_{TF}(\pm L) = n_{TF}(\pm L) = 0$ — which necessarily sets the value for the chemical potential at $\mu_{TF} = m\omega^2 L^2/2$. In this case the Thomas-Fermi radius is given by $L_{TF} = \sqrt{2\mu/(m\omega^2)}$.

2.3.4 Weak Excitations

Having gone over a few stationary properties, next we look at what happens when small-amplitude oscillations are present in a condensate. These constitute time-dependent solutions to the GPE and represent small spatio-temporal changes to the stationary solutions.

Bogoliubov was the first to study the effects of small (linear) excitations in a BEC [23, 33, 34], by adding a small perturbative term $\delta\varphi(x,t)$ to the stationary state ansatz (2.44):

$$\Psi_0(x,t) = (\varphi_0(x) + \delta\varphi(x,t))e^{-i\frac{\mu t}{\hbar}}. \tag{2.52}$$

This non-uniform solution was then inserted into the GPE (2.36) to yield [23, 34]:

$$\begin{cases} i\partial_t\delta\varphi = \left(-\frac{\hbar^2\nabla^2}{2m} + (2g|\varphi|^2 + V - \mu)\right)\delta\varphi + g\varphi^2\delta\varphi^* \\ i\hbar\partial_t\delta\varphi^* = \left(\frac{\hbar^2\nabla^2}{2m} - (2g|\varphi|^2 + V - \mu)\right)\delta\varphi^* - g\varphi^2\delta\varphi \end{cases} \tag{2.53}$$

These equations may be solved to find the excitation energy $\epsilon(p)$ (or equivalently $\omega(k)$). The dispersion law for the elementary excitations goes by the name of Bogoliubov spectrum [23, 34]:

$$\omega^2 = c^2k^2 + \frac{\hbar^2k^2}{4m^2}, \tag{2.54}$$

where we defined the Bogoliubov sound velocity [20, 33, 35–37],

$$c = \sqrt{\frac{gn_0}{m}}. \tag{2.55}$$

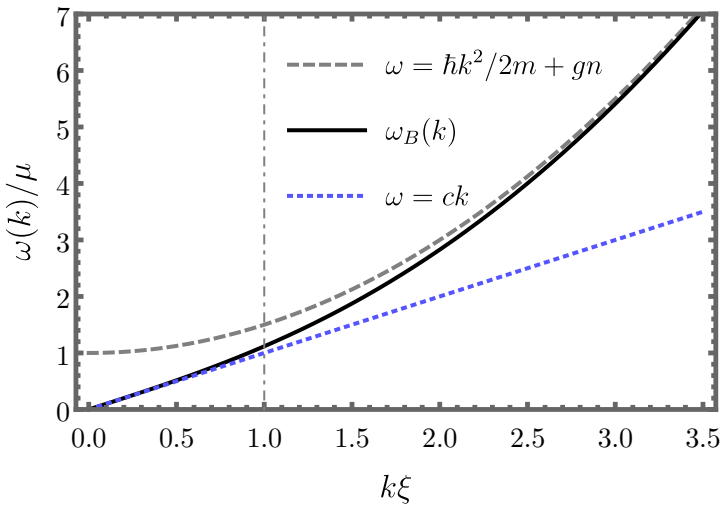

Figure 2.1: Dispersion relation of the Bogoliubov spectrum of elementary excitations (solid line). The dashed curve is the short-wavelength limit $k\xi \gg 1$ which delimits the free-particle regime; the dotted curve is the long wavelength limit $k\xi \to 0$ where phonon-like behaviour dominates.

This theoretical prediction has since been extensively corroborated through the observation of sound waves propagating in condensates [33]. The sound velocity (2.55) may be as well determined from the ground state energy of the BEC, by considering the equation of state for the pressure, $P = -\partial E/\partial V$, and the hydrodynamic relation $\partial n/\partial P = 1/(mc^2)$ [20]. Another alternative (hydrodynamic approach) is to recast the GPE into two equations — continuity (2.41) and Euler equations — and then introduce these excitations in the form of fluctuations in pressure and density [38, 39]. Depicted in Fig. 2.1 is the Bogoliubov spectrum of elementary excitations along with the corresponding approximated results in the short and long wavelength limits. The most useful of these in this work will be the long-wavelength (low-momenta) limit expression which represents the phonon or acoustic mode dispersion in an interacting Bose gas,

$$k \lesssim \xi \;\Rightarrow \omega \approx ck. \tag{2.56}$$

This is a consequence of the short-range nature of the interaction potential (a short-range potential is responsible for the acoustic mode, whereas a long-range potential generates the gapped mode).

2.3.5 Solitons

We now return to the stationary case in order to study a set of special solutions admitted by the GPE which go by the name of solitons [20, 34, 40–45].

Physically, solitons manifest as localised, solitary travelling waves which retain their size, shape and speed while propagating. Mathematically, they arise in non-linear differential equations due to the interplay between the dispersive ($\approx \frac{\hbar^2}{2m}\nabla^2$) spreading out/defocusing and non-linear ($\approx g|\Psi|^2$) steepening/focusing terms acting on localised perturbations, resulting in a balance which promotes the persis-

tence of localised structures and the preservation of their spatial profile. Whenever there is a disturbance in the balance of those terms, the soliton solution acquires more energy or develops new harmonics, and this results in the generation of small-amplitude density (sound) waves [46].

There can be distinguished two main types of soliton-like solutions, which emerge according to the nature of the inter particle interactions in the BEC [41]. When these are attractive ($g < 0$), the non-linear term in the GPE becomes negative, and the resulting soliton solutions are bright, i.e., characterized by a localized peak in the density. In the case the inter particle interactions are repulsive ($g > 0$), the non-linear term is positive, and the resulting solutions correspond to a localised dip or "suppression" in the density profile — dark solitons, fig. 2.2.

Now, while we are interested solely in dark solitons, there may still be distinguished two limiting cases of this particular solution: *black* solitons, whose density and velocity are zero — their depth is equal to the bulk density value — and across which there is a BEC phase shift $\varphi = \pi$; and *grey* solitons, in which the density does not completely drop to zero, propagating with a finite velocity, [40, 41]. In other words, the healing length will be given by the distance over which the kinetic energy and the interaction energy balance one another [32]. Mathematicaly, we find

$$\text{DISPERSIVE TERM:} \quad \frac{\hbar^2}{2m}\nabla^2 \sim \frac{h^2}{2m}\frac{1}{\xi^2}; \quad \text{NONLINEAR TERM:} \quad g|\Psi_0|^2 = \frac{4\pi\hbar^2 a}{m}n_0 \tag{2.57}$$

$$\Rightarrow \ \frac{h^2}{2m}\frac{1}{\xi^2} = \frac{4\pi\hbar^2 a}{m}n \ \Leftrightarrow \tag{2.58}$$

$$\Leftrightarrow \ \xi = \frac{1}{\sqrt{8\pi a n}} \simeq \frac{\hbar}{\sqrt{2mgn_0}} \tag{2.59}$$

In this work, we will redefine the healing length in order to avoid the $\sqrt{2}$ factor,

$$\boxed{\xi = \frac{\hbar}{\sqrt{mgn_0}}}. \tag{2.60}$$

A good intuition in regards to this quantity is to view it (much in the same way as Debye shielding in plasmas) as the distance over which the BEC wavefunction *heals* over defects; thus, the spatial widths of nonlinear excitations, such as grey and black solitons in 1D, and vortices in 2D, are of order $\sim \xi$ [20, 23, 28].

The Dark Soliton Solution

Solitons constitute exact one-dimensional solutions to the GP equation. These solutions propagate without change of form and are described by (see appendix A.4) [20, 32, 37, 44, 45]:

$$\Psi_{\rm s}(x) = \sqrt{n_0}\left(i\frac{v_s}{c} + \sqrt{1-\frac{v_s^2}{c^2}}\,\tanh\left(\frac{x-x_s}{\xi}\sqrt{1-\frac{v_s^2}{c^2}}\right)\right), \tag{2.61}$$

where v_s denotes the soliton velocity and c the BEC sound speed. For $v_s = 0$, we get the black soliton solution

$$\Psi_{\rm BS} = \sqrt{n_0}\tanh\left(\frac{x-x_s}{\xi}\right). \tag{2.62}$$

On the other hand, as the soliton velocity approaches c, $\Psi_{\rm s} \to 1$, i.e., the BEC density is unmarred and the soliton becomes indistinguishable from the motionless condensate. Thus the soliton with maximum speed is equivalent to the BEC ground state: faster solitons are less energetic than slower solitons. This sounds counter-intuitive, but becomes clearer upon realising that solitons have negative mass, and thus a negative kinetic energy. This interesting albeit counter-intuitive conclusion will be further explored in section 4.4.3.

It is important to remark that the presence of the hyperbolic tangent in this solution - more specifically, due to its asymmetry - is responsible for a jump or change in the phase of the wavefunction, $\Delta\varphi$, localised at the fsoliton centroid (i.e. at the soliton position $x_s = x$). In the dark soliton case this jump will be a discontinuous jump $\Delta\varphi = \pi$ and in other (grey soliton) cases the total phase change across the soliton will be given by, (see appendix (A.34)) [32]:

$$\Delta\varphi_s = \varphi[\Psi_{\rm s}(+\infty)] - \varphi[\Psi_{\rm s}(-\infty)] = \tag{2.63}$$

$$= -2\arccos\Big(\frac{v_s}{c}\Big). \tag{2.64}$$

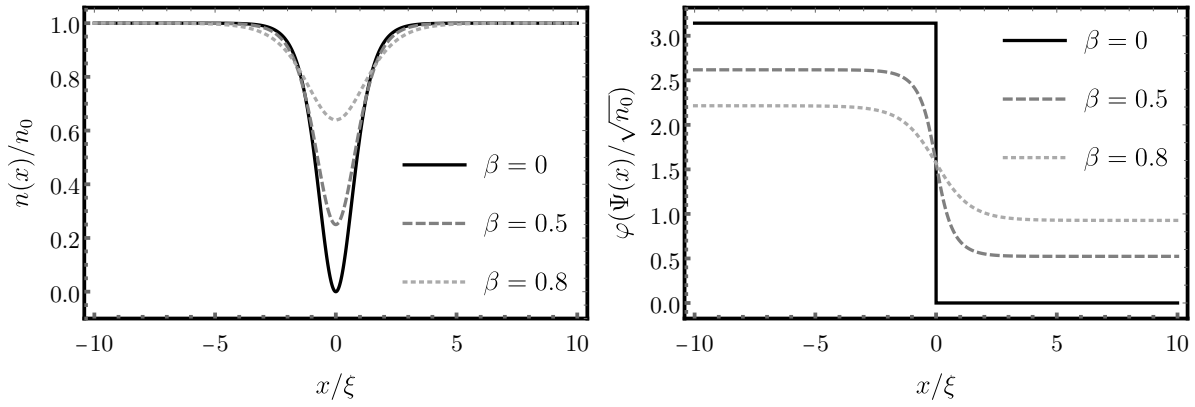

Figure 2.2: Representation of the density and phase of black and grey solitons. Continuous line corresponds to a dark ($\beta \equiv v/c = 0$) soliton, and the dashed and dotted lines correspond to two different-velocity-grey solitons.

Soliton Energy

Having established that topological excitations arise as a consequence of external perturbations or deformations to the system at hand, we may now write the total energy of a BEC as a sum of terms, containing the un-deformed ground-state BEC energy, E_g, and the energy of the deformation inserted into the system, E_d. As the system evolves and the introduced energy is siphoned into either phonons or solitons, which constitute the possible topological excitations in 1D, it becomes possible to divide the deformation energy into the sum of the total phonon and soliton energies,

$$E_d + E_g = E_s + E_{\rm ph} + E_g. \tag{2.65}$$

We observe that it is possible to determine the system excitation energy, $\epsilon \equiv E_d$, by calculating the difference between the grand canonical energy in the presence, E', and in the absence, E'_g, of the topological excitation(s) [20, 47].

$$\epsilon = E' - E'_g. \tag{2.66}$$

Extracting E' from Eq. (2.48), the total energy E from Eq. (2.38) and the ground state energy from E'_g, Eq. (2.68), we obtain [32]

$$E = \int \left(\frac{\hbar^2}{2m} |\nabla \Psi|^2 + \frac{g}{2} |\Psi|^4 \right) dx - \mu \int |\Psi_0(x)|^2 dx, \tag{2.67}$$

$$E'_g = \int \left(\frac{g}{2} |\Psi_g|^4 - \mu |\Psi_0|^2 \right) dx, \tag{2.68}$$

$$\epsilon = \int \left(\frac{\hbar^2}{2m} |\nabla \Psi|^2 + \frac{g}{2} |\Psi|^4 \right) dx - \mu \int |\Psi|^2 dx - \int \left(\frac{g}{2} |\Psi_0|^4 - \mu |\Psi_0|^2 \right) dx. \tag{2.69}$$

We need only make two other observations; firstly, the density of particles $n(x) = |\Psi(x)|^2$ assumes a finite constant value in the ground state $n_0 = |\Psi_0(x)|^2$, the background density in an unperturbed BEC, and may be accordingly replaced into Eq. (2.68); secondly, in a sufficiently large system and in the absence of an external potential, equation (2.51) is applicable, and as such we consider $\mu = g n_0$. It should be noted that despite the $\mu = g n_0$ result having been presented in the ground state context, the corrections to the chemical potential due to the presence of perturbations such as solitons are negligible[20, 47]. Substituting Eqs.(2.67) and (2.68) and applying the above considerations, equation (2.66) reads [20, 43]:

$$\begin{aligned} \epsilon &= \int \left(\frac{\hbar^2}{2m} |\nabla \Psi|^2 + \frac{g}{2} \left(|\Psi|^4 - 2n_0 |\Psi|^2 - n_0^2 + 2n_0^2 \right) \right) dx \\ \Leftrightarrow \epsilon &= \int \left(\frac{\hbar^2}{2m} |\nabla \Psi|^2 + \frac{g}{2} (|\Psi|^2 - n_0)^2 \right) dx. \end{aligned} \tag{2.70}$$

By replacing the soliton solution (2.61) into equation (2.70), one obtains the soliton energy, (see appendix A.5) [20, 32, 44, 48]:

$$\epsilon_s = \frac{4}{3} n_0 \hbar c \left(1 - \frac{v_s^2}{c^2} \right)^{\frac{3}{2}}. \tag{2.71}$$

An interesting conclusion obtained from this expression is relative to the soliton mass. In the limit $v_s \ll c$ we have,

$$\begin{cases} \epsilon_s \approx \frac{4}{3} n_0 \hbar c - 2 n_o \hbar c \frac{v_s^2}{c} \\ \epsilon_s = \epsilon_{rest} + \frac{1}{2} m_s v_s^2 \end{cases} \quad \Leftrightarrow \quad m_s = -\frac{4\hbar n_0}{c}, \tag{2.72}$$

which means the soliton mass is negative, in agreement with the fact that it actually represents a "hole", or absence of matter in a region and not a true "particle" [20, 49]. In the non-homogeneous case, when there is an external potential $V_{ext}(x)$ acting on the system, one must write $n_0(x) = (\mu - V(x))/g$, valid in the TF approximation. For a slowly varying external potential, the new expression for the soliton energy can be found by replacing the new TF density in (2.71) [32]. Rearranging the terms and using the sound velocity expression (2.55), we obtain,

$$\epsilon_s(x) = \frac{4}{3} \frac{\hbar}{g\sqrt{m}} \left(\mu - V(x) - v_s^2 m\right)^{\frac{3}{2}}. \tag{2.73}$$

2.3.6 Study of Soliton Collective Behaviour Within Kinetic Theory Formalism

As was previously motivated in chapter 1, the study of many-body systems such as ultracold gases and Bose-Einstein condensates, more specifically studying the behaviour of the macroscopic structures arising in BECs as a consequence of disturbances or turbulence — structures as described in previous sections and with a special focus on dark and grey solitons — may be the key to a better understanding of the characteristics of quantum turbulence in low-dimensional scenarios. It is with this in mind that we will resort to the kinetic theory formalism to model the coupled dynamics of interacting dark-solitons in turbulent scenarios. By employing a kinetic equation of the Vlasov type, we will be able to cast both the interactions and the statistics of dark solitons [50]. To do that, we review some general principles of kinetic theory in order to build up to the equations governing the collective behaviour of particles (or holes).

The most important ingredient is the probability distribution function, $f(\boldsymbol{r}_i, \boldsymbol{p}_i; t)$. This distribution describes the probability of the system being found in the vicinity of the point ($\boldsymbol{r}_i$,$\boldsymbol{p}_i$), i.e. it yields the probability to find the system in a certain $6N$ phase space state, and as such subject to the usual normalisation condition,

$$\int dV f(\boldsymbol{r}_i, \boldsymbol{p}_i; t) = 1 \; ; \quad dV = \prod_{i=1}^{N} d^3 r_i d^3 p_i. \tag{2.74}$$

Because the probability is locally conserved, it must obey the continuity equation [51]. In phase space, with a velocity vector given by $\boldsymbol{v} = (\dot{\boldsymbol{r}}_i, \dot{\boldsymbol{p}}_i)$ and the gradient given by $\boldsymbol{\nabla} = \left(\frac{\partial}{\partial \boldsymbol{r}_i}, \frac{\partial}{\partial \boldsymbol{p}_i}\right)$, this equation takes the form:

$$\frac{\partial f}{\partial t} + \frac{\partial (f \dot{\boldsymbol{r}}_i)}{\partial \boldsymbol{r}_i} + \frac{\partial (f \dot{\boldsymbol{p}}_i)}{\partial \boldsymbol{p}_i} = 0, \tag{2.75}$$

where Einstein's notation is applied (sum over repeated indexes). Using Hamilton's equations and some simple manipulation we are able to arrive at Liouville's teorem,

$$\frac{df}{dt} = \frac{\partial f}{\partial t} + \frac{\partial f}{\partial \boldsymbol{r}_i}\frac{\partial H}{\partial \boldsymbol{p}_i} - \frac{\partial f}{\partial \boldsymbol{p}_i}\frac{\partial H}{\partial \boldsymbol{r}_i} = 0. \tag{2.76}$$

Liouville's theorem states the conservation of the probability function in phase space as the incompressibility of $f(\boldsymbol{r}_i, \boldsymbol{p}_i; t)$.

Liouville's equation is then the starting point for the derivation of other fundamental equations of kinetic theory such as the Boltzmann and Vlasov equations. However, the N-particle distribution function we started with is impractical, as it leads to an equation which governs a complicated function of $N \sim O(10^{23})$ variables. We are able to obtain a much more tractable theory by introducing a one-particle distribution function, $f_1(\boldsymbol{r}, \boldsymbol{p}; t)$, normalised as $\int d\boldsymbol{r}d\boldsymbol{p} f_1(\boldsymbol{r}, \boldsymbol{p}; t) = N$, which yields the number of expected particles at $(\boldsymbol{r}, \boldsymbol{p})$, and thus reduces our description from $6N$ to an only 6-dimensional phase-space. This change is what allows the derivation of the Boltzmann equation which describes particle interactions through f_1 via a collision term integral. The latter term stores the particle interaction contributions which can be written in a chain-like sequence from the two-particle distribution up to the N-particle — the Bogoliubov-Born-Green-Kirkwood-Yvon (BBGKY) hierarchy [51]. The Boltzmann equation then reads,

$$\frac{\partial f_1}{\partial t} + \boldsymbol{v} \cdot \frac{\partial f_1}{\partial \boldsymbol{r}} + \boldsymbol{F} \cdot \frac{\partial f_1}{\partial \boldsymbol{p}} = \left(\frac{\partial f_1}{\partial t}\right)_{\text{coll}}, \tag{2.77}$$

where $\boldsymbol{F}$ accounts for external forces. The extraordinary value of this hierarchy resides in the fact that it can be truncated from a defined point on (dismissing higher order contributions), which results in different families of kinetic equations. In the case of dilute gases, the collisional term has little effect on the dynamics of the system, as the particles simply follow their Hamiltonian evolution for most of the time, colliding only very occasionally. For this reason, the collision integral is commonly neglected and the resultant equation governing the system's dynamics is the Vlasov equation,

$$\frac{df_1}{dt} = \frac{\partial f_1}{\partial t} + \boldsymbol{v}\frac{\partial f_1}{\partial \boldsymbol{r}} + \frac{\partial \boldsymbol{p}}{\partial t}\frac{\partial f_1}{\partial \boldsymbol{p}} = 0. \tag{2.78}$$

Importantly, $d\boldsymbol{p}/dt = \boldsymbol{F}$ accounts also for averaged, mean field forces[‡].

2.4 Lieb-Liniger Theory for a 1D Bose Gas Interacting Via a Repulsive δ Interaction

We have previously discussed the Bogoliubov theory, which models weakly-interacting bosons and reproduces the excitation spectrum arising in a BEC. But this theory does not treat or yield any solution resembling the nature of dark solitons. A relevant model is based on the Lieb-Liniger (LL) theory, first developed in [52] and [53], which describes a one-dimensional system of point-like bosons with repulsive contact interactions in the thermodynamic limit. This model is solvable exactly by the Bethe-Ansatz method, and its solutions have helped to better understand a few aspects of many-body problems in one-

[‡]Such as the mean field force exerted by all the other particles on the one particle.

dimension. Of these we point out the presence of two excitation branches in the dispersion spectrum, one of them — type-I — akin to the Bogoliubov particles in the weakly-interacting limit and another — type-II — which has been connected with dark-solitons in the GP equation. The latter have fermionic statistics [54–58]. The LL Hamiltonian reads [54, 55, 59, 60]:

$$H_{LL} = -\frac{\hbar^2}{2m}\sum_{i=1}^{N}\frac{\partial^2}{\partial x_i^2} + g_{1D}\sum_{i>j=1}^{N}\delta(x_i - x_j), \tag{2.79}$$

where $g_{1D} > 0$ is the strength of the two-body contact repulsive interactions. A key aspect of this theory is the interaction parameter $\gamma = mg_{1D}/(\hbar^2 n)$ which is inversely proportional to the density.

The Lieb-Liniger model is solvable through the Bethe-ansatz, which produces a set of 3 equations [55, 61]:

$$p(k;\gamma) = 2\pi\hbar Q(\gamma)\int_1^{k/Q(\gamma)}\rho(x)dx, \tag{2.80}$$

$$\epsilon(k;\gamma) = \frac{\hbar^2 Q^2(\gamma)}{m}\int_1^{k/Q(\gamma)} f(x)dx, \quad \text{and} \tag{2.81}$$

$$f(x;\lambda) = \frac{1}{\pi}\int_{-1}^{1}\frac{\lambda}{\lambda^2 + (x-y)^2}f(y) + x, \tag{2.82}$$

where $Q(\gamma) = n_0/\int_1^1 \rho(x)dx$ is the Fermi rapidity. This set of equations is quite cumbersome to tackle and can only be solved numerically. However, through an approximation in the low-momentum region (which is the relevant region in our study) we present the features of the Lieb-Liniger excitation spectrum in fig. 2.3.

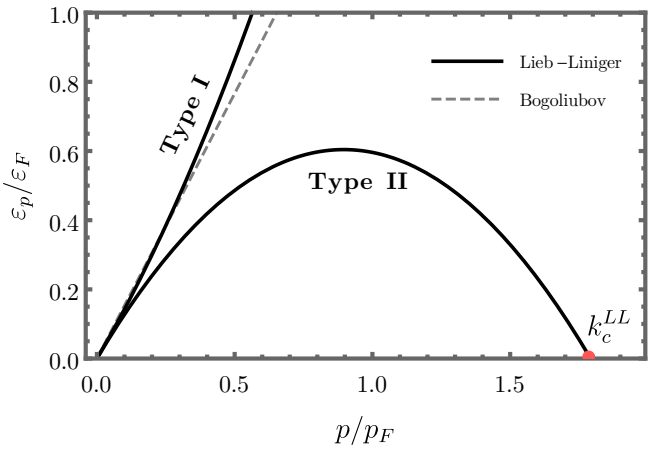

Figure 2.3: Excitation spectrum of the Lieb-Liniger gas in units of $\epsilon_F = \hbar^2\pi^2N^2/(2mL^2)$ and $p_F = \hbar\pi N/L$ for a representative case with $\gamma = 10$, $n = 0.3$. Full line represents the LL spectrum of excitations and the dotted line the Bogoliubov spectrum (2.54) is included for comparison. Image also includes the crtical point k_c^{LL} at which the LL lower-energy curve intersects the $\epsilon_p = 0$ axis.

Type I (or "particle") phonon-like excitations are described in the thermodynamic limit by an integral equation, yielding a curve contained between the asymptotic limits $\epsilon_I(k) = \hbar k^2/2m$ at $\gamma = 0$ and $\epsilon_I(k) = \hbar k^2/2m + 2\pi\hbar n|k|$ at $\gamma \to \infty$. Type II excitations or "hole" states are absent in Bogoliubov theory [58–60];

they have, however, a linear spectrum in the small momentum region with the same phase velocity as that of the phonons. Lieb explained the existence of these two types of excitations by calling attention to the fact that the present Bose system with an infinitely large interaction strength (simplest case to analyse) has an energy spectrum analogous to that of the 1D spinless Fermion system [56].

Tonks-Girardeau Limit

The Tonks-Girardeau (TG) gas is a limit case of the LL model, in the situation $\gamma \to \infty$, i.e. for a strongly-interacting gas. In these circumstances, the gas behaves as a gas of hard-core bosons [55], i.e. there is infinite repulsion between the particles, so much so that they are impenetrable and hence behave like non-interacting fermions [52, 58, 62]. This effect often receives the name of fermionisation [55, 63]. Accordingly, the TG gas energy spectrum resembles that of a one-dimensional gas of non-interacting fermions (even though their wavefunctions are still quite different) [32, 53]. The two branches of the dispersion relation for the Lieb-Liniger model in the Tonks-Girardeau limit are[§] [55]:

$$\omega_{\mathrm{TG}}^{I} = \frac{\hbar}{2m}\left[2k_F k\left(1-\frac{1}{N}\right)+k^2\right], \tag{2.83}$$

$$\omega_{\mathrm{TG}}^{II} = \frac{\hbar}{2m}\left[2k_F k\left(1+\frac{1}{N}\right)-k^2\right], \tag{2.84}$$

where N is the total number of particles.

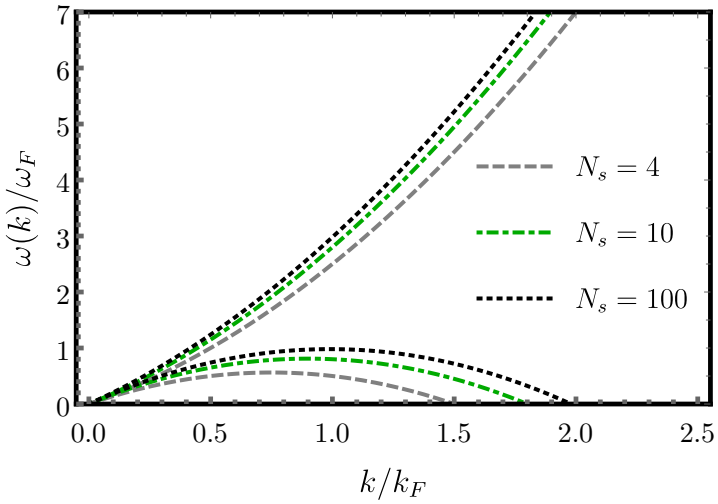

Figure 2.4: Excitation spectrum of the TG gas in units of $\omega_F = \hbar\pi^2 N^2/2mL^2$ and Fermi momentum $k_F = \pi N/L$.

[§]The method carried out to obtain these expressions is detailed in [55]. It requires solving the LL integral equations through the Bethe-ansatz method, but with matters greatly simplified in the TG regime, for a set of transcendental equations for k become linear in the latter.

Chapter 3

Kinetic Model for a Dark Soliton Gas

A comprehensive model of turbulence in one-dimensional superfluids needs to accurately model the dynamics of a dark soliton gas, capturing their statistical nature and interactions. Kinetic theory provides the grounds for the development of such a model: starting from the Vlasov equation, and accounting for (i) the relativistic nature of dark solitons ($-1 < \beta < 1$), (ii) the negativity of their mass ("hole-like" nature), and (iii) their interaction through a short-range potential (dependent on their velocity), it allows us to develop a fully analytical* equation governing the phase-space distribution function of a dark soliton gas.

For this reason we will start from the general form of the Vlasov Eq. (2.78) and adapt the theory in section 2.3.6 by dropping the f_1 subscript, modifying the expressions to our one-dimensional case $\boldsymbol{r} \to x$ and identifying the velocity $v \equiv dx/dt$ in this equation, we may rewrite it in the following way:

$$\frac{df}{dt} = \frac{\partial f}{\partial t} + v\frac{\partial f}{\partial x} + \frac{\partial p}{\partial t}\frac{\partial f}{\partial p} = 0. \tag{3.1}$$

An important consideration here is to understand we can go from the discrete dynamics to a continuous description in the phase space by making use of $f(x', v', t)$, allowing us to write the equation of motion $\partial p/\partial t = -\partial V/\partial x$, where V is the two-body interaction potential,

$$V(x, v, t) = \iint H(x - x', v - v')f(x', v', t)dx'dv', \tag{3.2}$$

which encodes all possible pairwise interactions by integrating the Hamiltonian weighed by $f(x', v', t)$, which accounts for every possible system state, over all positions and velocities. Eq. (3.2) constitutes a pseudo-potential dependent on both x and v which is a consequence of the relativistic nature of dark solitons: their mass depends on their velocity. Equation (3.1) now becomes,

$$\frac{\partial f}{\partial t} + v\frac{\partial f}{\partial x} - \frac{\partial V}{\partial x}\frac{\partial f}{\partial p} = 0. \tag{3.3}$$

Because we are interested in the mean-field behaviour of dark-soliton gases, we will separate our quantities into their ensemble averages plus small deviations $f \to \langle f \rangle + \delta f$ and $V \to \langle V \rangle + \delta V$. This yields:

*A feature that is virtually impossible with studies based on the Gross-Pitaevskii equation.

$$\frac{\partial\langle f\rangle}{\partial t}+v\frac{\partial\langle f\rangle}{\partial x}-\frac{\partial\langle V\rangle}{\partial x}\frac{\partial\langle f\rangle}{\partial p}=\langle\frac{\partial\delta V}{\partial x}\frac{\partial\delta f}{\partial p}\rangle, \tag{3.4}$$

whose rhs corresponds to the collision integral in (2.77), which might be truncated according to chosen applicable approximations through the BBGKY hierarchy. Given that we are considering dilute soliton gases, $N_0\xi \ll 1$, where $N_0 = 1/\langle d\rangle$ is the gas density determined by the averaged soliton separation $\langle d\rangle$, we may fully neglect the collision integral and obtain

$$\frac{\partial f}{\partial t}+v\frac{\partial f}{\partial x}-\frac{\partial\langle V\rangle}{\partial x}\frac{\partial f}{\partial p}=0\ ;\quad (f\equiv\langle f\rangle). \tag{3.5}$$

In order to obtain a dispersion relation for the soliton gas we sequentially linearise and Fourier transform (3.5). Linearisation is carried out by considering small amplitude oscillations around the equilibrium configuration $f(x,v,t) = f_0(v) + f_1(x,v,t)$,

$$\begin{cases}\dfrac{\partial f_1}{\partial t}+v\dfrac{\partial f_1}{\partial r}-\dfrac{\partial\langle V_1\rangle}{\partial x}\dfrac{\partial f_0}{\partial p}=0\\[2ex] \langle V_1(x,v)\rangle=\displaystyle\iint H(x-x',v-v')f_1(x',v',t)dx'dv',\end{cases} \tag{3.6}$$

wherein f_0 is the initial distribution function of solitons in the system. The Fourier transform is calculated by considering the small perturbations are of the type $f_1(x,v,t)\propto e^{i(kx-\omega t)}$, producing:

$$\begin{cases}\tilde{f}_1(k,v)=-i\dfrac{\partial\langle\tilde{V}_1\rangle}{\partial x}\dfrac{\partial f_0}{\partial p}\dfrac{1}{(\omega-vk)}\\[2ex] \langle\tilde{V}_1\rangle=\displaystyle\int\tilde{H}(k,v)\tilde{f}_1(k,v,\omega)dv,\end{cases} \tag{3.7}$$

where we have employed the Fourier transform of the convolution. Substituting $\tilde{f}_1$ into $\langle\tilde{V}_1\rangle$ leads to the desired formula — the general dispersion relation for a dark soliton gas:

$$\boxed{1=k\int\tilde{H}(k,v)\frac{\partial f_0}{\partial v}\frac{\partial v}{\partial p}\frac{1}{(kv-\omega)}dv.} \tag{3.8}$$

Determining the jacobean $\partial v/\partial p$ requires knowledge of the relation between v and p, which may not be trivial as DS are relativistic quasiparticles in relation to the speed of sound c. For this reason we determine $\partial p/\partial v$ in the more amenable case of a non-relativistic DS gas, distributed such that $v \ll c$. This implies $\tilde{H}(k,v)\approx\tilde{H}(k,0)$ and $\partial v/\partial p = 1/m^*$, where m^* is the soliton effective mass, which may be related to the soliton inertial mass $m^* = m_s/2$, Eq. (3.9), and which is calculated by integrating the background BEC density subtracted from the soliton density [49],

$$\begin{aligned} m^* &= m\int(n_0-|\Psi_{\rm s}|^2)dx = mn_0\int\left(1-\tanh^2\left(\frac{x}{\xi}\right)\right)dx\Leftrightarrow\\ \Leftrightarrow\ m^* &= -2mn_0\xi,\end{aligned} \tag{3.9}$$

or in other terms, we are determining the amount of matter emptied by the hole-like soliton in the BEC.

At this point it remains to determine the soliton distribution function f_0 and to model the interaction

potential $\tilde{H}(k)$. The former will be considered to be a Heaviside function which represents the uniform soliton velocity distribution,

$$f_0(v) = \frac{N_0}{2v_F}\Theta(v_F - |v|)\,; \quad v_F = \frac{\pi\hbar N_0}{m^*}. \tag{3.10}$$

This means solitons will have a velocity within the domain $|v| < v_F$, where $v_F = \pi\hbar N_0/m^*$ is the 1D Fermi velocity of the DS gas [50]. The reason for this choice is that even if one prepares a gas of solitons at rest, which would correspond to a Dirac delta $f_0 = N_0\delta(v)$ distribution of particles, the fermionisation† of the gas will widen their velocity distribution profile. Introducing f_0 in the dispersion relation (3.8) and solving for ω now yields:

$$\omega^2 = k^2\left(v_F^2 + \frac{N_0\tilde{H}(k)}{m^*}\right). \tag{3.11}$$

3.1 The Interaction Potential or Hamiltonian Dynamics of a Dark Soliton Pair

In order to develop a description of a soliton gas it is essential we are able to cast their interactions $\tilde{H}(k)$ into the model. To do this we consider pairwise interactions and describe the interaction between two dark-solitons within a BEC by seeking the Hamiltonian or energy for a two-soliton solution. This quantity remains the only unknown in (3.11). The two-soliton solution is simply the superposition of two solitons with symmetric velocities v separated by a distance d from each other,

$$\Psi(x,d,v) = n_0\left(\gamma\tanh\left[\frac{\gamma}{\xi}\left(x-\frac{d}{2}\right)\right]+i\beta\right)\left(\gamma\tanh\left[\frac{\gamma}{\xi}\left(x+\frac{d}{2}\right)\right]-i\beta\right), \tag{3.12}$$

where $\beta = v/c$ and $\gamma = \sqrt{1-(v/c)^2}$. In order to guarantee phase continuity in the system, multiple soliton solutions will form into symmetrical phase pairs $\Psi(x,x_1,0) = -\Psi(x,x_2,0)$. What is more, and in accordance with the theory in section 2.3.5, exchanging two solitons with one another will originate a phase shift of π. These phenomena occur for the fact that solitons obey fermionic statistics (despite being borne on a BEC formed by a gas of bosons) [50, 64]. This is also consistent with the connection made between dark solitons and type-I excitations in Lieb-Liniger theory, section 2.4.

We recuperate the expression for the energy of excitations in a dilute BEC already obtained in section section 2.3.5, and repeated here for convenience:

$$\tilde{H}(d) = \int\left(\frac{\hbar^2}{2m}|\nabla\Psi|^2 + \frac{g}{2}(|\Psi|^2 - n_0)^2\right)dx. \tag{3.13}$$

Analogously to the process carried out in section 2.3.5 to find the single soliton energy, we now replace the two-soliton solution (3.12), into equation (3.13) and obtain the desired total two-soliton energy. The integration over x in (3.13) means that this Hamiltonian will depend only on the distance between solitons, and d is thus the relevant parameter characterising interaction. Following this calculation process

†Solitons are fermions. This is motivated and explained in section 3.1.

one obtains the expression $H(d)$ in real space and, through Fourier transform, in the desired frequency domain,

$$\tilde{H}(k) = \frac{1}{144}\pi c^2 k^2 \xi^2 n_0^2 \left(-4\beta^2 + k^2 - 14\right)\left(-4\beta^2 + k^2 + 4\right) \operatorname{csch}^2\left(\frac{\pi k}{2\sqrt{1-\beta^2}}\right). \tag{3.14}$$

We also include the simpler expression in the case the soliton gas is cold, i.e. the solitons are initialised with zero initial velocity $\beta = 0$,

$$H(k, \beta = 0) = \frac{1}{144}\pi c^2 k^2 \xi^2 n_0^2 \left(k^2 - 14\right)\left(k^2 + 4\right) \operatorname{csch}^2\left(\frac{\pi k}{2}\right). \tag{3.15}$$

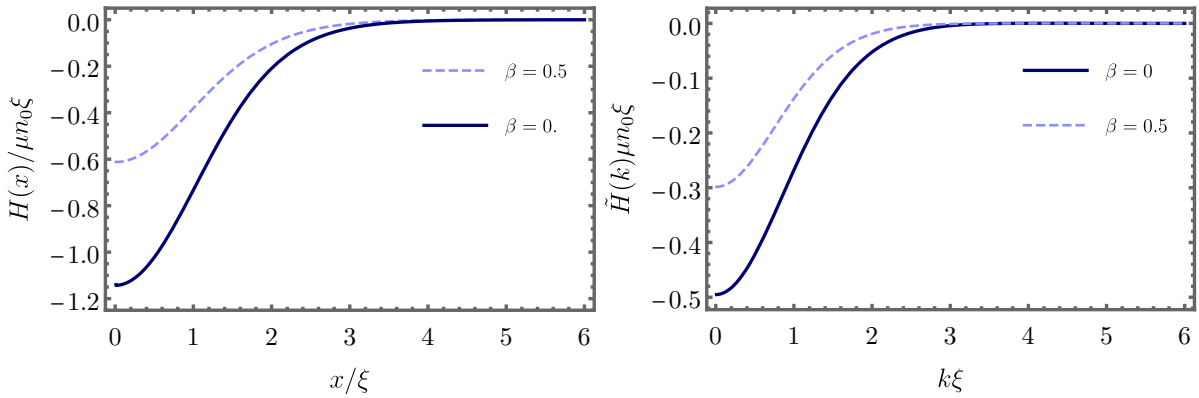

Figure 3.1: The obtained two-soliton interaction potential in real space (left) as a function of soliton separation; and momentum space (right) for two different values of the soliton velocities. The solid line represents $\beta = 0.5$ and the dashed line $\beta = 0$.

Fig. 3.1 depicts the profile of the potential determined in real and k-space for two different soliton gas velocities. It is interesting to notice that the resulting potential is negative, appearing to be attractive, whilst we expected repulsive soliton interactions. This holds, however, once we factor in the solitons' negative mass, which effectively sets the repulsive nature of interactions.

3.1.1 Soliton Gas Dispersion Relation

One may now replace the two-soliton interaction potential (3.14) into the dispersion relation (3.11) and obtain, at last, an expression for the soliton gas dispersion relation:

$$\omega(k) = \frac{1}{24}ck\sqrt{\frac{\pi N_0}{n_0^2\hbar^2}\left(144\pi N_0\hbar^2 - 2ck^2\xi^2 n_0^3\hbar\left(-4\beta^2 + k^2 - 14\right)\left(-4\beta^2 + k^2 + 4\right)\operatorname{csch}^2\left(\frac{\pi k}{2\sqrt{1-\beta^2}}\right)\right)}. \tag{3.16}$$

So that one may visualise these curves, they are plotted in fig. 3.2 for different soliton density and velocity values. The gas density is seen to be a much more predominant variable than the solitons' relative velocity.

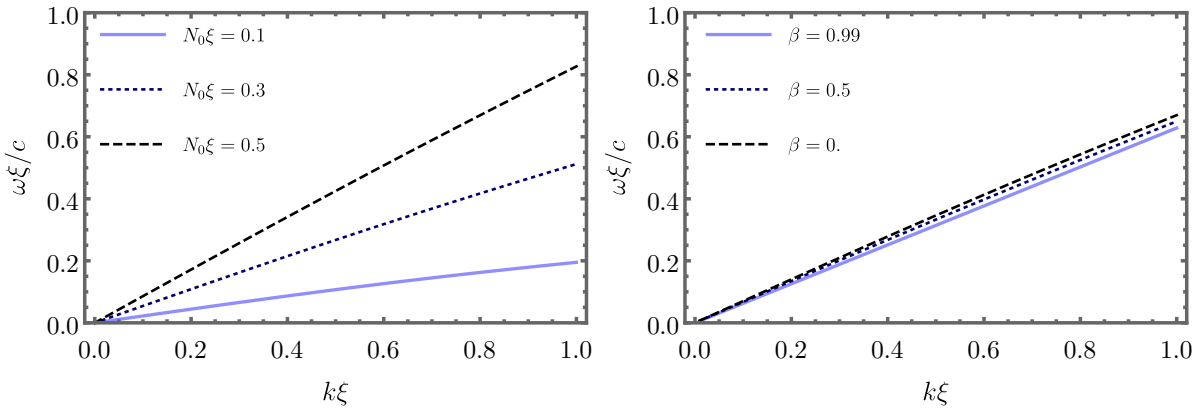

Figure 3.2: Left: Representation of the dispersion relation for a cold gas of solitons (3.16) for three different soliton density values. Right: Representation of the dispersion relation for three soliton gases (3.16) with different initial soliton velocities. The three represented cases correspond to a same gas density $N_0 = 0.3/\xi$.

Chapter 4

Implementation and Numerical Method

4.1 Dimensionalisation

Before advancing a method for discretisation and subsequent implementation of the GP equation, it is useful to study the interplay between the different quantities present in the equation, and to investigate which dimensionalisation or which set of variables are more adequate for the study of the desired phenomena and thus facilitate the physical interpretation of the results.

With this goal in mind we introduce a new set of dimensionless variables, which are defined in terms of the chosen adimensionalisation constants, x_0, t_0, v_0, Ψ_0,

$$\widetilde{x} = \frac{x}{x_0}; \quad \widetilde{t} = \frac{t}{t_0}; \quad \widetilde{v} = \frac{v}{v_0}; \quad \widetilde{\Psi} = \frac{\Psi}{\Psi_0}. \tag{4.1}$$

The redefinition of these variables allows the one-dimensional GP equation to be rewritten as

$$i\frac{\hbar\Psi_0}{t_0}\frac{\partial\widetilde{\Psi}(x,t)}{\partial t} = \left(-\frac{\hbar^2\widetilde{\boldsymbol{\nabla}}^2}{2mx_0^2} + V(x,t) + g|\widetilde{\Psi}(x,t)|^2|\Psi_0|^2\right)\Psi_0\widetilde{\Psi}(x,t). \tag{4.2}$$

We will promptly detail the relevant scenarios under study and the chosen dimensionalisation constants for each.

4.1.1 System With an External Trapping Potential

In the case that an external harmonic trapping potential of the type $V(x) = \frac{1}{2}mw^2x^2$ is applied to the system, the dimensionalisation constants are commonly defined in the following way [20, 25, 27, 32] :

$$\Psi_0 \equiv x_0^{-\frac{1}{2}}; \quad x_0 \equiv \sqrt{\frac{\hbar}{m\omega}}; \quad t_0 \equiv \frac{1}{\omega}; \quad v_0 = \sqrt{\frac{\hbar\omega}{m}}. \tag{4.3}$$

We additionally define $\omega \equiv \omega/\omega_0$, with $\omega_0 = 1$. As a consequence, the GPE becomes

$$i\partial_t \Psi = \left(-\frac{1}{2}\nabla^2 + \frac{1}{2}x^2 + \kappa|\Psi(x)|^2 \right) \Psi. \tag{4.4}$$

where we have already removed the tilde for simplicity and the new constant is given by $\kappa = g\sqrt{(\omega m^3/\hbar^5)} = (4\pi a/x_0)$.

4.1.2 Homogeneous System

On an homogeneous system, i.e., without an externally applied confining potential, it is useful to make use of the intrinsic scales of the system, ξ and c, such that

$$\Psi_0 \equiv \sqrt{n_0}\,; \quad x_0 \equiv \xi = \frac{\hbar}{\sqrt{mgn_0}}\,; \quad t_0 \equiv \frac{x_0}{c} = \frac{\hbar}{gn_0}\,; \quad v_0 \equiv c = \sqrt{\frac{gn_0}{m}}, \tag{4.5}$$

we get [46]

$$i\partial_t \Psi = \left(-\frac{1}{2}\nabla^2 + |\Psi|^2 \right) \Psi. \tag{4.6}$$

4.2 Imaginary time propagation

The imaginary time propagation method is essential to the numerical computation of the ground state of a certain physical system. It consists on making the replacement $t = -i\tau$ in an equation whose previous formal solution could be given by the evolution operator e^{-iHt}. Upon substitution, the system evolves instead in accordance with a new evolution operator $e^{-H\tau}$. As a consequence, all excited states of the problem decay exponentially to zero, and the system converges assymptotically to the ground state solution when $\tau \to \infty$ [65]. Performing this substitution, the dimensionless GPE becomes

$$\frac{\partial \Psi(x,t)}{\partial t} = \left(\frac{1}{2}\boldsymbol{\nabla}^2 - V(x,t) - |\Psi(x,t)|^2 \right) \Psi(x,t). \tag{4.7}$$

4.3 Time-Splitting Finite Difference (TSFD)

There exist several methods for discretising the NLSE/GPE equation in literature [25, 27, 66–70]. In this work, we employ a time-splitting finite difference (TSFD) method which consists in the separation of the equation into two splitting steps known as Strang-Splitting [27, 65]; these are then solved sequentially: whilst the nonlinear part is integrated analytically through the time-splitting technique, the linear part is discretised through a Crank-Nicolson finite-difference (CNFD) method [27, 67, 69].

4.3.1 Time-Splitting Technique

In the simplest two-step case, this technique consists in splitting the GP equation in two time steps, from t_n to t_{n+1}, [27, 71]:

$$\text{1st splitting step}: \quad i\partial_t\Psi(x,t) = -\frac{1}{2}\partial_{xx}\Psi(x,t) \tag{4.8a}$$

$$\text{2nd splitting step}: \quad i\partial_t\Psi(x,t) = V(x)\Psi(x,t) + |\Psi(x,t)|^2\Psi(x,t). \tag{4.8b}$$

Proof of validity of the Splitting Technique: Multiplying (4.8b) by $\Psi(x,t)^\dagger$, and its conjugated by $\Psi(x,t)$, and subtracting the latter from the former, we get

$$\begin{aligned}
&i\partial_t\Psi(x,t)\Psi(x,t)^\dagger = V(x)|\Psi(x,t)|^2 + |\Psi(x,t)|^2|\Psi(x,t)|^2 \\
&- \\
&i\partial_t\Psi(x,t)^\dagger\Psi(x,t) = V(x)|\Psi(x,t)|^2 + |\Psi(x,t)|^2|\Psi(x,t)|^2 \\
&= i[(\partial_t\Psi(x,t))\Psi(x,t)^\dagger + (\partial_t\Psi(x,t)^\dagger)\Psi(x,t)] = 0 \Leftrightarrow \\
&\Leftrightarrow \partial_t|\Psi(x,t)|^2 = 0.
\end{aligned}$$

From this we conclude that $\partial_t n(x,t) = 0$, i.e., the density is invariant in the second splitting step ($|\Psi(x,t_n)|^2 = |\Psi(x,t_{n+1})|^2$).

With this knowledge, one may keep the non-linear term in (4.8b) fixed, and integrate equation for $\Psi(x,t)$,

$$\Psi(t,x) = e^{-i[V(x)+|\Psi(x,t_n)|^2]\Delta t}\Psi(x,t_n). \tag{4.9}$$

Thus we solve the second splitting step equation (4.8b) spectrally, and are left with equation (4.8a). This one is solved using the CNFD method.

4.3.2 Crank-Nicolson Finite Difference (CNFD) or Semi-Implicit Crank-Nicolson method

The heat equation (4.8a), repeated here for convenience,

$$i\partial_t\Psi(x,t) = -\frac{1}{2}\partial_{xx}\Psi(x,t), \tag{4.10}$$

is discretised through the Crank–Nicolson finite difference (CNFD) method, which consists on applying a second-order centred difference scheme for spatial discretisation, and the Crank–Nicolson scheme for time discretisation. Implmenting this on Eq. (4.10) yields

$$i\frac{\Psi_j^{n+1} - \Psi_j^n}{\Delta t} = -\frac{1}{2}\left(C_I\,\delta_x^2\Psi_j^{n+1} + C_E\,\delta_x^2\Psi_j^n\right), \tag{4.11}$$

where δ_x^2 is the second-order central finite difference operator. The constants C_I and C_E, defined in the classical Crank-Nicolson method as $C_I = C_E = \frac{1}{2}$, represent the coefficients which allow us to tune the weight of the implicit and explicit parts of the discretisation, respectively [27, 67, 69]. For we have explicit access to Ψ^n, but have no such access to Ψ^{n+1} and must thus solve for it using an implicit method. Taking these values and developing the finite difference operator expressions, we obtain

$$\frac{\Psi_i^{n+1} - \Psi_i^n}{\Delta t} = \frac{i}{4}\left[\frac{\Psi_{i+1}^{n+1} - 2\Psi_i^{n+1} + \Psi_{i-1}^{n+1}}{\Delta x^2} + \frac{\Psi_{i+1}^{n} - 2\Psi_i^{n} + \Psi_{i-1}^{n}}{\Delta x^2}\right]. \tag{4.12}$$

Defining the simulation parameter $\lambda = \Delta t/\Delta x^2$, it can be written as

$$-\frac{i}{4}\lambda\Psi_{i-1}^{n+1} + \left(1 + \frac{i}{2}\lambda\right)\Psi_i^{n+1} - \frac{i}{4}\lambda\Psi_{i+1}^{n+1} = \Psi_i^n + \frac{i}{4}\lambda(\Psi_{i-1}^n - 2\Psi_i^n + \Psi_{i+1}^n). \tag{4.13}$$

This system (4.13) forms a tridiagonal matrix system with main diagonal $b = 1 + \frac{i}{2}\lambda$, and secondary diagonals $a = c = \frac{i}{4}\lambda$:

$$\begin{bmatrix} b & -c & 0 & \cdots & 0 \\ -a & b & -c & & \vdots \\ 0 & -a & \ddots & \ddots & 0 \\ \vdots & & \ddots & & -c \\ 0 & \cdots & 0 & -a & b \end{bmatrix} \begin{bmatrix} \Psi_1^{n+1} \\ \vdots \\ \Psi_i^{n+1} \\ \vdots \\ \Psi_{N-2}^{n+1} \end{bmatrix} = \begin{bmatrix} d_1 \\ \vdots \\ d_i \\ \vdots \\ d_{N-2} \end{bmatrix}. \tag{4.14}$$

Here we have defined $d_i = \frac{i}{4}\lambda(\Psi_{i-1}^n + \Psi_{i+1}^n) + \left(1 - \frac{i}{2}\lambda\right)\Psi_i^n$. Because (4.14) is diagonally dominant, we may apply the Jacobi method.

Jacobi Method

Considering the system (4.14) as $A\underline{\Psi} = \underline{d}$ and decomposing the tridiagonal matrix as $A = D - L - V$, where D is a diagonal matrix, V an upper diagonal matrix and L a lower diagonal matrix, this method is written as

$$\underline{\Psi}^{n+1} = D^{-1}(L + V)\underline{\Psi}^n + D^{-1}\underline{d}. \tag{4.15}$$

As a consequence, we obtain the following solution:

$$\begin{bmatrix} \Psi_1^{n+1} \\ \vdots \\ \Psi_i^{n+1} \\ \vdots \\ \Psi_{N-2}^{n+1} \end{bmatrix} = \frac{1}{b}\begin{bmatrix} 0 & c & 0 & \cdots & 0 \\ a & 0 & c & & \vdots \\ 0 & a & \ddots & \ddots & 0 \\ \vdots & & \ddots & & c \\ 0 & \cdots & 0 & a & 0 \end{bmatrix} \begin{bmatrix} \Psi_1^{n} \\ \vdots \\ \Psi_i^{n} \\ \vdots \\ \Psi_{N-2}^{n} \end{bmatrix} + \frac{1}{b}\begin{bmatrix} d_1 \\ \vdots \\ d_i \\ \vdots \\ d_{N-2} \end{bmatrix}, \tag{4.16}$$

which, upon substitution of a, b and c yields the simplified solution:

$$\Psi_i^{n+1} = \frac{1}{1+\frac{i}{2}\lambda}\left[\frac{i}{2}\lambda(\Psi_{i-1}^n + \Psi_{i+1}^n) + \left(1 - \frac{i}{2}\lambda\right)\Psi_i^n\right]. \tag{4.17}$$

Having concluded this derivation, the final form of the scheme from time $t = t_n$ to $t = t_n + 1$ with homogeneous Dirichlet boundary conditions ($\Psi(0,t) = \Psi(L,t) = 0$) is given by the system [27, 72],

TSFD method (real-time)

$$\begin{cases} \Psi_j^{(1)} = e^{-i[V_j + |\Psi_j^{(2)}|^2]\frac{\Delta t}{2}}\Psi_j^n\,; \quad 0 \leq j \leq J \\ i\frac{\Psi_j^{(2)} - \Psi_j^{(1)}}{\Delta t} = -\frac{1}{4}\left(\delta_x^2\Psi_j^{(2)} + \delta_x^2\Psi_j^{(1)}\right)\,; \quad 0 \leq j \leq J-1\,; \quad \Psi_0^{(2)} = \Psi_J^{(2)} = 0 \\ \Psi_j^{n+1} = e^{-i[V_j + |\Psi_j^{(2)}|^2]\frac{\Delta t}{2}}\Psi_j^{(2)}\,; \quad 0 \leq j \leq J, \end{cases} \tag{4.18}$$

where the splitting steps have been combined via the standard Strang-Splitting [27].

The scheme for the computation of a stationary simulation solves the same equation, only in this case the imaginary time method is first applied, section 4.2, making (4.7) the starting point for the discretisation. This results in a scheme similar to (4.18), except the time step now appears multiplied by the imaginary number, $\Delta t \to i\Delta t$, such that $\lambda \to i\lambda$.

We have presented the simplest case of the TSFD method using homogeneous Dirichlet boundary conditions; however, if one wishes to apply periodic boundary conditions ($\Psi(0,t) = \Psi(L,t)$, $\partial_x\Psi(0,t) = \partial_x\Psi(L,t)$), the simplest way to implement this is to make Ψ_0 into a ghost point which stores the wave function information from the opposite end of the 1D system. To do so and to retain system size ($J+1$ positions), the iterations $0 \leq j \leq J$ in (4.18) must be changed to $1 \leq j \leq J+1$, and the intermediate step changes to $1 \leq j \leq J$; in addition, instead of making the wavefunction vanish on both ends ($\Psi_0^{(2)} = \Psi_J^{(2)} = 0$) this step is accompanied by a new boundary prescription,

$$\begin{cases} \Psi_1^{n+1} = \Psi_{J+1}^{n+1} \\ \Psi_0^{n+1} = \Psi_J^{n+1}. \end{cases} \tag{4.19}$$

Conserved Quantities

The TSFD method conserves the mass (2.37) at the discretised level throughout the simulation and it is also time transverse invariant. It does not, however, conserve energy (2.38) [67].

4.3.3 Stability Analysis

The TSFD method is particularly favourable because it is unconditionally stable, time reversible, second-order accurate in both time and space, it conserves mass (or total particle number) and is time transverse invariant [27, 67]. In addition, as it is an implicit scheme where only a linear system needs be solved at each time step, it has a memory cost of only $\mathcal{O}(J)$ operations in the one-dimensional case. The only slight drawback to this method is that it does not have an energy conservation property [67, 73].

We will observe further on, however, that in every simulation run energy is actually conserved with the same degree of precision as the mass.

Now, the part of the code where there could be an introduction of error would be in the iterative scheme used to solve the Crank-Nicolson implicit method. The latter is unconditionally stable according to linear analysis*, however, in the actual implementation, the simulation may become unstable because nonlinear terms may play a dominant role in the dynamics [75], and this could compromise the convergence of the method. For this reason we set a time step $\delta t = 0.0001$ and a spatial discretisation step $\delta x = 0.1$, which results in a simulation parameter of the order $\lambda = 0.01$ that is verified to guarantee convergence of the method in all scenarios.

4.4 Verification

This section aims to evaluate the physical applicability and quality of the developed code. This is achieved by considering several well-documented features of the GP equation and comparing them to our own results, generated through the code.

4.4.1 Relaxation

Any simulation is preceded by a relaxation of the system to its global minimum solution, which then serves as starting point for real-time evolution. This relaxation relies on the imaginary time method, section 4.2, which iteratively causes the exponential decay of all excited states, providing the ground state of the system. The end to this iterative process is imposed by a stopping criterion [72],

$$||\psi^{n+1} - \psi^n||_\infty < \epsilon\, \delta t, \tag{4.20}$$

where $||\cdot||_\infty$ is the uniform norm defined as $||\varphi||_\infty = \max(|\varphi(x)|)$ and ϵ is a chosen parameter setting the precision. To illustrate this process, we start with a simple case of a BEC in a harmonic trap $V_{ext}(x) = \frac{1}{2}m\omega^2 x^2$ with trapping frequency $\omega/\omega_0 = 1$. The system is initialised from the Thomas-Fermi solution and evolves towards the ground state. Fig. 4.1 presents the evolution of the energy and different final ground states obtained for different ϵ values.

*The equation being solved, (4.14), is a strictly diagonally dominant tri-diagonal matrix system, and as such it gathers sufficient condition for guaranteed convergence of the Jacobi iterative method [74].

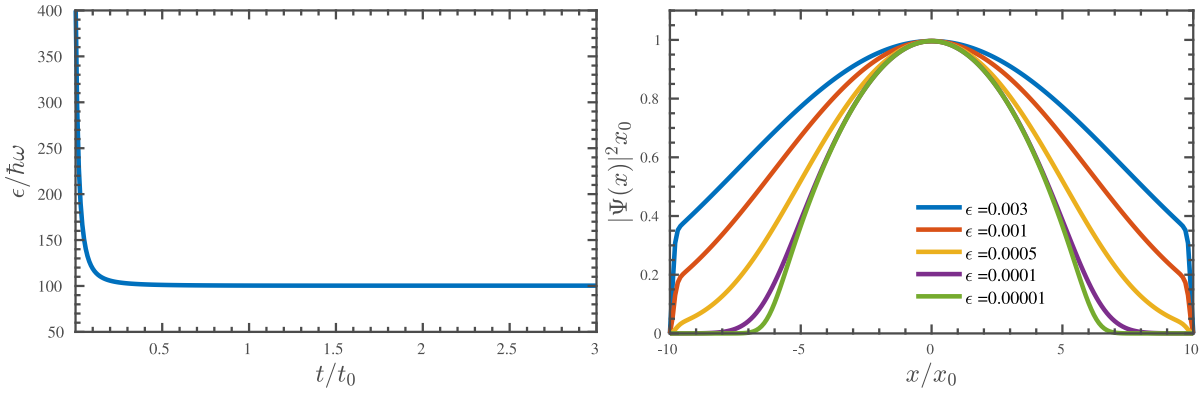

Figure 4.1: Relaxation of a harmonically trapped BEC through employment of the imaginary time method for a $L = 25x_0$ system and a fixed time step of $\delta t = 0.0001$. Left: Energy evolution when $\epsilon = 0.1 \times 10^{-4}$; right: ground-state solutions obtained for different stopping criteria values.

4.4.2 Pure BEC

With the purpose of validating the simulation, we will start by observing a few key well-documented examples of BEC dynamics.

It seems natural to start from the simplest situation: a pure condensate confined by a harmonic trap, and whose center of mass is displaced a small distance x_{CM} from the center of the trap. As a result, the BEC exhibits dipolar oscillation of amplitude x_{CM} and frequency corresponding to the trap frequency of the BEC (Kohn's Theorem) [76]. This is depicted in fig. 4.2

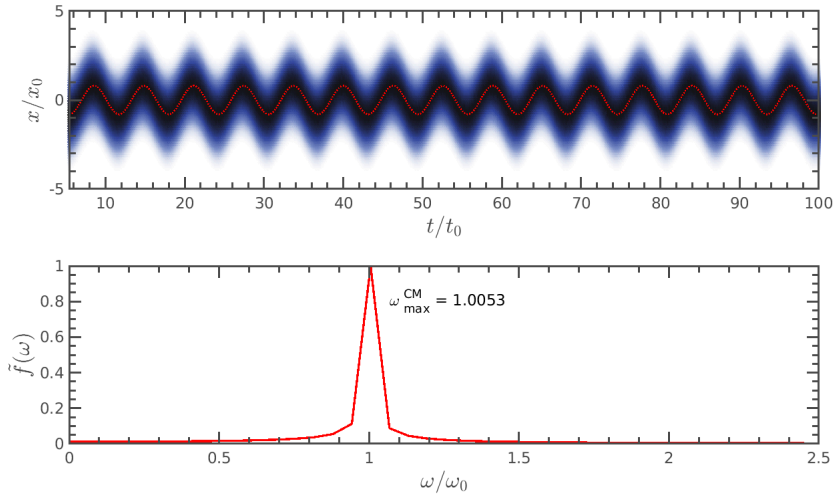

Figure 4.2: Top: Evolution of the BEC density and centre of mass position after a small displacement; the dotted line indicates the center of mass x_{CM} position. Bottom: Fourier transform of the CM position signal.

In the numerical simulation, we used a trap frequency $\omega/\omega_0 = 1$ and obtained a corresponding CM oscillation frequency of $\omega_{\mathrm{CM}}/\omega_0 = 1.0053$, which means the prediction $\omega_x = \omega_{\mathrm{CM}}$ is accurate up to the

third decimal placement.

Finally, we also plot the energy (2.38) and particle number (2.37) evolution of the system, fig. 4.3, and confirm the numerical conservation of the two quantities.

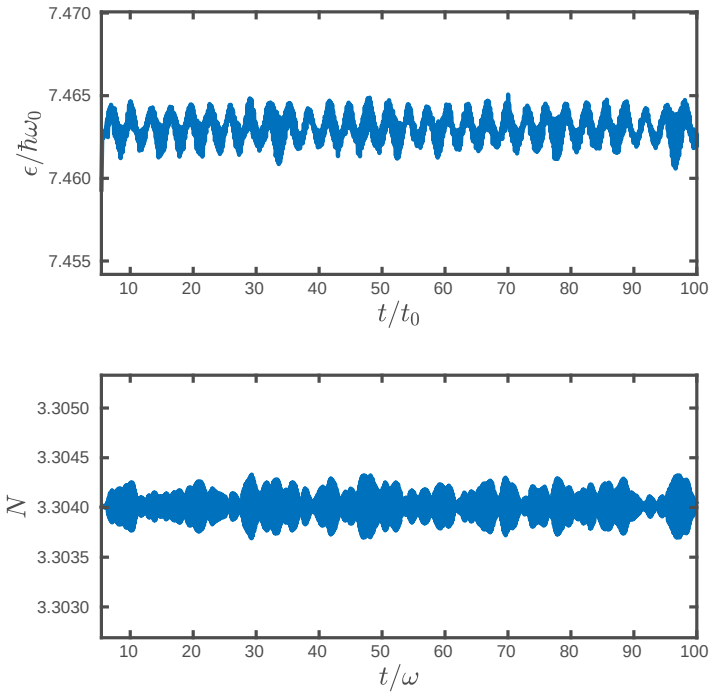

Figure 4.3: Top: Evolution of the BEC energy with time. Fluctuations are under $\sim 10^{-2}\epsilon/\hbar\omega_0$. Bottom : Evolution of the number of particles with time. Fluctuations are under $\sim 10^{-3}N$.

4.4.3 Soliton on a BEC

Now, having studied the behaviour of a BEC with no added perturbation, we add a new degree of complexity by introducing a soliton into the system. We start with the simplest scenario by introducing a $v = 0$ soliton into the centre of the trap. As we have detailed, in the theoretical description (section 2.3.5), we may introduce the soliton by multiplying the TF wave function by the expression (2.61). This expression should be an exact solution of the GP equation, however, we evolve the system in imaginary time for a few time steps to guarantee the exact numerical stationary solution. was found. We obtain the solution as depicted in fig. 4.4.

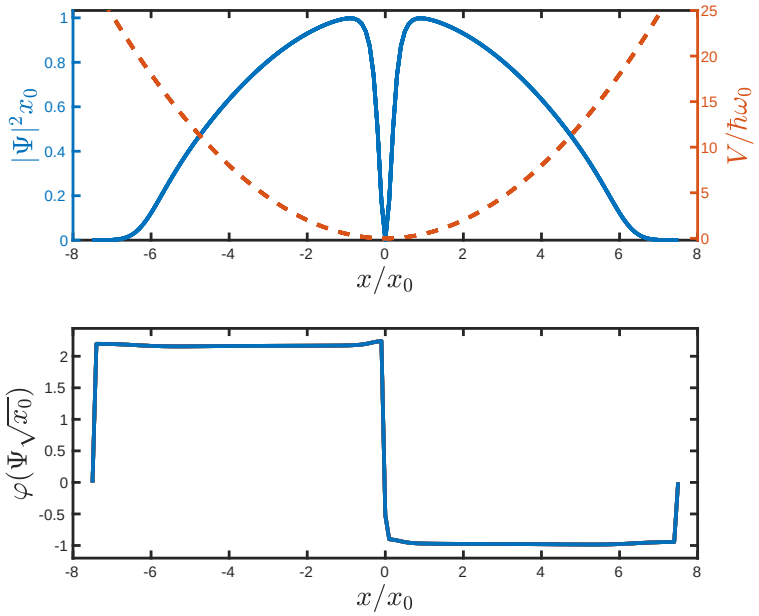

Figure 4.4: Top: BEC density (solid) and the external trapping potential (dashed). Bottom : Phase of the BEC wave function (solid). The phase jump $\Delta\varphi \approx \pi$. Simulation run in an $L = 15x_0$ box with soliton solution placed in the centre of the trap. Trapping frequency $\omega_x/\omega_0 = 1$.

Because we have created a soliton with zero velocity in the middle of the trap, this soliton will have a depth equal to the maximum density, $n_d = n_0$, and is therefore a black soliton whose position will remain unaltered during dynamical real-time simulations [42]. If, however, we create a gray soliton, (see fig. 2.2), by either initialising the soliton a distance away from the centre — its depth will consequently be $n_d < n_0$ — or with a velocity $v_s \neq 0$, then this soliton is expected to acquire oscillatory motion [42, 45]. we may observe this feature in fig. 4.5.

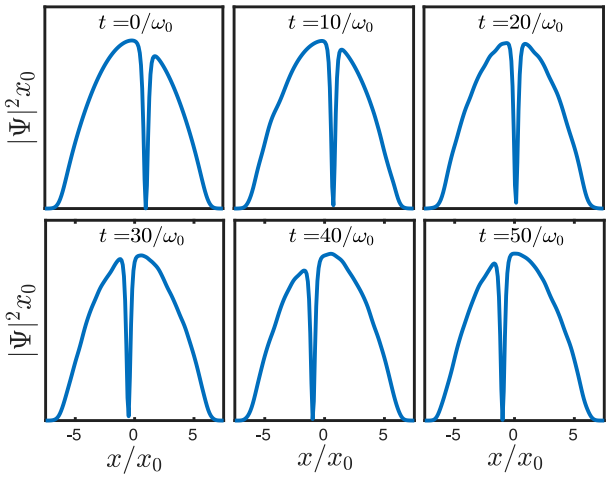

Figure 4.5: Evolution of the BEC density in several temporal moments. The grey soliton oscillates through the condensate. Simulation run in an $L = 10x_0$ box with a soliton solution placed in $x = 1x_0$.

It may be worth noting that the deeper a soliton is, the larger its mass (in module, for the soliton mass is negative), and slower its velocity. Conversely, a shallow soliton will move considerably faster. In this way, dissipative effects result in an acceleration of the soliton motion.

An extensively reported scenario consists on inserting a grey soliton into a BEC confined via a harmonic trap potential and observing the motion it acquires. The cases for $\omega/\omega_0 = 1$ and $\omega/\omega_0 = 2$ are presented in fig. 4.6, including Fourier transforms of the soliton and center-of-mass (CM) trajectories.

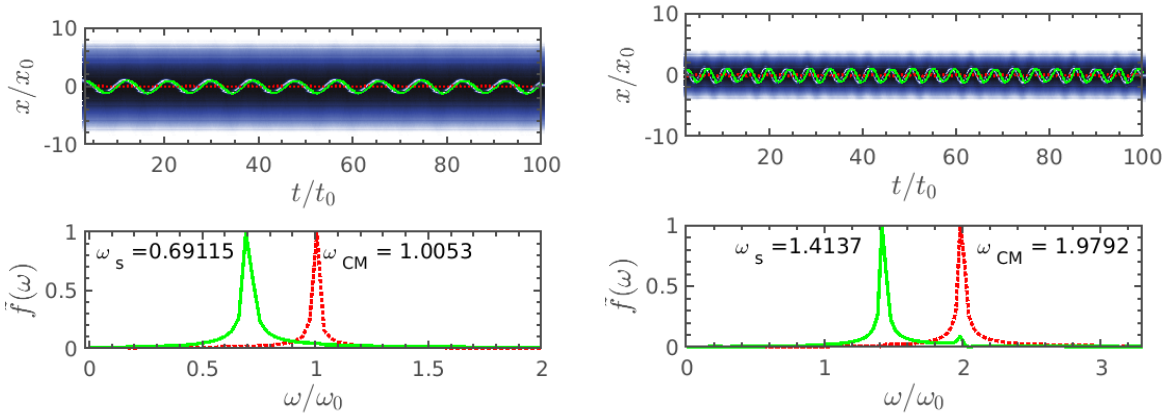

Figure 4.6: Top: Evolution of the BEC density, centre of mass position (dotted) and soliton position (solid) after a small displacement. Bottom: Fourier transform of the CM (dotted) and soliton (solid) positions. Left panel corresponds to a trap frequency $\omega_x/\omega_0 = 1$, and the right panel to $\omega_x/\omega_0 = 2$. Simulation with $\kappa = 30$, $L = 20x_0$, $\Delta t = 200t_0$ and initial soliton position $x = 1x_0$.

We verify that whilst centre of mass oscillate to the trap frequency, the solitons oscillate harmonically at a frequency $\omega_s = \omega/\sqrt{2}$. This is known as the "anomalous mode" (see appendix A.6 for a derivation) and constitutes an extensively documented phenomenon which seems to contradict the Ehrenfest theorem [37, 42, 44, 48, 77–79]. The latter states that the centre of mass of the whole BEC always oscillates with the trap frequency ω_0[†].

fig. 4.6	ω/ω_0	$\omega/\sqrt{2}\omega_0$	$\omega_{\mathrm{CM}}/\omega_0$	$\omega_{\mathrm{s}}/\omega_0$	$\epsilon_r(\%)$
left	1.	0.707	1.005	0.691	2.210
right	2.	1.414	1.979	1.414	0.036

Table 4.1: Results of two simulations investigating the oscillating frequency of a grey soliton in a BEC confined by an external harmonic trap $V(x) = \frac{1}{2}m\omega^2x^2$.

The fact that the motion of the dark soliton is accompanied by a deformation of the system density is responsible for the decoupling between the dark soliton motion and the centre of mass motion [79].

Numerical Calculation of the Phonon Spectrum

To further test the code, we simulate a gas of phonons, describing the small excitations on top of a BEC. A gas of phonons is generated by imprinting many high-velocity soliton-like solutions in a 1Db box

[†]Ehrenfest theorem states $m\frac{d\langle x\rangle}{dx} = \langle p\rangle$, with $\frac{d\langle p\rangle}{dx} = -\langle\frac{dV}{dx}\rangle$; which relates the way in which the expectation value for the position and momentum of a particle is dependent on the external potential, V, acting on it.

of length L. The excitations evolve according to the GP equation as observed in fig. 4.7.

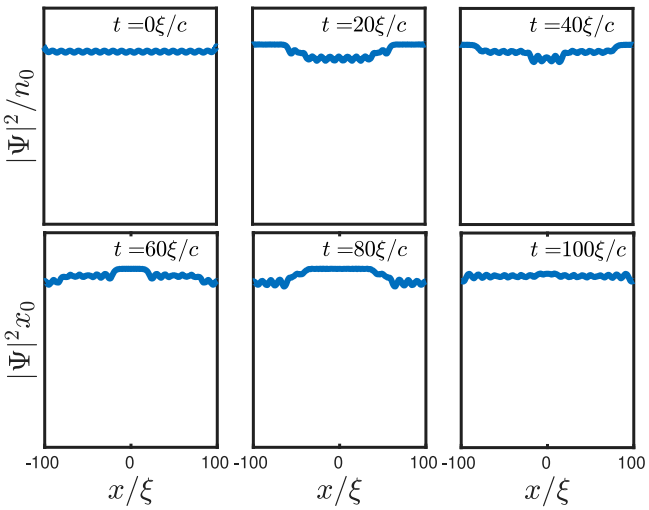

Figure 4.7: Time-stamped snapshots of a numerical simulation of a phonon gas, $v_p h \approx 0.98c$.

We simulate phonon gases with different densities‡ and characterise the resulting spectra by making use of the dynamical structure factor,

$$S(\omega, k) = \int\int e^{-i\omega t + ikx} |\Psi(x,t)|^2 dx dt, \tag{4.21}$$

depicted in figures 4.8 and 4.9.

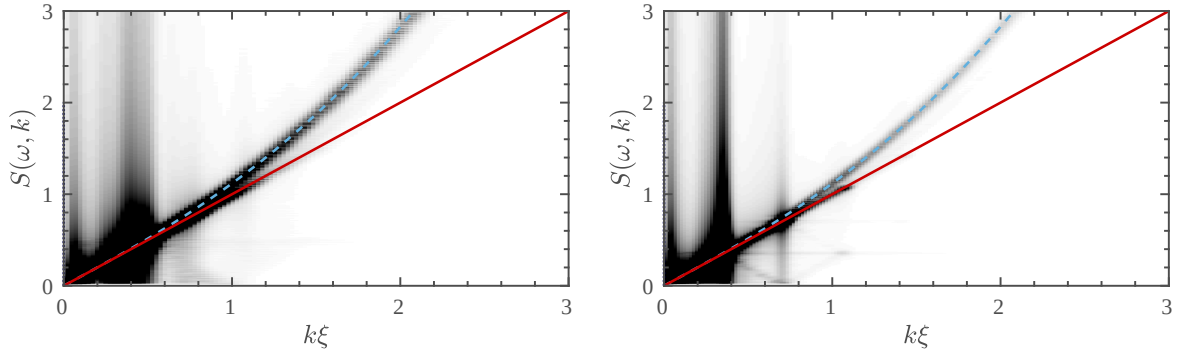

Figure 4.8: Dynamic structure factor $S(\omega, k)$ as obtained from the numerical simulation, for 20 phonons in a $L = 250\xi$ box (left) and a $L = 350\xi$ box (right). In both images, the dashed line corresponds to the Bogoliubov mode (2.54). The lower full line included in the graph is a linear curve depicting the limit of this expression in low k (2.56).

The resulting spectra are characterised by a single mode with a linear phonon-like form in the region $k \lesssim \xi$; as the momentum increases it approaches the free-particle law. This mode is consistent with the Bogoliubov spectrum of elementary excitations (2.54).

‡Observing instances with different system dimensions reduces the risk of encountering numerical artifacts.

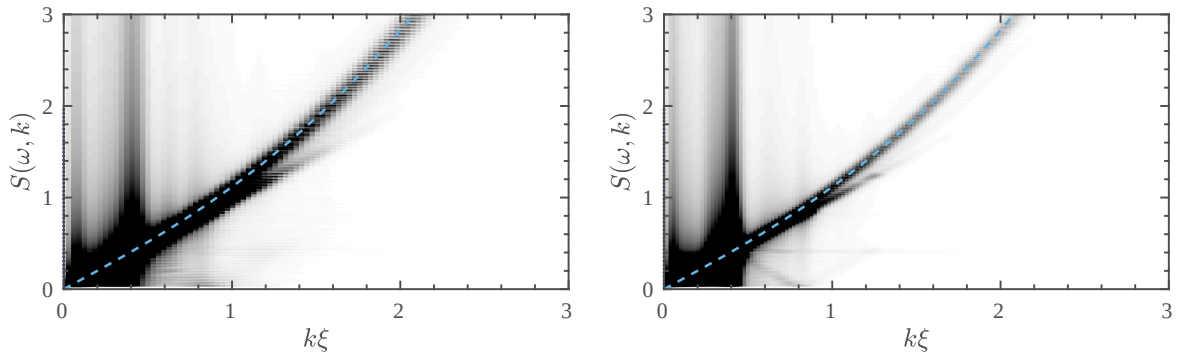

Figure 4.9: Dynamic structure factor $S(\omega, k)$ as obtained from the numerical simulation, for 20 phonons in a $L = 200\xi$ box (left) and a $L = 300\xi$ box (right). In both images, the dashed line corresponds to the Bogoliubov mode (2.54).

Omitting the linear long-wavelength expression in this new set of spectra, fig. 4.9, we are left free to simply verify the accordance between the curve obtained from simulation and the expected results from the theory. For all observed phononic systems this yields a complete agreement.

Chapter 5

Simulation of Dark Soliton Dynamics

In this section we finally examine the results obtained through simulation, and look to compare these with our theoretical predictions, section 2.3.6.

5.1 Soliton interaction features

A first obvious subject is to look into individual soliton interaction. Two solitons coming into contact with one another cause a phase shift of their wavefunctions which gets translated into a displacement of their trajectories. This displacement depends on their relative velocity before contact and may thus be used to characterise the interaction. Simulating this behaviour we can, in fact, observe the phase shifts of the soliton wavefunctions: in fig. 5.1 we observe colliding solitons in two different situations (different initial relative velocities).

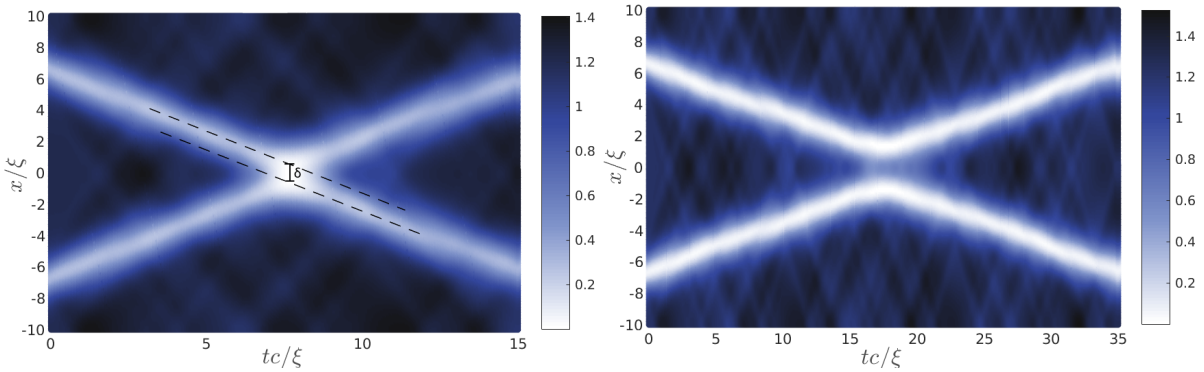

Figure 5.1: Simulation with 2 solitons in an $L = 20\xi$ box . time step $\Delta x = 0.1\xi$ and $\Delta t = 0.0001\xi/c$. Ran for 15000 iterations which yields a simulation time of $t = 15$ (time is normalised to $\xi/(cs)$). Left: $v_s = 0.6/c$ which means that the relative velocity between solitons $\delta v_s = 1.2c > c$ is relativistic; Right: $v_s = 0.2c$ which means that the relative velocity between solitons $\Delta v = 0.4c < c$ is not relativistic. Trajectory displacement δ is represented in the left picture.

Fig.5.1 contains a representative example of two solitons coming into contact with the relative initial velocities of $\Delta v_s = 1.2c$ and $\Delta v_s = 0.4c$. Not only does it become clear that a higher relative velocity implies a smaller trajectory displacement, but we also observe that a relativistic velocity difference $\Delta v_s >$

c permits the solitons to "cross" one another. Indeed, in this case the wavefunction of the two solitons coalesces — there appears only one single depression in the density, with depth that of the two solitons combined — whereas a difference in velocity under the sound speed $\Delta v_s < c$ causes the solitons instead to repel one another. In the latter case their wavefunctions never coalesce, and are scattered with a more significant trajectory displacement than in the previous case.

There are thus three different scenarios: for $v_s < 0.5c$, the solitons, which are quite deep and slower-moving, repel one another and never come into full contact, always presenting two separate density minima; for $v_s = 0.5c$ the solitons come into contact and at their junction the BEC density drops to exact zero; for $v_s > 0.5c$ the shallower solitons are transmitted through one another, forming a single soliton with their combined depth at their collision point, after which they move away separated again.

This behaviour is replicated in larger scale, section 5.1, which represent sections of the density evolution of soliton gases where one may observe the many different soliton interactions and scattering, which is the cause of fermionisation. We may observe that the dominant soliton interaction is non-relativistic, which is consistent with a progressively fermionised gas but that was initially cold and in which no perturbation or energy form was added into.

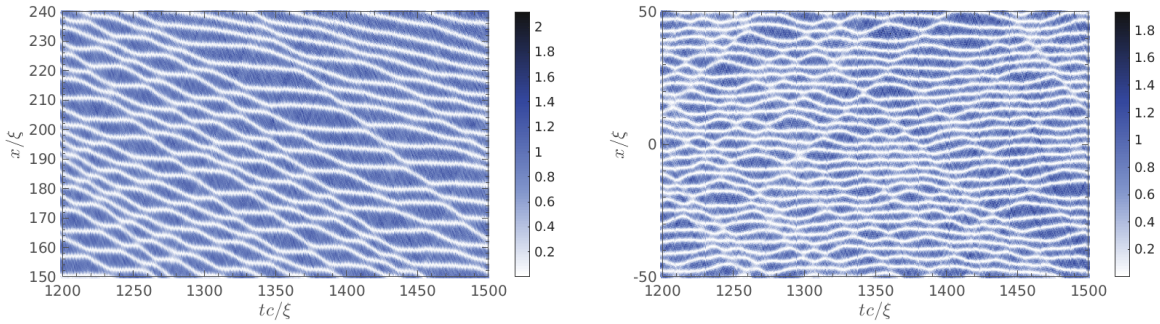

Figure 5.2: Two representative cases of many-soliton interaction in gases of initially cold solitons. Both panels represent a detail in the full density evolution of a $N = 100$ dark soliton gas.

5.2 Soliton gas

The study of the collective behaviour of a gas in a soliton requires the generation of a set of $N \gg 1$ solitons at a same velocity in a BEC whose motion and interaction will then be observed. The simulations heretofore presented are generated in a simple homogeneous BEC system (no external acting potentials), and follow the considerations made in section 4.1 including the dimensionalisation of each variable.

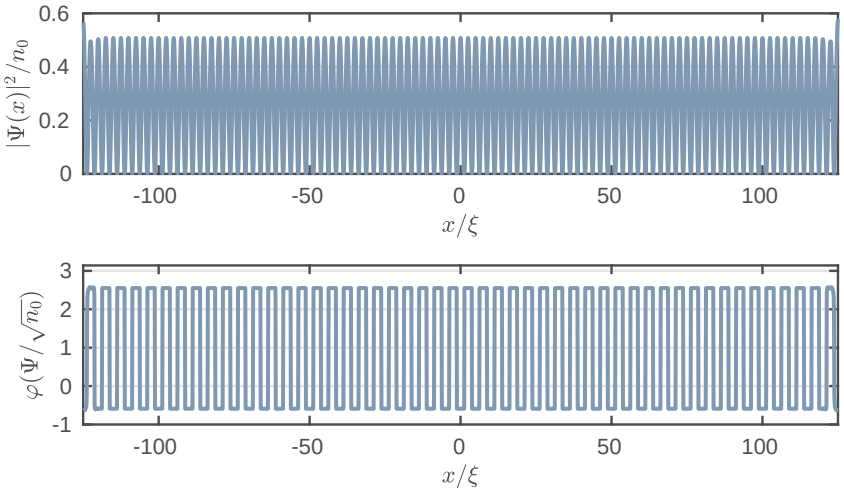

Figure 5.3: Initial state of a simulation, represented in both the density and the phase of the BEC. This simulation is of a single soliton gas, with 100 solitons and density $N_0\xi = 0.4$ which means each soliton is at a distance of $d = 2.5\xi$ from their neighbours, and common initial velocity $v_s/c = 0$.

We consider dark soliton gases. Because there is no initial velocity, motion is caused by two things: interactions between solitons and interactions between solitons and phonons; these may be excited due to numerical noise.

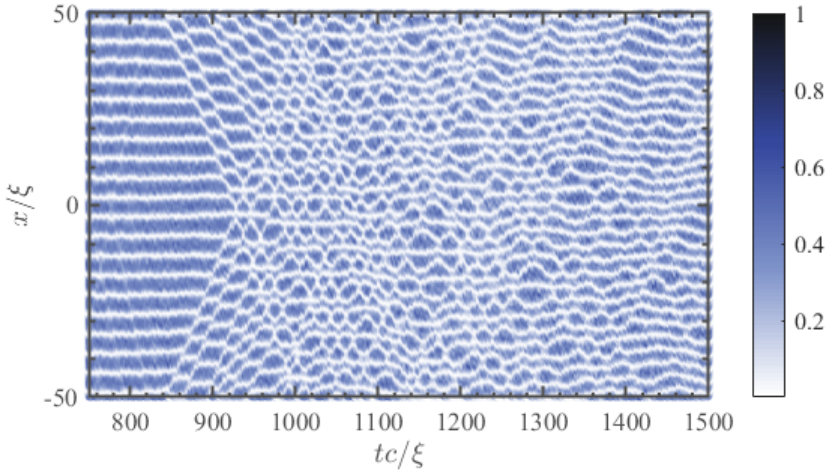

Figure 5.4: Numerical simulation of a cold dark-soliton gas, $v_s = 0$. Colouring represents the density $|\Psi|^2/n_0$. Soliton density equals $N_0 = 0.2$. One observes the formation of an acoustic mode, which preludes the solitonic turbulence

Guaranteeing homogeneity and consistency, all results from here on will have been produced with a system normalised to the background density.

A real-space representation of a single soliton gas with zero initial velocity, simulated using the code developed in this thesis, is shown in fig. 5.4.

Figure 5.4 provides visual confirmation that the system is behaving in an expected manner — we see

the solitons at rest initially, and over time the generation of small ripples of movement in the gas (acoustic mode) in the long wavelength limit. This develops into bigger events, wherein there is significant soliton interplay. Further investigation to other aspects of the simulation is needed if we want to corroborate our hypothesised kinetic equation for the collective-soliton behaviour.

In order to investigate collective modes, we look at the k-space representation. Once again we rely on the dynamical structure factor $S(\omega, k)$.to analyse several soliton gases. What differs between the cases showcased here is the density of the gas. The derived expression (3.16) should be valid in the dilute configuration, $N_0\xi \ll 1$.

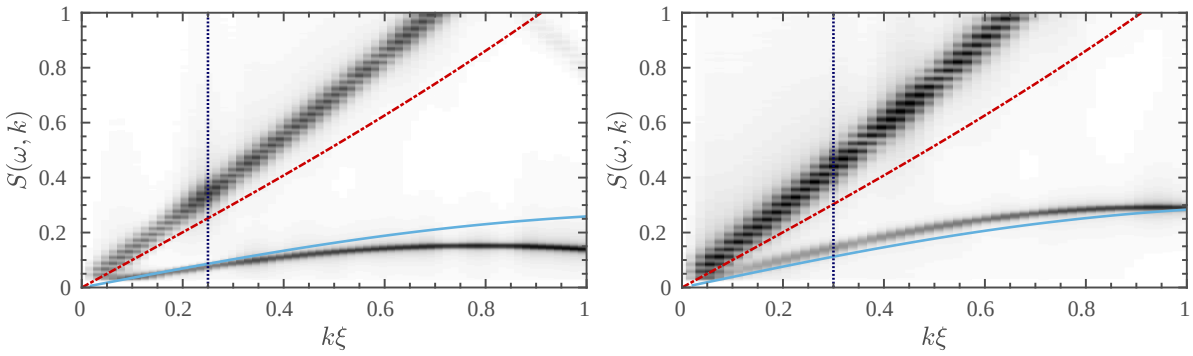

Figure 5.5: Dynamic structure factor $S(\omega, k)$ as obtained from the numerical simulation, for $N_0\xi = 0.25$ (left) and $N_0\xi = 0.3$ (right). In both images, the mode (3.16) is plotted with no adjustable parameters, while the top curve is compared against the Bogoliubov mode (dashed line), (2.54). The vertical dotted lines depicts the limit of the expected validity of the Vlasov equation (3.4), $k = N_0$.

Before further analysis, it is relevant to remark that the developed model based on the Vlasov equation predicts a single mode, which finds a good agreement with the less-energetic mode in the numerical spectra, Fig. 5.5, especially in the region $k \lesssim N_0$, i.e. for wavelengths lying above the inter-particle separation $1/N_0$. Above this value, the intersoliton separation is of the same order of magnitude as the wavelength of the phenomena, and the coarse-graining assumption of the phase space breaks down. Moreover, for shorter wavelengths in the range $k \sim \xi$, the description of DS as hole-like particles fails and the internal structure of the solitons becomes important, and this hinders the validity of the kinetic equation. Beside this, an additional higher-energetic mode $\omega \simeq v_2 k$ with $v_2 > c$ is present in the spectra. The relativistic nature of this mode excludes it from being solitonic. We thus compare it to the low-lying Bogoliubov excitations on top of the BEC, Fig. 5.5, to which it doesn't show particular agreement. We hypothesise that this mode may come about as a result of mode repulsion between the higher-energetic Bogoliubov modes and the lower energetic solitonic modes.

These figures, fig. 5.5, represent the interval of densities $N_0\xi \simeq 0.2 - 0.3$ which we show the best agreement with the proposed theory. However, the range for the validity of the theory should continue to lower densities $N_0\xi < 0.2$. We are not able to verify this as in this density range the spectra display a higher number of modes, Fig. fig. 5.6, which become difficult to discern. The likely cause is that the distance between solitons in this density range is too large for the simulation to efficiently detect the higher intensity solitonic mode within the executed time frame (or number of iterations), showing instead a larger number of lower intensity modes.

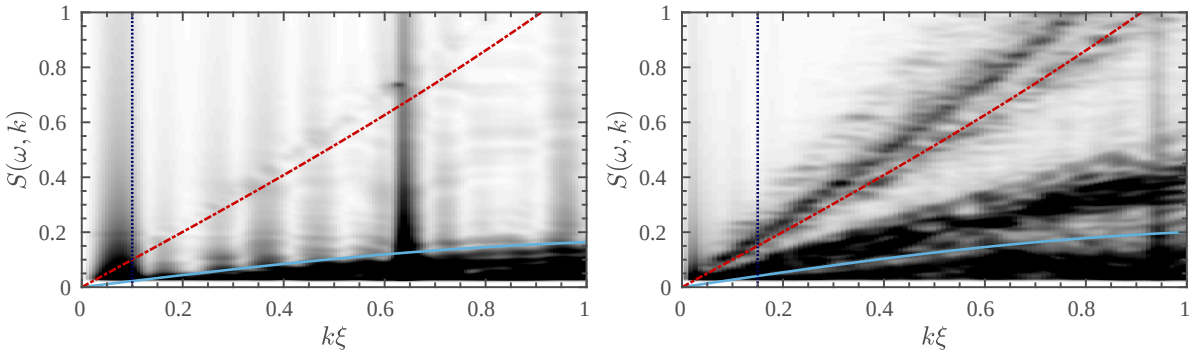

Figure 5.6: Dynamic structure factor $S(\omega, k)$ as obtained from the numerical simulation, for $N_0\xi = 0.1$ (left) and $N_0\xi = 0.15$ (right). In both images, the solid line corresponds to the first-sound mode in (3.16), plotted with no adjustable parameters, while the top curve is compared against the Bogoliubov mode (dashed line), (2.54). The vertical dotted lines depicts the limit of the expected validity of the Vlasov equation (3.4), $k = N_0$.

The spectra obtained for $N_0\xi = 0.1$ and $N_0\xi = 0.15$ are nevertheless shown, particularly because it may be interesting to note that as the density decreases, the Bogoliubov curve approaches the top curve in the spectra. This fact would further support the hypothesis that the upper mode in the spectra corresponds to a Bogoliubov mode that is hybridised with the lower solitonic mode. In this density range, the solitonic modes take longer to be excited and are much less predominant in the dynamics, as such, the hybridisation phenomenon is expected to be less pronounced.

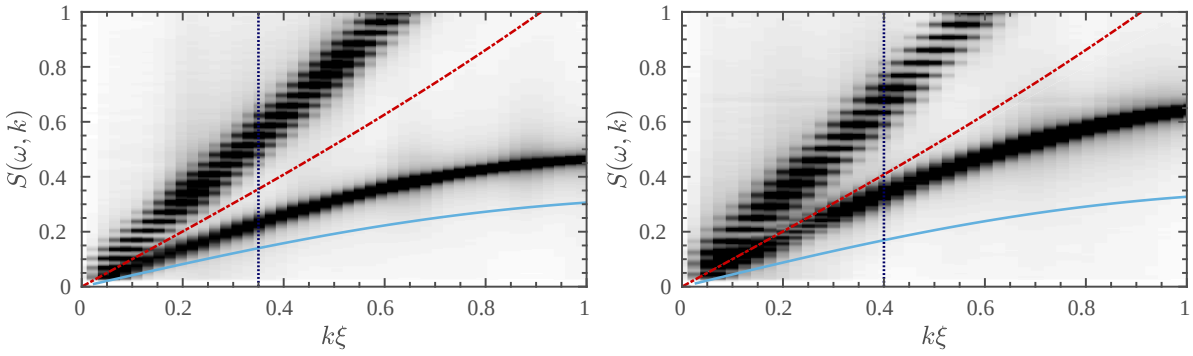

Figure 5.7: Dynamic structure factor $S(\omega, k)$ as obtained from the numerical simulation, for $N_0\xi = 0.35$ (left) and $N_0\xi = 0.4$(right). In both images, the solid line corresponds to the mode (3.16), plotted here with no adjustable parameters, while the top curve is compared against the Bogoliubov mode (dashed line), (2.54). The vertical dotted lines depicts the limit of the expected validity of the Vlasov equation (3.4), $k = N_0$.

Despite there being some consistency between theory and simulation, there are some aspects which escape a fully satisfactory explanation so far, such as the behaviour of the spectra for non-intermediate densities — specifically high-density $N_0\xi \lesssim 0.3$ when solitons are closer than $\sim 3\xi$ distance, fig. 5.7. At these densities, it is increasingly possible that higher order effects — such as three-soliton interaction — become non-negligible in our determination of the interaction potential, or even become dominant enough that the collision term in the Boltzmann equation, (2.77), becomes non-negligible.

Comparison with the Lieb-Liniger Model

The Lieb-Liniger (LL) model, as detailed in section 2.4, predicts two types of elementary excitations: one is identified with the phonon mode (type I excitation) which has been shown to be in close agreement with the Bogoliubov spectrum; and the other, type II excitation (or "hole" state), with less energetic than the type I excitation. This model is therefore quite compelling to compare to our spectra, for it presents a spectrum with two branches, fig. 2.3, much like the one-obtained in our numerical simulations, fig. 5.5, with a top branch similarly identified with a Bogoliubov mode and a bottom branch which has an established association with solitonic modes [55–58, 64]. Moreover, solitons are fermionic quasiparticles on top of a 1D Bose gas (a BEC in our case), much like the conditions of the type-II excitations in LL theory, which are also fermionic and borne on a 1D Bose gas with repulsive interactions. A good measure of the compatibility between the kinetic model and LL is the predicted critical point k_c^{LL} where the type-II branch "returns" to the momentum axis ($\omega = 0$), at $k_c^{LL} = 2k_F$, fig. 2.3. In order to compare this to our results, we investigated the critical k_c value at which the less-energetic curve in our spectra return to the $\omega = 0$ axis for different densities and obtained the linear fitting equation $k_c \approx (6.28 \pm 1.52 \times 10^{-4})N_0 + (2.31 \pm 5.77) \times 10^{-5}$, fig. 5.8.

The critical k_c^{LL} value in Lieb-Liniger theory is given by the expression (5.1) which is dependent on the Fermi wavevector k_F.

$$k_c^{LL} = 2k_F = 2\frac{\pi N}{L} = 2\pi N_0 \simeq 6.283 N_0 \tag{5.1}$$

Disregarding the value at zero (which is $\sim 10^{-5}$), we get $k_c \approx 6.28 N_0$ which in its full form is exactly equal to the expected LL critical k_c up to the fifth decimal place. So, short of a numerical comparison between the models, this extremely accurate prediction allows us to find evidence to support the connection between type-II excitations in the LL model and dark solitons.

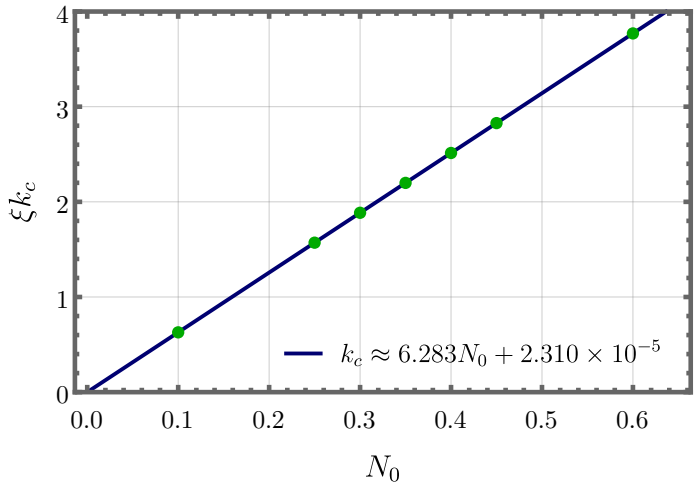

Figure 5.8: Fit of the critical wavevector value, k_c , at which point the lower curve in the spectra, fig. 3.2 returns to frequency zero.

The Tonks-Girardeau Gas

The Tonks-Girardeau gas, section 2.4, describes the state of a gas of hard-core bosons, i.e., interacting with infinite repulsion. This is, of course, a limit case, but which might still be relevant in order for one to understand further aspects of the soliton gas spectrum. The kinetic model developed in this thesis does lose its predictive nature for higher density systems, which leads one to consider that in such a case, if the model does fail due to the increasingly non-negligible interactions between particles, then eventually one may find themselves in a dense enough case (in which interaction is so dominant) that the Tonks-Girardeau limit becomes applicable. As such, we compare a few of our most dense situations, in this case a gas with $N_0\xi = 0.55$ and $N_0\xi = 0.6$ densities, both cases in which our theory has broken down, and compare them to the TG regime predictions, section 2.4.

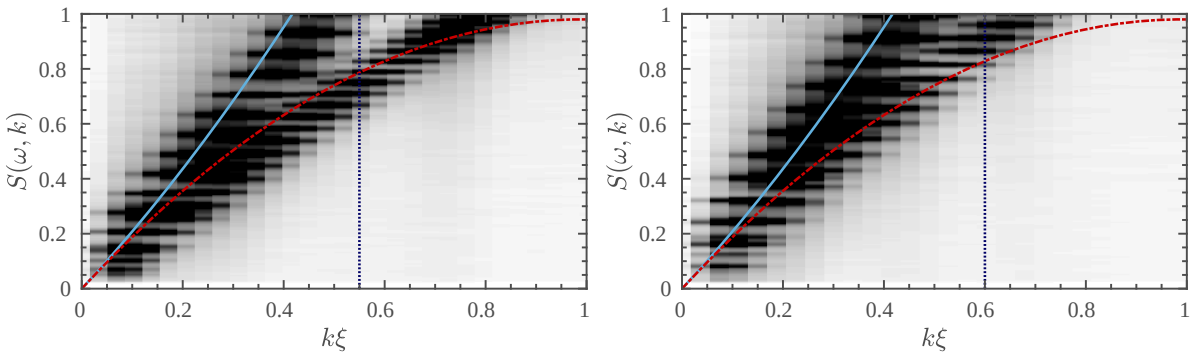

Figure 5.9: Comparison between the limit Tonks-Girardeau gas predictions and the soliton gas obtained spectrum for two density cases. Left: $N_0\xi = 0.55$; and Right: $N_0\xi = 0.6$.

The two spectra in fig. 5.9 superimpose the TG limit dispersion, (2.83), with our spectra; we may recognise that up until the reference line $N_0\xi = k\xi$ there is a rather satisfactory agreement between the two. And whilst this may not be enough to confidently make a connection between the TG regime and denser soliton gases, it does strengthen our hypothesis that the theory breaks down due to increasingly dominant soliton interaction terms.

Different Soliton Distribution Functions

When developing the kinetic model here proposed, we had at one point to postulate the soliton velocity distribution function (A.26), which was considered to be approximately a Heaviside function around zero with symmetric maxima at v_F. This was justified by the fermionisation of a gas of solitons, which would, in principle, make these particles evolve to such a configuration, even if they were initialised at rest.

But what if this initial assumption was wrong? What if the most correct soliton velocity distribution is, in fact, a dirac delta distribution around v, or even what if the correct result is actually a mix between these two modalities?

This question was promptly answered by developing new $\omega(k)$ dispersion for these two different possibilities for f_0. The comparison between different results can be seen in fig. 5.10, where it should

be noted that in the case the distribution is a mixture between the dirac delta and heaviside options, $f_0 = (N_0/2)\delta(v)+(N_0/4v_F)\Theta(v_F-|v|)$, the expression actually yields two positive results, corresponding to two modes in the spectrum.

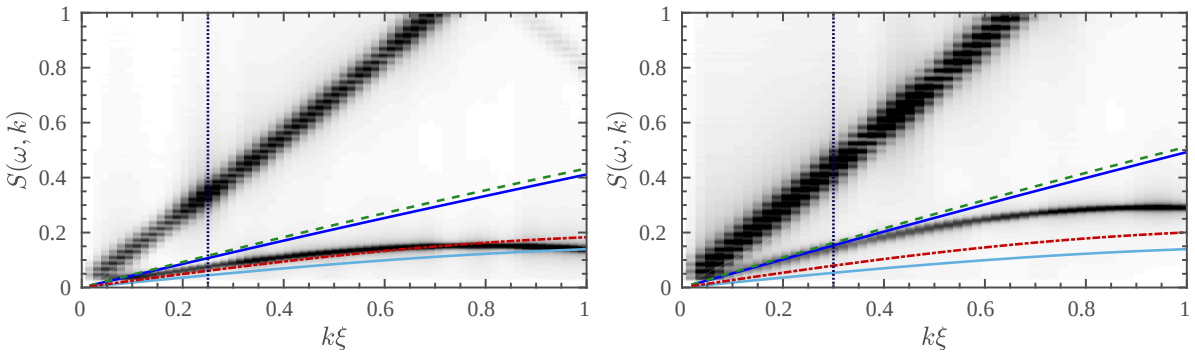

Figure 5.10: Dynamic structure factor $S(\omega, k)$ obtained from the numerical simulation, for $N_0\xi = 0.25$ (left) and $N_0\xi = 0.3$(right). Different curves represent different solutions resulting from the utilisation of different f_0 soliton velocity distributions. The dashed line corresponds to $f_0 = N_0/(2v_F)\Theta(|v| - v_F)$, the dotted-dashed line to a $f_0 = N_0\delta(v)$ and the two solid lines, both the less and more energetic modes correspond to the mixture between these two possibilities. The dotted line is the reference $k\xi = N_0\xi$.

These figures represent the full $\omega(k)$ spectra, corresponding to fig. 5.5, and the dotted line here represented is the exact same as the solid line in those figures. In general the different f_0 don not modify the spectra too drastically, but we do observe that the closest approximation is our first hypothesis, the $f_0 = \Theta(|v| - v_F)$ distribution which takes into account soliton fermionisation; the top mode from the distribution mixture is quite close the former, but can be excluded because we do only see one unique mode in the corresponding energy region, and not the two that this distribution predicts.

Chapter 6

Conclusions

In this work we set out to describe a gas of interacting solitons in a quantum fluid through a kinetic theory approach. Having laid the groundwork for this theory by exploring the statistical, quantum and finally kinetic formalisms needed to build and understand it, we relied on the Vlasov equation to illustrate the evolution of the one-soliton distribution function. Understanding the fermionic quality of solitons and assuming interactions under an ensemble-averaged pairwise potential we were able to develop that equation into a kinetic description of the phase-space evolution of a gas of dark solitons. The resulting equation presents a unique set of advantages in comparison with other approaches to the same issue, as it is an analytical description, which relies on the particles' statistical nature, and which is easily solvable, at least when compared with adjacent theories such as the Lieb-Liniger theory, which can only be solved numerically through the cumbersome Bethe-ansatz method, or even the very own Gross-Pitaevskii equation, which is solved numerically in this work.

This last consideration takes us into the second big undertaking of this thesis, which was the development of a computer code (based in C++ language) which solves the GP equation statistically an dynamically for virtually any specific case in one-dimension. The code is valid for any choice of applied external potential, allowing different sets of boundary conditions (homogeneous infinite systems or bounded trapped BECs are the most common) and allows one to introduce the soliton gas with any initial velocity distribution, and in any density configuration. It is also possible to introduce other excitations such as phonons, or to include more than one soliton gas (by introducing two or more sets of solitons at different group velocities). This extremely versatile code provided the backdrop — the numerical confirmation and visual materialisation — of the studied systems.

6.1 Achievements or a Summary of Results

From these two main endeavours we gleaned a few interesting results regarding the behaviour of soliton gases. We learned that the produced soliton gases, even if initialised completely cold, undergo fermionisation and we have observed how the interactions between the quasiparticles occur depending on their relative velocities; we have verified the Bogoliubv spectrum of excitations if, instead of a soliton

gas, a phonons gas is initialised; and to finalise we were able to produce the dynamical structure factors from the simulations' densities $|\Psi(x,t)|^2$ which allow us to observe the k-space spectra for any simulated system, and to compare our numerical results to the theoretical predictions from the developed model.

A substantial and interesting result is the observation of two modes in the spectra. An upper — more-energetic but less intense — mode, which is associated to the Bogoliubov BEC mode, but which shows weak agreement with the latter due to mode hybridisation with the second, lower mode — less-energetic but more distinguishable —- which is the one associated with solitons. The spectra shows good agreement between theory and numerics in the long wavelength region, where the validity of the Vlasov equation holds, even though the developed theory does break down in higher gas densities which imply soliton distances approaching the order of magnitude of ξ. Spectra for lower densities are harder to interpret, as the solitonic modes are less intense and take a much longer time to develop, which means the expression of otherwise negligible modes. Our spectra do have features in many ways similar to Lieb-Liniger theory, which, beside the two excitation branches depicting an upper acoustic mode and a lower solitonic mode, include a common critical wavevector k_c^{LL} value which is very accurately measured and consistent with this theory. The Tonks-Girardeau limit of infinite-strength interaction is also compared to find relative agreement to our spectra in the stronger densities after our model has broken down. Finally, experimentation with different solitonic velocity distribution functions confirms that a Heaviside-like distribution based on the recognition of naturally occurring fermionisation in the system is the most adequate and consistent with our results.

Filtering out these several results, the major takeaway of this work is the production of a kinetic equation for the description of a dark soliton gas, which shows consistency with the numerical description, even if still in a density limited domain. This is the description may mean further significant knowledge of the physics of strong quantum turbulence in low-dimensional quantum fluids.

6.2 Future Work

This work is actually quite ripe with ideas for future work. Some of which were actually thought of during the development of the work, but would either imply a whole new thesis or were avenues that didn't yield results right away and were discarded for a later time or a deeper investigation.

In terms of finding a better agreement between our model and the obtained spectra, a considered option was to study the Casimir effect, as a force which could arise between two solitons in the BEC, with a few phonon-like or small excitations in between; the solitons would act as Casimir plates being pushed together due to the small quantum fluctuations, even though the influence of this effect could potentially be small. Undeniably, the interaction between solitons and phonons should provide a correction to our results. Another idea is the consideration of higher order terms in the soliton interaction potential, or not neglecting the collision integral in the Vlasov equation. This work contemplates only two-body interaction, and corrections to this term could mean a higher consistency of the model to bigger densities; Three-body interactions, however, produce a Hamiltonian which involves quite cumbersome integrations and this would entail a longer mathematical study to solve. It would also be interesting to fully solve the

Lieb-Liniger equations for a full spectra, in order to compare it to our own and be able to fully establish the compatibility between these theories. IMoreover, the developed programme allows freedom to explore other investigation avenues. For example investigating the interaction between more than one interacting soliton gases, and possibly watching the appearance of other interaction modes and instabilities in the spectra. Control over the number of solitons is also conducive to statistical studies, such as getting a better measure of the system fermionisation procedure.

Bibliography

[1] R. Feynman, R. Leighton, and M. Sands. *The Feynman Lectures on Physics*. The Feynman Lectures on Physics. Addison-Wesley, 1964.

[2] M. S. Paoletti and D. P. Lathrop. Quantum turbulence. *Annual Review of Condensed Matter Physics*, 2:213–234, 2011. ISSN 1947-5454. doi: 10.1146/annurev-conmatphys-062910-140533. URL https://doi.org/10.1146/annurev-conmatphys-062910-140533.

[3] M. I. Shaukat, E. V. Castro, and H. Terças. Quantum dark solitons as qubits in bose-einstein condensates. *Physical Review A*, 95:053618, 5 2017. ISSN 2469-9926. doi: 10.1103/PhysRevA.95.053618. URL https://link.aps.org/doi/10.1103/PhysRevA.95.053618,http://link.aps.org/doi/10.1103/PhysRevA.95.053618.

[4] N. G. Parker, A. J. Allen, C. F. Barenghi, and N. P. Proukakis. *A quantum storm in a teacup*, chapter 1, pages 1–23. Cambridge University Press, 2015.

[5] C. F. Barenghi, L. Skrbek, and K. R. Sreenivasan. Introduction to quantum turbulence. *Proceedings of the National Academy of Sciences of the United States of America*, 111:4647–4652, 3 2014. ISSN 1091-6490. doi: 10.1073/pnas.1400033111. URL http://www.ncbi.nlm.nih.gov/pubmed/24704870,http://www.pubmedcentral.nih.gov/articlerender.fcgi?artid=PMC3970860,https://arxiv.org/abs/1404.1909.

[6] L. Madeira, M. A. Caracanhas, F. E. A. dos Santos, and V. S. Bagnato. Quantum Turbulence in Quantum Gases. *Annual Review of Condensed Matter Physics*, 11(1):37–56, 2020. doi: 10.1146/annurev-conmatphys-031119-050821. URL https://doi.org/10.1146/annurev-conmatphys-031119-050821.

[7] S. Inouye, M. R. Andrews, J. Stenger, H.-J. Miesner, D. M. Stamper-Kurn, and W. Ketterle. Observation of Feshbach resonances in a Bose–Einstein condensate. *Nature*, 392(6672):151–154, 1998. ISSN 1476-4687. doi: 10.1038/32354. URL https://doi.org/10.1038/32354.

[8] A. Gorlitz, J. M. Vogels, A. E. Leanhardt, C. Raman, T. L. Gustavson, J. R. Abo-Shaeer, A. P. Chikkatur, S. Gupta, S. Inouye, T. P. Rosenband, D. E. Pritchard, and W. Ketterle. Realization of Bose-Einstein condensates in lower dimensions. *Physical Review Letters*, 87(13):130402/1–130402/4, apr 2001. ISSN 00319007. doi: 10.1103/PhysRevLett.87.130402. URL http://arxiv.org/abs/cond-mat/0104549,http://dx.doi.org/10.1103/PhysRevLett.87.130402.

[9] M. H. Anderson, J. R. Ensher, M. R. Matthews, C. E. Wieman, and E. A. Cornell. Observation of bose-einstein condensation in a dilute atomic vapor. *Science (New York, N.Y.)*, 269:198–201, 7 1995. ISSN 0036-8075. doi: 10.1126/science.269.5221.198. URL http://www.ncbi.nlm.nih.gov/pubmed/17789847,http://science.sciencemag.org/content/269/5221/198.

[10] R. P. Feynman. *Chapter II Application of Quantum Mechanics to Liquid Helium*, volume 1, pages 17–53. Elsevier, 1955. ISBN 9780444533074. doi: 10.1016/S0079-6417(08)60077-3. URL http://www.sciencedirect.com/science/article/pii/S0079641708600773.

[11] M. Kobayashi and M. Tsubota. Quantum turbulence in a trapped bose-einstein condensate. *Phys. Rev. A*, 76:45603, 10 2007. ISSN 10502947. doi: 10.1103/PhysRevA.76.045603. URL https://link.aps.org/doi/10.1103/PhysRevA.76.045603.

[12] N. G. Parker and C. S. Adams. Emergence and decay of turbulence in stirred atomic bose-einstein condensates. *Phys. Rev. Lett.*, 95:145301, 9 2005. ISSN 0031-9007. doi: 10.1103/PhysRevLett.95.145301. URL https://link.aps.org/doi/10.1103/PhysRevLett.95.145301.

[13] M. Tsubota and M. Kobayashi. Quantum turbulence in trapped atomic bose-einstein condensates. In *Journal of Low Temperature Physics*, volume 150, pages 402–409, 2 2008. doi: 10.1007/s10909-007-9560-1. URL https://doi.org/10.1007/s10909-007-9560-1.

[14] A. J. Allen, N. G. Parker, N. P. Proukakis, and C. F. Barenghi. Quantum turbulence in atomic bose-einstein condensates. *Journal of Physics: Conference Series*, 544:12023, 10 2014. ISSN 1742-6588. doi: 10.1088/1742-6596/544/1/012023. URL http://stacks.iop.org/1742-6596/544/i=1/a=012023http://stacks.iop.org/1742-6596/544/i=1/a=012023?key=crossref.f4e89a1c503e60d68c207fead5a5aeba.

[15] M. Tsubota. Quantum hydrodynamics and turbulence in atomic bose-einstein condensates. In *Frontiers in Optics 2014*. OSA, 10 2014. ISBN 1-55752-286-3. doi: 10.1364/LS.2014.LTu1H.1. URL https://www.osapublishing.org/abstract.cfm?URI=LS-2014-LTu1H.1.

[16] A. C. White, N. P. Proukakis, A. J. Youd, D. H. Wacks, A. W. Baggaley, and C. F. Barenghi. Turbulence in a bose-einstein condensate. *Journal of Physics: Conference Series*, 318:62003, 12 2011. ISSN 1742-6596. doi: 10.1088/1742-6596/318/6/062003. URL http://stacks.iop.org/1742-6596/318/i=6/a=062003?key=crossref.199ac3d4f6b1057ac155aa1aff19cdc3.

[17] A. C. White, C. F. Barenghi, N. P. Proukakis, A. J. Youd, and D. H. Wacks. Nonclassical Velocity Statistics in a Turbulent Atomic Bose-Einstein Condensate. *Physical Review Letters*, 104 (7):075301, feb 2010. ISSN 0031-9007. doi: 10.1103/PhysRevLett.104.075301. URL https://link.aps.org/doi/10.1103/PhysRevLett.104.075301.

[18] M. Kobayashi and M. Tsubota. Kolmogorov Spectrum of Superfluid Turbulence: Numerical Analysis of the Gross-Pitaevskii Equation with a Small-Scale Dissipation. *Physical Review Letters*, 94(6):065302, feb 2005. ISSN 0031-9007. doi: 10.1103/PhysRevLett.94.065302. URL https://link.aps.org/doi/10.1103/PhysRevLett.94.065302.

[19] T. Araki, M. Tsubota, and S. K. Nemirovskii. Energy Spectrum of Superfluid Turbulence with No Normal-Fluid Component. *Physical Review Letters*, 89(14):145301, sep 2002. ISSN 0031-9007. doi: 10.1103/PhysRevLett.89.145301. URL https://link.aps.org/doi/10.1103/PhysRevLett.89.145301.

[20] L. P. Pitaevskii and S. Stringari. *Bose-Einstein Condensation*. Oxford University Press, 2003.

[21] L. F. Yin. *Analytical and numerical studies of Bose-Einstein condensates*. PhD thesis, National University of Singapore, 2008. URL http://scholarbank.nus.edu.sg/handle/10635/16603.

[22] T. David. Statistical physics. Lectures Notes: Part II Mathematical Tripos, 2012 and 2013. URL http://www.damtp.cam.ac.uk/user/tong/statphys.html.

[23] F. Dalfovo, L. Pitaevskii, and S. Stringari. Bose einstein condensates. *Uspekhi Fizicheskikh Nauk - USP FIZ NAUK*, 167, 2005. doi: 10.3367/UFNr.0167.199706d.0649. URL https://www.researchgate.net/publication/228849160_Bose_Einstein_Condensates.

[24] D. Tong. Quantum field theory. Lecture Notes: Part III Mathematical Tripos, 2006 and 1007. URL http://www.damtp.cam.ac.uk/user/tong/qft.html.

[25] W. Bao. Mathematical models and numerical methods for bose-einstein condensation. *ArXiv e-prints*, 3 2014. URL https://arxiv.org/abs/1403.3884.

[26] P. L. Krapivsky, S. Redner, and E. Ben-Naim. *A Kinetic View of Statistical Physics*. Cambridge University Press, 2010. ISBN 9780511780516. doi: 10.1017/CBO9780511780516. URL http://ebooks.cambridge.org/ref/id/CBO9780511780516.

[27] W. Bao and Y. Cai. Mathematical theory and numerical methods for bose-einstein condensation. *ArXiv e-prints*, 6:1–135, 12 2012. ISSN 19375093. doi: 10.3934/krm.2013.6.1. URL http://arxiv.org/abs/1212.5341,http://dx.doi.org/10.3934/krm.2013.6.1.

[28] P. G. Kevrekidis, D. J. Frantzeskakis, and R. Carretero-González. *Basic Mean-Field Theory for Bose-Einstein Condensates*. Springer Berlin Heidelberg, 2008. ISBN 978-3-540-73591-5. doi: 10.1007/978-3-540-73591-5_1. URL https://doi.org/10.1007/978-3-540-73591-5_1,http://link.springer.com/10.1007/978-3-540-73591-5_1.

[29] F. V. Pepe. *Bose-Einstein condensation: static and dynamical aspects*. PhD thesis, Università degli studi di Bari Aldo Moro, 2013. URL http://www.infn.it/thesis/PDF/getfile.php?filename=8684-Pepe-dottorato.pdf.

[30] S. Stringari. Collective excitations of a trapped bose-condensed gas. *Physical Review Letters*, 77:2360–2363, 9 1996. ISSN 0031-9007. doi: 10.1103/PhysRevLett.77.2360. URL https://link.aps.org/doi/10.1103/PhysRevLett.77.2360.

[31] I. F. Barna, M. A. Pocsai, and L. Mátyás. Analytic solutions of the Madelung equation. *Journal of Generalized Lie Theory and Applications*, 11(2), mar 2017. ISSN 17364337. doi: 10.4172/1736-4337.1000271. URL http://arxiv.org/abs/1703.10482.

[32] C. J. Pethick and H. Smith. *Bose–Einstein Condensation in Dilute Gases*. Cambridge University Press, 2nd edition, 2008. ISBN 9780511802850. doi: 10.1017/CBO9780511802850. URL http://ebooks.cambridge.org/ref/id/CBO9780511802850.

[33] M. R. Andrews, D. M. Kurn, H.-J. J. Miesner, D. S. Durfee, C. G. Townsend, S. Inouye, and W. Ketterle. Propagation of sound in a bose-einstein condensate. *Physical Review Letters*, 79:553–556, 7 1997. ISSN 10797114. doi: 10.1103/PhysRevLett.79.553. URL https://link.aps.org/doi/10.1103/PhysRevLett.79.553.

[34] R. Balakrishnan and I. I. Satija. Solitons in bose–einstein condensates. *Pramana - Journal of Physics*, 77:929–947, 12 2011. ISSN 0304-4289. doi: 10.1007/s12043-011-0187-z. URL http://link.springer.com/10.1007/s12043-011-0187-z.

[35] R. Meppelink, S. B. Koller, and P. van der Straten. Sound propagation in a bose-einstein condensate at finite temperatures. *Physical Review A - Atomic, Molecular, and Optical Physics*, 80:1–7, 9 2009. ISSN 10502947. doi: 10.1103/PhysRevA.80.043605. URL http://arxiv.org/abs/0909.3455, http://dx.doi.org/10.1103/PhysRevA.80.043605.

[36] T. D. Lee, K. Huang, and C. N. Yang. Eigenvalues and eigenfunctions of a bose system of hard spheres and its low-temperature properties. *Physical Review*, 106:1135–1145, 6 1957. ISSN 0031-899X. doi: 10.1103/PhysRev.106.1135. URL https://link.aps.org/doi/10.1103/PhysRev.106.1135.

[37] V. V. Konotop. Dark solitons in bose-einstein condensates: Theory. *Emergent Nonlinear Phenomena in Bose-Einstein Condensates: Theory and Experiment*, 45:65, 2008. doi: 10.1007/978-3-540-73591-5_4. URL http://www.springerlink.com/content/h47033234971111x/fulltext.pdf,https://doi.org/10.1007/978-3-540-73591-5_4.

[38] E. Zaremba. Sound propagation in a cylindrical bose-condensed gas. *Physical Review A - Atomic, Molecular, and Optical Physics*, 57:518–521, 1998. ISSN 10941622. doi: 10.1103/PhysRevA.57.518.

[39] G. M. Kavoulakis and C. J. Pethick. Quasi-one-dimensional character of sound propagation in elongated bose-einstein condensed clouds. *Physical Review A - Atomic, Molecular, and Optical Physics*, 58:1563–1566, 1998. ISSN 10941622. doi: 10.1103/PhysRevA.58.1563.

[40] Y. S. Kivshar and B. Luther-Davies. Dark optical solitons: physics and applications. *Physics Reports*, 298:81–197, 5 1998. ISSN 0370-1573. doi: https://doi.org/10.1016/S0370-1573(97)00073-2. URL http://www.sciencedirect.com/science/article/pii/S0370157397000732, https://www.sciencedirect.com/science/article/pii/S0370157397000732.

[41] B. P. Anderson, P. C. Haljan, C. A. Regal, D. L. Feder, L. A. Collins, C. W. Clark, and E. A. Cornell. Watching dark solitons decay into vortex rings in a bose-einstein condensate. *Phys. Rev. Lett.*, 86:2926–2929, 4 2001. doi: 10.1103/PhysRevLett.86.2926. URL https://link.aps.org/doi/10.1103/PhysRevLett.86.2926.

[42] H. L. C. L. C. Couto and W. B. B. Cardoso. Dark soliton in quasi-one-dimensional bose-einstein condensates with a gaussian trap. *ArXiv e-prints*, pages 1–7, 11 2013. URL https://arxiv.org/abs/1311.2087.

[43] B. Jackson, N. P. Proukakis, and C. F. Barenghi. Dark-soliton dynamics in bose-einstein condensates at finite temperature. *Phys. Rev. A*, 75:51601, 5 2007. ISSN 1050-2947. doi: 10.1103/PhysRevA.75.051601. URL https://link.aps.org/doi/10.1103/PhysRevA.75.051601,https://journals.aps.org/pra/pdf/10.1103/PhysRevA.75.051601,https://arxiv.org/abs/cond-mat/0612218.

[44] N. G. Parker, N. P. Proukakis, and C. S. Adams. Dark soliton decay due to trap anharmonicity in atomic bose-einstein condensates. *Phys. Rev. A*, 81:33606, 3 2010. ISSN 10502947. doi: 10.1103/PhysRevA.81.033606. URL https://link.aps.org/doi/10.1103/PhysRevA.81.033606.

[45] S. Burger, K. Bongs, S. Dettmer, W. Ertmer, K. Sengstock, A. Sanpera, G. V. Shlyapnikov, and M. Lewenstein. Dark solitons in bose-einstein condensates. *Physical Review Letters*, October 1999. doi: 10.1103/PhysRevLett.83.5198. URL http://arxiv.org/abs/cond-mat/9910487, http://dx.doi.org/10.1103/PhysRevLett.83.5198.

[46] M. Sciacca, C. F. Barenghi, N. G. Parker, C. F. Barenghi, and N. G. Parker. Matter-wave dark solitons in box-like traps. *Physical Review A*, 95:13628, 2017. ISSN 24699934. doi: 10.1103/PhysRevA.95.013628.

[47] C. B. Prieto. Dark solitary waves in 1d bose-einstein condensates. In *Treballs Finals de Grau (TFG) - Física*, 2016. URL http://hdl.handle.net/2445/102763,http://diposit.ub.edu/dspace/bitstream/2445/102763/1/TFG_%20FIS_Bravo_Prieto_Carlos.pdf. Facultat de Física, Universitat de Barcelona.

[48] V. A. A. Brazhnyi, V. V. V. Konotop, and L. P. P. Pitaevskii. Dark solitons as quasiparticles in trapped condensates. *Physical Review A - Atomic, Molecular, and Optical Physics*, 73:1–14, 5 2006. ISSN 10941622. doi: 10.1103/PhysRevA.73.053601. URL https://link.aps.org/doi/10.1103/PhysRevA.73.053601.

[49] H. M. Hurst, D. K. Efimkin, I. B. Spielman, and V. Galitski. Kinetic theory of dark solitons with tunable friction. *Physical Review A*, 95:1–12, 2017. ISSN 24699934. doi: 10.1103/PhysRevA.95.053604.

[50] H. Terças, D. D. D. Solnyshkov, and G. Malpuech. Topological wigner crystal of half-solitons in a spinor bose-einstein condensate. *Physical Review Letters*, 110:35303, 1 2013. doi: 10.1103/PhysRevLett.110.035303. URL http://adsabs.harvard.edu/abs/2013PhRvL.110c5303T.

[51] D. Tong. Kinetic theory. Lecture Notes: Graduate Course on Kinetic Theory, 2012. URL http://www.damtp.cam.ac.uk/user/tong/kinetic.html.

[52] E. H. Lieb and W. Liniger. Exact analysis of an interacting bose gas. i. the general solution and the ground state. *Physical Review*, 130:1605–1616, 1963. ISSN 0031899X. doi: 10.1103/PhysRev.130.1605.

[53] E. H. Lieb. Exact analysis of an interacting bose gas. ii. the excitation spectrum. *Physical Review*, 130:1616–1624, 1963. ISSN 0031899X. doi: 10.1103/PhysRev.130.1616.

[54] S. S. Shamailov and J. Brand. Quantum dark solitons in the one-dimensional bose gas. *arXiv e-prints*, 99:arXiv:1805.07856, 5 2018. ISSN 24699934. doi: 10.1103/PhysRevA.99.043632.

[55] G. Lang, F. Hekking, and A. Minguzzi. Ground-state energy and excitation spectrum of the lieb-liniger model : accurate analytical results and conjectures about the exact solution. *SciPost Physics*, 3:003, 9 2017. ISSN 2542-4653. doi: 10.21468/scipostphys.3.1.003. URL `http://arxiv.org/abs/1609.08865http://dx.doi.org/10.21468/SciPostPhys.3.1.003`, `https://scipost.org/10.21468/SciPostPhys.3.1.003`.

[56] M. Ishikawa and H. Takayama. Solitons in a one-dimensional bose system with the repulsive delta-function interaction. *Journal of the Physical Society of Japan*, 49:1242–1246, 10 1980. ISSN 0031-9015. doi: 10.1143/JPSJ.49.1242. URL `http://journals.jps.jp/doi/10.1143/JPSJ.49.1242`.

[57] J. Sato, R. Kanamoto, E. Kaminishi, and T. Deguchi. Quantum dark solitons in the 1d bose gas and the superfluid velocity. *Proceedings of the 20th USENIX Security Symposium*, pages 1–5, 4 2012. URL `http://arxiv.org/abs/1204.3960`.

[58] R. Kanamoto, L. D. Carr, and M. Ueda. Metastable quantum phase transitions in a periodic one-dimensional bose gas. ii. many-body theory. *Physical Review A - Atomic, Molecular, and Optical Physics*, 81:1–14, 2010. ISSN 10502947. doi: 10.1103/PhysRevA.81.023625.

[59] N. Fabbri, M. Panfil, D. Clément, L. Fallani, M. Inguscio, C. Fort, and J.-S. Caux. Revealing elementary excitations of one-dimensional bose gases through their dynamical structure factor. *Physical Review A - Atomic, Molecular, and Optical Physics*, 91:1–5, 6 2014. doi: 10.1103/PhysRevA.91.043617. URL `http://arxiv.org/abs/1406.2176`.

[60] J. S. Caux and P. Calabrese. Dynamical density-density correlations in the one-dimensional bose gas. *Physical Review A - Atomic, Molecular, and Optical Physics*, 74:1–4, 2006. ISSN 10502947. doi: 10.1103/PhysRevA.74.031605.

[61] Z. Ristivojevic. Excitation spectrum of the lieb-liniger model. *Physical Review Letters*, 113:1–6, 2014. ISSN 10797114. doi: 10.1103/PhysRevLett.113.015301.

[62] L. Pollet, S. M. Rombouts, and P. J. Denteneer. Ultracold atoms in one-dimensional optical lattices approaching tonnks-girardeau regime. *Physical Review Letters*, 93, 2004. ISSN 00319007. doi: 10.1103/PhysRevLett.93.210401.

[63] V. Guarrera, D. Muth, R. Labouvie, A. Vogler, G. Barontini, M. Fleischhauer, and H. Ott. Spatiotemporal fermionization of strongly interacting one-dimensional bosons. *Physical Review A*, 86(2):021601, aug 2012. ISSN 1050-2947. doi: 10.1103/PhysRevA.86.021601. URL `https://link.aps.org/doi/10.1103/PhysRevA.86.021601`.

[64] T. Karpiuk, T. Sowiński, M. Gajda, K. Rzazewski, and M. Brewczyk. Correspondence between dark solitons and the type ii excitations of the lieb-liniger model. *Physical Review A - Atomic, Molecular, and Optical Physics*, 91:1–5, 2015. ISSN 10941622. doi: 10.1103/PhysRevA.91.013621.

[65] P. Bader, S. Blanes, and F. Casas. Solving the schrödinger eigenvalue problem by the imaginary time propagation technique using splitting methods with complex coefficients. *The Journal of Chemical Physics*, 139:124117, 2013. doi: 10.1063/1.4821126. URL http://adsabs.harvard.edu/abs/2013JChPh.13914117B,https://doi.org/10.1063/1.4821126.

[66] W. Bao. The nonlinear schrodinger equation and applications in bose-einstein condensation and plasma physics. *Dynamics in models of coarsening, coagulation, condensation and quantization*, 9:141, 2007. doi: 10.1142/9789812770226_0003.

[67] W. B. Xavier Antoine and C. Besse. Computational methods for the dynamics of the nonlinear schrödinger/gross–pitaevskii equations. *Computer Physics Communications*, 184:2621–2633, 12 2013. ISSN 0010-4655. doi: 10.1016/J.CPC.2013.07.012. URL https://www.sciencedirect.com/science/article/pii/S0010465513002403,http://www.sciencedirect.com/science/article/pii/S0010465513002403.

[68] W. Bao and Q. Du. Computing the ground state solution of bose-einstein condensates by a normalized gradient flow. *Society*, 25:1674–1697, 3 2003. URL http://arxiv.org/abs/cond-mat/0303241.

[69] W. Bao, D. Jaksch, and P. A. Markowich. Numerical solution of the gross-pitaevskii equation for bose-einstein condensation. *Journal of Computational Physics*, 187:318–342, 3 2003. ISSN 00219991. doi: 10.1016/s0021-9991(03)00102-5. URL https://arxiv.org/abs/cond-mat/0303239.

[70] W. Bao, S. Jin, and P. A. Markowich. On time-splitting spectral approximations for the schrödinger equation in the semiclassical regime. *Journal of Computational Physics*, 175:487–524, 2002. ISSN 0021-9991. doi: 10.1006/jcph.2001.6956. URL http://www.sciencedirect.com/science/article/pii/S0021999101969566.

[71] M. Dehghan and A. Taleei. A compact split-step finite difference method for solving the nonlinear schrödinger equations with constant and variable coefficients. *Computer Physics Communications*, 181:43–51, 2009. ISSN 00104655. doi: 10.1016/j.cpc.2009.08.015. URL http://www.sciencedirect.com/science/article/pii/S0010465509002768,https://linkinghub.elsevier.com/retrieve/pii/S0010465509002768.

[72] X. Antoine and R. Duboscq. Gpelab, a matlab toolbox to solve gross-pitaevskii equations i: Computation of stationary solutions. *Computer Physics Communications*, 185:2969–2991, 11 2014. ISSN 00104655. doi: 10.1016/j.cpc.2014.06.026. URL https://www.sciencedirect.com/science/article/pii/S0010465514002318?via%3Dihub.

[73] W. Bao, Q. Tang, and Z. Xu. Numerical methods and comparison for computing dark and bright solitons in the nonlinear schrödinger equation. *Journal of Computational Physics*, 235:423–445, 2013. ISSN 0021-9991. doi: https://doi.org/10.1016/j.jcp.2012.10.054. URL http://dx.doi.org/10.1016/j.jcp.2012.10.054http://www.sciencedirect.com/science/article/pii/S0021999112006602.

[74] K. K. HarpindervKaur and H. HarpinderKaur. Convergence of jacobi and gauss-seidel method and error reduction factor. *IOSR Journal of Mathematics*, 2:20–23, 2012. ISSN 2319765X. doi: 10.9790/5728-0222023.

[75] Y. Y. Choy, W. N. Tan, K. G. Tay, and C. T. Ong. Crank-nicolson implicit method for the nonlinear schrodinger equation with variable coefficient. In *AIP Conference Proceedings*, volume 1605, pages 76–82, 2014. doi: 10.1063/1.4887568. URL https://aip.scitation.org/doi/abs/10.1063/1.4887568http://aip.scitation.org/doi/abs/10.1063/1.4887568.

[76] A. de Freitas Smaira. Dinâmica de um condensado de bose-eintein contendo sólitons. Master's thesis, Universidade de São Paulo, February 2015. URL http://www.teses.usp.br/teses/disponiveis/76/76132/tde-02042015-170017/.

[77] T. Busch and J. R. R. Anglin. Mossbauer effect for dark solitons in bose-einstein condensates. *arXiv e-prints*, 1998. URL http://arxiv.org/abs/cond-mat/9809408.

[78] J. Denschlag, J. E. Simsarian, D. L. Feder, C. W. Clark, L. A. Collins, J. Cubizolles, L. Deng, E. W. Hagley, K. Helmerson, W. P. Reinhardt, S. L. Rolston, B. I. Schneider, and W. D. Phillips. Generating solitons by phase engineering of a bose-einstein condensate. *Science*, 287:97–101, 2000. ISSN 0036-8075. doi: 10.1126/science.287.5450.97. URL https://science.sciencemag.org/content/287/5450/97.

[79] A. M. Kamchatnov and M. Salerno. Dark soliton oscillations in bose–einstein condensates with multi-body interactions. *Journal of Physics B: Atomic, Molecular and Optical Physics*, 42:185303, 9 2009. ISSN 0953-4075. doi: 10.1088/0953-4075/42/18/185303. URL http://stacks.iop.org/0953-4075/42/i=18/a=185303?key=crossref.0d873af1bc1c7f3a333e842d4a2a48d0.

[80] T. Busch and J. R. Anglin. Motion of dark solitons in trapped bose-einstein condensates. *Physical Review Letters*, 84:2298–2301, 2000. ISSN 10797114. doi: 10.1103/PhysRevLett.84.2298.

[81] T. Busch and J. R. Anglin. Dark-bright solitons in inhomogeneous bose-einstein condensates. *Physical Review Letters*, 87:010401/1–010401/4, 2001. ISSN 00319007. doi: 10.1103/physrevlett.87.010401.

Appendix A

Derivations and extra calculations

A.1 Applying the Heisenberg equation to the rare Bose gas hamiltonian to obtain a nonlinear Schrödinger - type equation

- $[\hat{\Psi}(\boldsymbol{r},t),\hat{\Psi}^{\dagger}(\boldsymbol{r}',t)]=\delta(\boldsymbol{r}-\boldsymbol{r}')\,;\quad [\hat{\Psi}(\boldsymbol{r},t),\hat{\Psi}'(\boldsymbol{r}',t)]=0$ (A.1)
- $\hat{H}=\frac{\hbar^2}{2m}\int(-\hat{\Psi}^{\dagger}\boldsymbol{\nabla}^2\hat{\Psi})d\boldsymbol{r}+\int\hat{\Psi}^{\dagger}V_{\text{ext}}\hat{\Psi}dx+\frac{1}{2}\int\hat{\Psi}^{\dagger}\hat{\Psi}^{\dagger'}V(\boldsymbol{r}'-\boldsymbol{r})\hat{\Psi}\hat{\Psi}'d\boldsymbol{r}'d\boldsymbol{r}\equiv\hat{A}+\hat{B}+\hat{C}$ (A.2)

$$i\hbar\frac{\partial\hat{\Psi}}{\partial t}=[\hat{\Psi},\hat{H}]\equiv[\hat{\Psi}'',\hat{A}]+[\hat{\Psi}'',\hat{B}]+[\hat{\Psi}'',\hat{C}] \tag{A.3}$$

$$\begin{aligned}[\hat{\Psi}'',\hat{A}]&=-\frac{\hbar^2}{2m}\int[\hat{\Psi}'',\hat{\Psi}^{\dagger}\boldsymbol{\nabla}^2\hat{\Psi}]dr=-\frac{\hbar^2}{2m}\int([\hat{\Psi}'',\hat{\Psi}^{\dagger}]\boldsymbol{\nabla}^2\hat{\Psi}+\hat{\Psi}^{\dagger}[\hat{\Psi}'',\boldsymbol{\nabla}^2\hat{\Psi}])dr=\\&=-\frac{\hbar^2}{2m}\int(\boldsymbol{\nabla}^2\hat{\Psi}\delta(r''-r)+\hat{\Psi}^{\dagger}\hat{\Psi}''\boldsymbol{\nabla}^2\hat{\Psi}-\hat{\Psi}^{\dagger}(\boldsymbol{\nabla}^2\hat{\Psi})\hat{\Psi}'')dr\\&=-\frac{\hbar^2}{2m}\left(\boldsymbol{\nabla}^2\hat{\Psi}''+\int\boldsymbol{\nabla}^2\hat{\Psi}[\hat{\Psi}^{\dagger}\hat{\Psi}''-\hat{\Psi}^{\dagger}\hat{\Psi}'']\right)dr\\&=-\frac{\hbar^2}{2m}\boldsymbol{\nabla}^2\hat{\Psi}''\end{aligned} \tag{A.4}$$

$$\begin{aligned}[\hat{\Psi}'',\hat{B}]&=\int[\hat{\Psi}'',\hat{\Psi}^{\dagger}V_{\text{ext}}\hat{\Psi}]dr=\\&=\int([\hat{\Psi}'',\hat{\Psi}^{\dagger}]V_{\text{ext}}\hat{\Psi}+\hat{\Psi}^{\dagger}[\hat{\Psi}'',V_{\text{ext}}]\hat{\Psi}+\hat{\Psi}^{\dagger}V_{\text{ext}}[\hat{\Psi}'',\hat{\Psi}])dr=\\&=V_{\text{ext}}\hat{\Psi}''+\int[\hat{\Psi}^{\dagger}\hat{\Psi}''V_{\text{ext}}\hat{\Psi}-\hat{\Psi}^{\dagger}V_{\text{ext}}\hat{\Psi}''\hat{\Psi}]dr=\\&=V_{\text{ext}}\hat{\Psi}''\end{aligned} \tag{A.5}$$

$$
\begin{aligned}
[\hat{\Psi}'', \hat{C}] &= \frac{1}{2}\int [\hat{\Psi}'', \hat{\Psi}^\dagger \hat{\Psi}^{\dagger\prime} V(r'-r)\hat{\Psi}\hat{\Psi}']dr'dr = \\
&= \frac{1}{2}\int ([\hat{\Psi}'', \hat{\Psi}^\dagger]\hat{\Psi}^{\dagger\prime} V(r'-r)\hat{\Psi}\hat{\Psi}' + \hat{\Psi}^\dagger[\hat{\Psi}'', \hat{\Psi}^{\dagger\prime}]V(r'-r)\hat{\Psi}\hat{\Psi}' + \hat{\Psi}^\dagger\hat{\Psi}^{\dagger\prime}[\hat{\Psi}'', V(r'-r)]\hat{\Psi}\hat{\Psi}' + \\
&+ \hat{\Psi}^\dagger\hat{\Psi}^{\dagger\prime} V(r'-r)[\hat{\Psi}'', \hat{\Psi}]\hat{\Psi}' + \hat{\Psi}^\dagger\hat{\Psi}^{\dagger\prime} V(r'-r)\hat{\Psi}[\hat{\Psi}'', \hat{\Psi}'])drdr' = \\
&= \frac{1}{2}\left[\int \hat{\Psi}^{\dagger\prime} V(r'-r'')\hat{\Psi}''\hat{\Psi}'dr' + \int \hat{\Psi}^\dagger V(r''-r)\hat{\Psi}\hat{\Psi}''dr\right] = \\
&= \frac{1}{2}\int \hat{\Psi}^{\dagger\prime} V(r'-r)\hat{\Psi}\hat{\Psi}'dr' + \frac{1}{2}\int \hat{\Psi}^\dagger V(r'-r)\hat{\Psi}\hat{\Psi}'dr = \\
&= \frac{1}{2}\int \hat{\Psi}^{\dagger\prime} V(r'-r)\hat{\Psi}\hat{\Psi}'dr' + \frac{1}{2}\int \hat{\Psi}^\dagger V(r'-r)\hat{\Psi}\hat{\Psi}'dr = \\
&= \left[\int \hat{\Psi}^{\dagger\prime} V(r'-r)\hat{\Psi}'dr'\right]\hat{\Psi};\ \text{with } V(r'-r) = V(r-r') \quad \text{Symmetric external potential.}
\end{aligned} \tag{A.6}
$$

$$
\begin{aligned}
\Rightarrow \quad i\hbar\frac{\partial\hat{\Psi}}{\partial t} &= -\frac{\hbar^2}{2m}\boldsymbol{\nabla}^2\hat{\Psi}'' + V_{\text{ext}}\hat{\Psi} + \left[\int \hat{\Psi}^{\dagger\prime} V(r'-r)\hat{\Psi}'dr'\right]\hat{\Psi} = \\
&= \left[-\frac{\hbar^2}{2m}\boldsymbol{\nabla}^2 + V_{\text{ext}} + \int \hat{\Psi}^{\dagger\prime} V(r'-r)\hat{\Psi}'dr'\right]\hat{\Psi}
\end{aligned} \tag{A.7}
$$

A.2 Obtaining the energy functional for the GPE equation from the hamiltonian of a rarefied (weakly interacting) Bose gas

- $\hat{H} = \frac{\hbar^2}{2m}\int(-\hat{\Psi}^\dagger\boldsymbol{\nabla}^2\hat{\Psi})d\boldsymbol{r} + \int \hat{\Psi}^\dagger V_{\text{ext}}\hat{\Psi}dx + \frac{1}{2}\int \hat{\Psi}^\dagger\hat{\Psi}^{\dagger'} V(\mathbf{r}'-\boldsymbol{r})\hat{\Psi}\hat{\Psi}'d\boldsymbol{r}'d\boldsymbol{r} \equiv \hat{A}+\hat{B}+\hat{C}.$ (A.8)
- $E(\Psi) = \frac{\langle\Psi|\,\hat{H}\,|\Psi\rangle}{\langle\Psi|\Psi\rangle}.$ (A.9)

In order to find the energy functional we also need relation

$$
\int \boldsymbol{\nabla}\hat{\Psi}^\dagger\boldsymbol{\nabla}\hat{\Psi}d\boldsymbol{r} = -\int \hat{\Psi}^\dagger\boldsymbol{\nabla}^2\hat{\Psi}d\boldsymbol{r}. \tag{A.10}
$$

Which can be proven quite straightforwardly by expanding $\boldsymbol{\nabla}\left[\hat{\Psi}^\dagger(\boldsymbol{\nabla}\hat{\Psi})\right]$, integrating the different parts in $\boldsymbol{r}$,

$$
\int \boldsymbol{\nabla}\left[\hat{\Psi}^\dagger(\boldsymbol{\nabla}\hat{\Psi})\right]d\boldsymbol{r} = \int \boldsymbol{\nabla}\hat{\Psi}^\dagger\boldsymbol{\nabla}\hat{\Psi}d\boldsymbol{r} + \int \hat{\Psi}^\dagger\boldsymbol{\nabla}^2\hat{\Psi}d\boldsymbol{r}, \tag{A.11}
$$

and finally noticing that the first term is a total divergence, and as such goes to zero (upon employment of the divergence theorem).

Finally, we may find the energy:

$$
\langle\Psi|\,\hat{H}\,|\Psi\rangle \equiv \langle\Psi|\,\hat{A}\,|\Psi\rangle + \langle\Psi|\,\hat{B}\,|\Psi\rangle + \langle\Psi|\,\hat{C}\,|\Psi\rangle \tag{A.12}
$$

$$\langle\Psi|\,\hat{A}\,|\Psi\rangle = -\frac{\hbar^2}{2m}\int\int \Psi^{\dagger\prime}\Psi^{\dagger}(\boldsymbol{\nabla}^2\Psi)\Psi' d\boldsymbol{r}d\boldsymbol{r}' = \frac{\hbar^2}{2m}\int \Psi^{\dagger\prime}[\boldsymbol{\nabla}\Psi^{\dagger}\boldsymbol{\nabla}\Psi]\Psi' d\boldsymbol{r}\boldsymbol{r}' =$$
$$= \frac{\hbar^2}{2m}\int |\boldsymbol{\nabla}\Psi|^2 d\boldsymbol{r}\int \Psi^{\dagger\prime}\Psi' d\boldsymbol{r} = \frac{\hbar^2}{2m}\langle\Psi|\Psi\rangle\int |\boldsymbol{\nabla}\Psi|^2 d\boldsymbol{r} \tag{A.13}$$

$$\langle\Psi|\,\hat{B}\,|\Psi\rangle = \int\int \Psi^{\dagger\prime}\Psi^{\dagger}V_{\text{ext}}\Psi\Psi' d\boldsymbol{r}d\boldsymbol{r}' = \int \Psi^{\dagger}V_{\text{ext}}\Psi d\boldsymbol{r}\int \Psi^{\dagger}\Psi' d\boldsymbol{r}' =$$
$$= \langle\Psi|\Psi\rangle\int |\Psi|^2 V_{\text{ext}} d\boldsymbol{r} \tag{A.14}$$

$$\langle\Psi|\,\hat{C}\,|\Psi\rangle = \frac{1}{2}\int\int\int \Psi^{\dagger\prime\prime}\Psi^{\dagger}\Psi^{\dagger\prime}V(\boldsymbol{r}'-\boldsymbol{r})\Psi\Psi'\Psi'' d\boldsymbol{r}' d\boldsymbol{r} d\boldsymbol{r}'' =$$
$$= \frac{1}{2}\int \Psi^{\dagger\prime\prime}\Psi'' d\boldsymbol{r}''\int\int \Psi^{\dagger}\Psi^{\dagger\prime}V(\boldsymbol{r}'-\boldsymbol{r})\Psi\Psi' d\boldsymbol{r}' d\boldsymbol{r}$$

Replacing the interaction potential, $V(\boldsymbol{r}'-\boldsymbol{r}) = g\delta(\boldsymbol{r}'-\boldsymbol{r})$, in accordance with (2.33)

$$\langle\Psi|\,\hat{C}\,|\Psi\rangle = \frac{1}{2}\langle\Psi|\Psi\rangle\int |\Psi|^2\int\int |\Psi'|^2 g\delta(\boldsymbol{r}-\boldsymbol{r}) d\boldsymbol{r}' d\boldsymbol{r} =$$
$$= \frac{g}{2}\langle\Psi|\Psi\rangle\int |\Psi|^4 d\boldsymbol{r} \tag{A.15}$$

$$\Rightarrow E(\Psi) = \frac{\langle\Psi|\,\hat{H}\,|\Psi\rangle}{\langle\Psi|\Psi\rangle} = \int\left[\frac{\hbar^2}{2m}|\boldsymbol{\nabla}\Psi|^2 + V_{\text{ext}}|\Psi|^2 + \frac{g}{2}|\Psi|^4\right] d\boldsymbol{r} \tag{A.16}$$

A.3 Conservation of the number of particles in the GPE from the continuity equation

- LEIBNIZ RULE $\quad \dfrac{d}{dt}\left(\displaystyle\int_a^b f(x,t)dx\right) = \int_a^b \frac{\partial f(x,t)}{\partial t}dx\ ; \quad a, b$ constants (A.17)
- $\hat{H} = \dfrac{\hbar^2}{2m}\displaystyle\int(-\hat{\Psi}^{\dagger}\boldsymbol{\nabla}^2\hat{\Psi})d\boldsymbol{r} + \int\hat{\Psi}^{\dagger}V_{\text{ext}}\hat{\Psi}dx + \frac{1}{2}\int\hat{\Psi}^{\dagger}\hat{\Psi}^{\dagger'}V(\boldsymbol{r}'-\boldsymbol{r})\hat{\Psi}\hat{\Psi}' d\boldsymbol{r}' d\boldsymbol{r} \equiv \hat{A}+\hat{B}+\hat{C},$ (A.18)
- CONTINUITY EQUATION $\quad \dfrac{\partial n}{\partial t} + \boldsymbol{\nabla}\cdot\mathbf{j} = 0.$ (A.19)

We start off by integrating both sides of the continuity equation,

$$\Rightarrow \quad \int\frac{\partial \mathbf{n}}{\partial t}d\boldsymbol{r} = -\int\boldsymbol{\nabla}\cdot\mathbf{j}d\boldsymbol{r}. \tag{A.20}$$

Then, the application of the Leibniz rule (A.17) to the left-hand side of equation (A.20) allows one to take the partial derivative out of the integral as a total derivative. In turn, the right-hand side term can be made to vanish by using the divergence theorem to obtain a contour integral of the current, which goes to zero either by considering a confined system or cyclic boundaries; and thus finally, simply by substituting the definition of $N = \int|\Psi(x)|^2 dx$one reaches the desired conservation law

$$\frac{d}{dt}\left(\int d\boldsymbol{r} n(\boldsymbol{r},t)\right)=0 \quad \Leftrightarrow \quad \frac{dN}{dt}=0. \tag{A.21}$$

A.4 Arriving at the Soliton Wavefunction Equation

$$\bullet \text{ 1D GPE} \quad i\frac{\partial\Psi(x,t)}{\partial t}=\left(-\frac{\hbar^2}{2m}\boldsymbol{\nabla}^2+g|\Psi(x,t)|^2\right)\Psi(x,t). \tag{A.22}$$

With the knowledge that solitons constitute actual solutions to equation (A.22), one may look for these solutions by substituting an ansatz

$$\Psi(x,t)=f(x-ut)e^{-i\frac{\mu t}{\hbar}}, \tag{A.23}$$

where u is the soliton velocity and μ the chemical potential (corresponds to the eigenvalue of the ground state solution), into the latter, and investigating only solutions which tend to a finite (background) value for the density $n_0 \neq 0$ when x goes to infinity, $|\Psi_{\text{SOL}}(\pm\infty)|^2 \to n_0$. Introducing the ansatz into eq.(A.22) yields

$$i(-i\mu)f(x-ut)+i\hbar\frac{\partial f(x-ut)}{\partial t}=-\frac{\hbar^2}{2m}\frac{\partial^2 f(x-ut)}{\partial x^2}+g|f(x-ut)|^2 f(x-ut) \tag{A.24}$$

and further reparametrizing the above equation by $\bar{x}=x-ut$ one obtains:

$$-\frac{\hbar^2}{2m}\frac{\partial^2 f(\bar{x})}{\partial \bar{x}^2}+g|f(\bar{x})|^2 f(\bar{x})=-i\hbar u\frac{\partial f(\bar{x})}{\partial \bar{x}}+\mu f(\bar{x}). \tag{A.25}$$

Before progressing we establish a few further considerations; it becomes useful to — first - –replace $\bar{x}$ by a new variable scaled to the soliton's natural dimensions, $\bar{\bar{x}}=\frac{\bar{x}}{\xi}$, where ξ is the healing length (2.60) and - second - to separate f into real and imaginary parts

$$f=f_0\left[\alpha(\bar{\bar{x}})+i\beta(\bar{\bar{x}})\right]; \quad f_0\equiv f(\bar{\bar{x}}\to\pm\infty). \tag{A.26}$$

Remembering the background density condition, we may now - third - rewrite it in terms of $|f_0|^2 \equiv |f(\bar{\bar{x}}\to\pm\infty)|^2=n_0$, and as for the chemical potential, given that we are using its stationary solution in the absence of an external potential we may — fourth — write $\mu=gn_0$. Note also that the boundary condition, together with (A.26) translates into a condition for the newly introduced α and β, which is that

$$\alpha(\pm\infty)^2+\beta(\pm\infty)^2=1. \tag{A.27}$$

Applying all these considerations into (A.25), and separating the resulting expression into real and imaginary parts yields,

$$\begin{cases} \text{RE}: & \alpha'' - \alpha(\alpha^2+\beta^2) = -u\sqrt{\frac{2m}{gn_0}}\beta' - \alpha \\ \text{IM}: & \beta'' - \beta(\alpha^2+\beta^2) = u\sqrt{\frac{2m}{gn_0}}\alpha' - \beta \end{cases}, \tag{A.28}$$

where we have simplified the notation to $''$ and $'$ denoting the second and first derivates with respect to $\bar{\bar{x}}$, respectively. Considering only possible solutions for which the imaginary part is equal to a constant everywhere [32], $\beta \equiv \beta_0$, we reach the system (A.29) in which c_s is the velocity of sound in the BEC (2.55), and whose condition of self-consistency will lead us to an expression for β_0:

$$\begin{cases} \alpha'' + (1+\alpha^2+\beta_0^2)\alpha = 0, & \text{(A.29a)} \\ (\,1-\alpha^2-\beta_0^2)\beta_0 = \sqrt{2}\dfrac{u}{c_s}\alpha'. & \text{(A.29b)} \end{cases}$$

In order to check the consistency between (A.29a) and (A.29b), we start by multiplying (A.29a) by $\partial\alpha$ and then find its primitive:

$$\int d\bar{\bar{x}}\ \ \alpha''\alpha\alpha'\alpha + \int d\bar{\bar{x}}\ \ (1-\alpha^2-\beta_0^2)\alpha\alpha' = cte \quad \Leftrightarrow \tag{A.30}$$

$$\Leftrightarrow \quad \frac{1}{2}(\alpha')^2 - \frac{1}{4}\int d\bar{\bar{x}}\ \ [(1-\alpha^2-\beta_0)^2]' = cte \quad \Leftrightarrow \tag{A.31}$$

$$\Leftrightarrow \quad \frac{1}{2}(\alpha')^2 - \frac{1}{4}(1-\alpha^2-\beta_0^2) = \cancelto{0}{cte}, \tag{A.32}$$

Where we have used integration by parts in the leftmost term - $\int \alpha''\alpha' = (\alpha')^2 - \int \alpha'\alpha''$ - and used the boundary condition - $\alpha^2(\pm\infty) = \beta_0^2 \ \Rightarrow\ \alpha'(\pm\infty) = 0$ - to conclude that the constant in the *rhs* should be zero. We henceforth have

$$2(\alpha')^2 = (1-\alpha^2-\beta_0^2), \tag{A.33}$$

which is only made consistent with (A.29b) if

$$\boxed{\beta_0^2 = \frac{u^2}{c_s^2}}. \tag{A.34}$$

Having found out the β_0 constant value one needs only solve (A.29) for α in order to fully define f (A.26) and thus obtain the soliton solution.

Under the boundary conditions $x(\pm\infty) = x_0$, where x_0 is some constant - in our case, $|\Psi(\pm\infty)|^2 = 1 \ \Rightarrow\ \alpha(\pm\infty)^2 = 1-\beta_0$ - and $x(0) = 0$ or an equivalent - there will be a minimum at $\Psi(ut) \ \Rightarrow\ \alpha(ut)$, which is the local density dip where the soliton is localised, and which will only be zero in the special case that the soliton is dark - such an equation may be solved using an hyperbolic tangent* [32],

$$x(t) = x_0 \tanh\left(\frac{x_0}{\sqrt{2}}x\right), \tag{A.35}$$

*Notice that between the hyperbolic functions the tangent is in this case the most appropriate, seeing as it has a zero in $x = 0$, which the cosine does not, and it tends to a finite value when $x \to \infty$, which the sine does not.

which in our system will translate into (and taking into account the analogy developed in the last paragraph):

$$\alpha(\bar{\bar{x}}) = \alpha_0 \tanh\left(\frac{\bar{\bar{x}}\alpha_0}{\sqrt{2}}\right) \;\Leftrightarrow$$
$$\Leftrightarrow \quad \alpha(x) = \alpha_0 \tanh\left(\frac{(x-ut)\alpha_0}{\xi\sqrt{2}}\right). \tag{A.36}$$

Finally, we employ the boundary condition to find α_0

$$\alpha(\pm\infty) = \alpha_0 \tanh(\pm\infty) = \alpha_0 \;\Rightarrow\; \alpha_0^2 = \alpha(\pm\infty)^2 = 1 - \beta_0^2,$$

$$\Rightarrow \quad \boxed{\alpha_0 = \sqrt{1 - \frac{u^2}{c_s^2}}}. \tag{A.37}$$

Circling back to equation (A.26) and to our ansatz (A.23) we may substitute in the expressions obtained and at last find a solution for Ψ:

$$\Psi(x,t)_{\text{SOL}} = f_0\left[\alpha_0 \tanh\left(\frac{(x-ut)\alpha_0}{\xi\sqrt{2}}\right) + i\beta_0\right], \tag{A.38}$$
$$= \sqrt{n_0}\left[i\frac{u}{c_s} + \sqrt{1-\frac{u}{c_s}}\tanh\left(\frac{x-ut}{\sqrt{2}\xi}\sqrt{1-\frac{u^2}{c_s^2}}\right)\right]. \tag{A.39}$$

For completeness we additionally determine the phase jump across a soliton,

$$\Delta\varphi_{\text{SOL}} = \varphi[\Psi_{\text{SOL}}(+\infty)] - \varphi[\Psi_{\text{SOL}}(-\infty)] =$$
$$\text{(A.26)} \;\Rightarrow\; = \varphi[f(+\infty)] - \varphi[f(-\infty)] =$$
$$= \arctan\left(\frac{\beta_0^+}{\alpha(+\infty)}\right) - \arctan\left(\frac{\beta_0^-}{\alpha(-\infty)}\right) =$$
$$= \arctan\left(\frac{\beta_0^+}{\alpha(+\infty)}\right) - \left[\pi - \arctan\left(\frac{\beta_0^+}{\alpha(+\infty)}\right)\right] =$$
$$\beta_0 \equiv \beta_0^+ \;\Rightarrow\; = 2\arctan\left(\frac{\beta_0}{\sqrt{1-\beta_0^2}}\right) - \pi =$$
$$= -2\arccos\left(\frac{u}{c_s}\right). \tag{A.40}$$

A.5 Determination of soliton energy

- SOLITON ENERGY INTEGRAL $\quad \epsilon = \int\left(\frac{\hbar^2}{2m}|\boldsymbol{\nabla}\Psi|^2 + \frac{g}{2}(|\Psi|^2 - n_0)^2\right)dx.$ (A.41)
- SOLITON SOLUTION $\quad \Psi_{\text{SOL}} = \sqrt{n_0}\left(i\frac{v_s}{c} + \sqrt{1-\frac{v_s^2}{c^2}}\tanh\left[\frac{x-x_s}{\xi}\sqrt{1-\frac{v_s^2}{c^2}}\right]\right).$ (A.42)

First of all we start by determining the derivative of Ψ_{SOL} in order to replace it onto (A.41):

$$\boldsymbol{\nabla}\Psi_{\text{SOL}} = \sqrt{n_0}\left(1-\frac{v_s^2}{c^2}\right)\frac{1}{\xi}\,\text{sech}^2\left(\frac{x-x_s}{\xi}\sqrt{1-\frac{v_s^2}{c^2}}\right),$$

$$\Rightarrow \quad |\boldsymbol{\nabla}\Psi_{\text{SOL}}|^2 = n_0\left(\left(1-\frac{v_s^2}{c^2}\right)^2\frac{1}{\xi^2}\,\text{sech}^4\left[\frac{x-x_s}{\xi}\sqrt{1-\frac{v_s^2}{c^2}}\right]\right), \tag{A.43}$$

$$|\Psi_{\text{SOL}}|^2 = n_0\left(\left(1-\frac{v_s^2}{c^2}\right)\tanh^2\left[\frac{x-x_s}{\xi}\sqrt{1-\frac{v_s^2}{c^2}}\right]+\frac{v_s^2}{c^2}\right). \tag{A.44}$$

Substituting (A.43) and (A.44) into (A.41):

$$\begin{aligned}\epsilon_s = \int\Bigg(&\frac{\hbar^2}{2m}n_0\left(1-\frac{v_s^2}{c^2}\right)^2\frac{1}{\xi^2}\,\text{sech}^4\left[\frac{x-x_s}{\xi}\sqrt{1-\frac{v_s^2}{c^2}}\right]+\\&+\frac{g}{2}n_0^2\left[\left(1-\frac{v_s^2}{c^2}\right)\tanh^2\left[\frac{x-x_s}{\xi}\sqrt{1-\frac{v_s^2}{c^2}}\right]-\left(1-\frac{v_s^2}{c^2}\right)\right]^2\Bigg)dx=\\=\int\Bigg(&\frac{\hbar^2}{2m}\frac{mgn_0}{\hbar^2}n_0\left(1-\frac{v_s^2}{c^2}\right)^2\text{sech}^4\left(\frac{x-x_s}{\xi}\sqrt{1-\frac{v_s^2}{c^2}}\right)-\\&-\frac{g}{2}n_0^2\left(1-\frac{v_s^2}{c^2}\right)^2\text{sech}^4\left[\frac{x-x_s}{\xi}\sqrt{1-\frac{v_s^2}{c^2}}\right]\Bigg)dx.\end{aligned} \tag{A.45}$$

Where we have replaced the healing length definition (2.60) in the rhs and we have utilized the trigonometric relation $1-\tanh^2=\text{sech}^2$ in the lhs. Performing the variable substitution $y=\frac{x-x_s}{\xi}\sqrt{1-\frac{v_s^2}{c^2}}$; $dy=\frac{1}{\xi}\sqrt{1-\frac{v_s^2}{c^2}}dx$,

$$\begin{aligned}\epsilon_s &= \int\left(\frac{gn_0^2}{2}\frac{\hbar}{mgn_0}\left(1-\frac{v_s^2}{c^2}\right)^{\frac{3}{2}}\text{sech}^4(y)-\frac{g}{2}n_0^2\frac{\hbar}{\sqrt{mgn_0}}\left(1-\frac{v_s^2}{c^2}\right)^{\frac{3}{2}}\text{sech}^4(y)\right)dy=\\&=\int\left(\frac{gn_0}{m}\frac{n_0\hbar}{2}2\left(1-\frac{v_s^2}{c^2}\right)^{\frac{3}{2}}\text{sech}^4(y)\right)dy=\hbar cn_0\left(1-\frac{v_s^2}{c^2}\right)^{\frac{3}{2}}\int\text{sech}^4(y)dy.\ \Leftrightarrow\end{aligned} \tag{A.46}$$

Finally, due to the fact that $\int_{-\infty}^{+\infty}\text{sech}^4(y)dy=\frac{4}{3}$ we finally reach

$$\Leftrightarrow\ \epsilon_s=\frac{4}{3}\hbar cn_0\left(1-\frac{v_s^2}{c^2}\right)^{\frac{3}{2}}. \tag{A.47}$$

A.6 Soliton oscillation frequency

SOLITON ENERGY IN THE ABSENCE OF AN EXTERNAL POTENTIAL

- (2.71) $\epsilon_s=\frac{4}{3}n_0\hbar c\left(1-\frac{v_s^2}{c^2}\right)^{\frac{3}{2}}=\frac{4}{3}\frac{\hbar}{g\sqrt{m}}\left(\mu-v_s^2m\right)^{\frac{3}{2}}.$ (A.48)

SOLITON ENERGY IN THE PRESENCE OF AN EXTERNAL POTENTIAL

- (2.73) $\epsilon_s=\frac{4}{3}\frac{\hbar}{g\sqrt{m}}\left(\mu-V(x_s)-v_s^2m\right)^{\frac{3}{2}}.$ (A.49)

In the absence of an external potential,

$$\text{the stationary solution is found by making : } \frac{\partial \epsilon}{\partial t} = 0 \quad \Leftrightarrow$$

$$\Leftrightarrow \quad 2\frac{\hbar}{g\sqrt{m}}\left(\mu - v_s^2 m\right)^{\frac{1}{2}}\left(-2v_s m\frac{dv_s}{dt}\right) = 0 \quad \Leftrightarrow$$

$$\Leftrightarrow \quad \begin{cases} \mu = v_s^2 m \;\Leftrightarrow\; v_s = \sqrt{\frac{\mu}{m}} = \pm\sqrt{\frac{gn}{m}} = c \quad \rightarrow \text{no soliton,} \\ \frac{dv_s}{dt} = 0 \rightarrow v_s = cte \quad \rightarrow \text{grey soliton,} \\ v_s = 0 \quad \rightarrow \text{dark soliton.} \end{cases} \tag{A.50}$$

$$\Leftrightarrow \quad x_s(t) = v_0 t + x_0 \;; \quad 0 \leq v_0 \leq c. \tag{A.51}$$

Whereas in the presence of an external potential,

$$\frac{\partial \epsilon}{\partial t} = 0 \quad \Leftrightarrow$$

$$\Leftrightarrow \quad -\frac{4}{3}\frac{\hbar}{g\sqrt{m}}\left(\mu - V(x_s) - v_s^2 m\right)^{\frac{1}{2}}\left(\frac{dV(x)}{dx_s}\frac{dx_s}{dt} + 2\frac{dx_s}{dt}m\frac{d^2x_s}{dt^2}\right) = 0 \quad \Leftrightarrow .$$

(forgoing the trivial solution $v_s = \sqrt{\frac{\mu - V(x)}{m}} = c$),

$$\Leftrightarrow \quad \frac{d^2x_s}{dt^2} + \frac{1}{2m}\frac{dV(x)}{dx_s} = 0 \quad \Leftrightarrow$$

considering a potential harmonic potential $V(x_s) = \frac{1}{2}mw^2x^2$,

$$\Leftrightarrow \quad \frac{d^2x_s}{dt^2} + \frac{1}{2}\omega^2 x = 0 \;; \; \boxed{\omega_s = \frac{\omega}{\sqrt{2}}} \quad \Leftrightarrow \tag{A.52}$$

$$\Leftrightarrow \quad x_s(t) = v_0\cos(\omega_s t + \varphi_0) + x_0. \tag{A.53}$$

This result for the frequency of the oscillation of the dark soliton, implies the following equation of motion for a dark soliton:

$$\frac{d^2x}{dt^2} = -\frac{1}{2}\frac{dV}{dx}. \tag{A.54}$$

This equation may be obtained directly through other means — involving lengthier and more complicated calculations, which are not included here, but methods for its derivation can be found in [80, 81]. ———

———————————————————————-

A.7 Vector identities

$$\boldsymbol{\nabla} \times (\boldsymbol{\nabla}\phi) = 0 \tag{A.55}$$

$$\boldsymbol{\nabla} \cdot (\boldsymbol{\nabla} \times \mathbf{u}) = 0 \tag{A.56}$$